MILD ADOLESCENT IDIOPATHIC SCOLIOSIS (AIS) CLASSIFICATION USING 3D ULTRASOUND IMAGING METHODS

YANG DE

PhD

The Hong Kong Polytechnic University

2023

The Hong Kong Polytechnic University

Department of Biomedical Engineering

Mild Adolescent Idiopathic Scoliosis (AIS) Classification Using 3D Ultrasound Imaging Methods

YANG De

A thesis submitted in partial fulfillment of the requirements for the degree of

Doctor of Philosophy

August 2022

CERTIFICATE OF ORIGINALITY

I hereby declare that this thesis is my own work and that, to the best of my knowledge and belief, it reproduces no material previously published or written, nor material that has been accepted for the award of any other degree or diploma, except where due acknowledgement has been made in the text.

_______________________________(Signed)

______YANG De_________________ (Name of Student)

ABSTRACT

Mild adolescent idiopathic scoliosis (AIS), with Cobb<20°, together with high bone maturity grade, was hypothesized as the right stage to intervene to prevent progression. AIS curve can be categorized into either structural or non-structural depending on the spine morphology (flexibility). Lenke classification is the state-of-the-art scoliosis classification scheme for pre-surgery AIS planning. However, no study has reported the scoliosis classification scheme for mild AIS curve-correction exercise assessment, which requires the knowledge of curve types in different spinal segments. Using X-ray to characterize AIS curves remains the clinical gold standard while compromising the risks of radiation exposure. For non-radiative alternatives, 3D ultrasound imaging has demonstrated its reliability for the coronal spinal curvature measurement. The overall objective of this study is to investigate the validity and reliability of a measurement parameter, Bending Asymmetry Index (BAI), originated from the 3D ultrasound imaging. BAI is derived from bilateral bending of spine, reflecting the curve type in spinal morphology of scoliosis, and can be used for mild AIS classification purposes. Non-structural curve demonstrates a quasi-symmetrical pattern in bilateral bending, while structural curve shows distinctive asymmetrical pattern. The BAI methods were validated through different anatomical landmarks: 1) vertebral body centroid; 2) spinous process; and 3) transverse process features.

In the present study, several features have been applied for the BAI methods. Vertebral body centroid was used to validate the pre-surgery AIS patients' classification in X-ray for ethical concerns. Two ultrasound-based BAI methods, namely as BAIsp (using spinous process) and BAItp (using transverse process

features), were validated for mild AIS patients classification. These BAI methods all demonstrated promising results for AIS curve type classification. Ultrasound BAI methods not only classify mild AIS curves, but also take an important role in AIS screening referrals.

Further studies are worthwhile to investigate whether deep learning approaches could liberate the manual procedures for the current semi-automatic BAI methods. Due to the radiation-free nature of ultrasound, it will also be very meaningful to conduct follow-up investigation of patients with AIS for monitoring BAI changes as a progression indication.

PUBLICATIONS RELATED TO THIS THESIS

Journal Papers

1. **Yang D**, Lee TTY, Lai KKL, Lam TP, Castelein RM, Cheng JCY, Zheng YP. Semi-automatic method for pre-surgery scoliosis classification on X-ray images using Bending Asymmetry Index. *International Journal of Computer Assisted Radiology and Surgery* **17**,2239-2251 (2022). https://doi.org/10.1007/s11548-022-02740-x **(Published)**

2. **Yang D**, Lee TTY, Lai KKL, Lam TP, Chu WCW, Castelein RM, Cheng JCY, Zheng YP. Semi-automatic ultrasound curve angle measurement for adolescent idiopathic scoliosis. *Spine Deformity* **10**, 351–359 (2022). https://doi.org/10.1007/s43390-021-00421-4 (**Published)**

3. **Yang D**, Lee TTY, Lai KKL, Wong YS, Wong LN, Yang JL, Lam TP, Castelein RM, Cheng JCY, Zheng YP. A novel classification method for mild adolescent idiopathic scoliosis using 3D ultrasound imaging. *Medicine in Novel Technology and Devices* **11**, 100075 (2021) https://doi.org/10.1016/j.medntd.2021.100075 **(Published)**

4. Huang ZX, Zhao R, Leung FHF, Banerjee S, Lee TTY, **Yang D**, Lun DPK, Lam KM, Zheng YP, Ling SH. Joint spine segmentation and noise removal from ultrasound volume projection images with selective feature sharing. *IEEE Transactions on Medical Imaging*, 41(7), 1610-1624 (2022) https://doi.org/10.1109/TMI.2022.3143953 **(Published)**

5. Banerjee S, Lyu J, Huang Z, Leung HFF, Lee TTY, **Yang D**, Su S, Zheng YP, Ling SH. Ultrasound spine image segmentation using multi-scale feature fusion skip-inception U-Net (SIU-Net). Biocybernetics and Biomedical Engineering. **42** (1):341-361 (2022) https://doi.org/10.1016/j.bbe.2022.02.011 **(Published)**

6. Banerjee S, Lyu J, Huang Z, Leung HFF, Lee TTY, **Yang D**, Su S, Zheng YP, Ling SH. Light-Convolution dense selection U-Net (LDS U-Net) for ultrasound lateral bony feature segmentation. *Applied Sciences*. **11**(21):10180. (2021) https://doi.org/10.3390/app112110180 **(Published)**

7. Lyu J, Bi XJ, Banerjee S, Huang Z, Leung HFF, Lee TTY, **Yang D**, Zheng YP, Ling SH. Dual-task ultrasound spine transverse vertebrae segmentation network with contour. *Computerized Medical Imaging and Graphics*. **89**:101896. (2021) https://doi.org/10.1016/j.compmedimag.2021.101896 **(Published)**

8. Lyu J, Ling SH, Banerjee S, Zheng JY, Lai KL, **Yang D**, Zheng YP, Bi XJ, Su S, Chamoli U. Ultrasound volume projection image quality selection by ranking from convolutional RankNet. Computerized Medical Imaging and Graphics. **89**:101847. (2021) https://doi.org/10.1016/j.compmedimag.2020.101847 **(Published)**

Conference Proceedings

1. **Yang D**, Lee TTY, Lai KKL, Wong YS, Wong LN, Lam TP, Castelein RM, Cheng JCY, Zheng YP. A glimpse of using 3D ultrasound imaging in the adolescent idiopathic scoliosis curve classification. *The 15th Society on Scoliosis Orthopaedic and Rehabilitation Treatment (SOSORT) Annual Meeting*, 2020.

2. **Yang D**, Lee TTY, Lai KKL, Wong YS, Wong LN, Lam TP, Castelein RM, Cheng JCY, Zheng YP. A pilot study to investigate the adolescent idiopathic scoliosis screening referral status using 3D ultrasound imaging. *The 15th Society on Scoliosis Orthopaedic and Rehabilitation Treatment (SOSORT) Annual Meeting*, 2020.

3. **Yang D**, Lee TTY, Lai KKL, Wong YS, Wong LN, Lam TP, Castelein RM, Cheng JCY, Zheng YP. Adolescent idiopathic scoliosis curve classification: a preliminary study using 3D ultrasound imaging. *The 9th World Congress on Bioengineering (WACBE)*,2019.

4. Zhao R, Huang ZX, Liu TS, Leung FHF, Ling SH, **Yang D**, Lee TTY, Lun DPK, Zheng YP, Lam KM. Structure-Enhanced attentive learning for spine segmentation from ultrasound volume projection images. *CASSP 2021-2021 IEEE International Conference on Acoustics, Speech and Signal Processing (ICASSP).*

5. Huang ZX, Zhao R, Leung FHF, Lam KM, Ling SH, Lyu J, Banerjee S, Lee TTY, **Yang D**, Zheng YP. DA-GAN: learning structured noise removal in ultrasound volume projection imaging for enhanced spine segmentation. *2021 IEEE 18th International Symposium on Biomedical Imaging (ISBI).*

6. Huang ZX, Wang LW, Leung FHF, Banerjee S, **Yang D**, Lee TTY, Lyu J, Ling SH, Zheng YP. Bone feature segmentation in ultrasound spine image with robustness to speckle and regular occlusion noise. *2020 IEEE International Conference on Systems, Man, and Cybernetics (SMC).*

ACKNOWLEDGEMENTS

I am very grateful to all those people who have helped and supported me throughout my Ph.D. study in the Hong Kong Polytechnic University. Firstly, I would like to express my deepest appreciation to my chief supervisor, Professor Zheng Yongping, for his all-time guidance and support throughout the entire period of my Ph.D. study. He is always there to provide me insightful suggestions and valuable comments to improve my research outputs and enhance the quality of my written documents and presentation skills. It is my great honor to have him as my research advisor and mentor.

At the same time, I would like to express my special thanks to my parents for their unconditional support and encouragement during my struggle for my study endeavor. This thesis would never have been completed without them. I also would like to express my thanks to Meng Meng, who is always keeping his companion during my thesis writing period. He always sleeps behind my laptop, sometimes snored, but never messed up with my keyboards.

Besides, I would also like to express many thanks to the research members of our group. Especially, I would like to thank Dr. Timothy Lee for his valuable ideas and comments to my research works, Kelly and Heidi for delivering great quality scanning scans, Meng Qiang and Zhou Guangquan for providing the scoliosis analysis software, Henry and William for technical support, Prof. Tsz-Ping Lam, Prof. Chun-yiu Cheng and Prof. Rene Castelein for the valuable comments on my research directions.

TABLE OF CONTENTS

LIST OF FIGURES

Figure 3.8 Illustration of structural curve characterized by BAI from a real subject. **(a)** An example of three-posture coronal spine images from the same subject with the 3D ultrasound imaging method. The spinous lines (interpolated by the curve passing through centers of spinous process from all levels, T1-L5) for standing erect (E-SPL, yellow), bending to left (L-SPL, red) and bending to right (R-SPL, green) are superimposed with the original ultrasound images with end points labelled with (Left/Right Upper/Lower) markers. **(b)** the extracted L-SPL and R-SPL from **(a)** and **(c)** with alignment of end points, L-SPL is flipped to match with R-SPL to examine the asymmetrical pattern. For this curve, the BAIsp value is 2330 pixel or 269.01 mm^2 , which is larger than the threshold for structural curve (200 pixel or 23.09 mm^2); it implicates that the thoraco-lumbar curve presented in E-SPL(a) is structural.

Figure 3.9 The modified Lenke distribution of mild AIS classification (m-Lenke) results (N=87). Scolioscan 3D ultrasound classification results (Matched cases in orange, mismatched cases in grey) are compared with the gold-standard EOS X-ray classification results (blue). A matched case indicates both ultrasound-based BAIsp method and X-ray ground-truth arrive at identical classification result. The ensemble comprises m-Lenke type 1–6 with two proximal thoracic-dominant variants: PT* (structural curve in proximal thoracic) and PT + L (structural curve in proximal thoracic and lumbar), and the detection of non-structural curves (NSC).

Figure 3.10 The major curve distribution of mild AIS classification results. Scolioscan 3D ultrasound classification results (Matched cases in orange, mismatched cases in grey) are compared with the gold-standard EOS X-ray classification results (blue). A matched case means both ultrasound and X-ray arrive at identical major curve detection result. The ensemble comprises major curve located in proximal thoracic (PT), thoracic (T), lumbar (L) or not detected (N/A, for non-structural curves).

Figure 3.11 Curved-based AUC analysis of ultrasound estimating X-ray Cobb ≥ 20 °. i) green line: using USSPA; ii) yellow line: using BAI; iii) blue line: using USSPA and BAI together. The purple line is served as a reference line to indicate AUC=0.500.

Figure 3.12 Patient-based AUC analysis of ultrasound estimating X-ray Cobb ≥ 20 °. i) green line: using USSPA; ii) yellow line: using BAI; iii) blue line: using USSPA and BAI together. The purple line is served as a reference line to indicate AUC=0.500.

Figure 4.1 Diagrams illustrating how points for line placements were assigned to acquire UCA: **a)** For thoracic region, if a white dot, which corresponded to the echo of a transverse process, could be seen, the center of the white dot will be used to place the point (left); If no white dot could be observed, the centre of the black region, which corresponded to the shadow of a transverse process, will be used to place the point (right); **b)** For (thoraco)lumbar region, the lump shadow would be considered as a combination of a triangle (yellow dotted line) and a rectangle (green dotted line) (left). Dots will be placed at locations proximal to the centre of the bilateral sides of the rectangle (right). UCA: Ultrasound Curve Angle. (Lee et al. 2021)

Figure 4.2 Diagram illustrating the **(a)** UCA measured on coronal ultrasound image and **(b)** Cobb angle measured on coronal X-ray images. The pair of T12 ribs was first identified to distinguish the rest of the vertebrae level (green dashed line). For cases with the most tilted vertebrae on T12 or above, line was placed though the centre of the bilateral transverse processes echoes or shadows, whereas for cases with the most tilted vertebrae below T12, the line was drawn though the centre of the bilateral superior articular processes shadows, which composed of the widest bilateral part of the lump. (Image reproduced from Lee et al. 2021)

Figure 4.3 **(a)** An example of X-ray Cobb angle (XCA) method* on coronal X-ray imaging, lines were drawn to cross the middle of the most tilted vertebra to characterize a scoliotic curve. Two curves were presented, thoracic curve (T6-T11) and thoracolumbar curve (T11-L3). * This is a revised XCA method in order to directly compare with UCA method. Lines were drawn passing through the midpoint of each investigated vertebra; **(b)** an example of ultrasound cobb angle (UCA) on ultrasound coronal VPI image, lines were drawn linking the centers of transverse processes in thoracic region and passing through the lower boundary of lumps in lumbar region to characterize a scoliotic curve. Two curves were presented, thoracic curve (T6-T11) and thoracolumbar curve (T11-L3). Both scans were taken on the same subject on the same day.

Figure 4.4 **(a)** Illustration of semi-automatic transverse process-related features used by the Ultrasound Cobb Angle (UCA) method. The contours are used in UCA calculation. **(b)** An example of the contour showing a pair of thoracic transverse process. **(c)** An example of the contour showing a typical lumbar lump (combined shadow of the laminae of the superior vertebrae and the articular processes of the inferior vertebrae). The principle of the manual UCA method is a reiteration from Lee et al. 2020.

Figure 4.5 Illustration of the process of the proposed semi-automatic UCA method using transverse process-related features. **(a)** Raw ultrasound VPI image; **(b)** spinal transverse process-related features identification (contours were drawn manually): green - thoracic transverse process; blue - rib; red - lumbar lump; **(c)** transverse process-related features mask generation for image processing purpose; **(d)** automatic angle calculation based on the masks.

Figure 4.6 Schematic diagram of the automatic program (the proposed semi-automatic UCA method, Stage 2) for computing angles based on transverse process-related features. The block diagrams are color coded according to the respective color of masks (Thoracic transverse process: green; Lumbar lump: red; Rib: blue. Each mask was processed in parallel until the curve characteristics (number of curves, start/end levels) were understood by the program; then the angles were automatically calculated.

Figure 4.7 Correlation and linear equations between manual calculated Ultrasound Cobb Angle (UCA) (x) and the proposed semi-automatic UCA method (y). **(a)** Thoracic angles; **(b)** thoracolumbar/lumbar angles; **(c)** combined angles of **(a)**&**(b)**.

Figure 4.8 Correlation and linear equations between manual measured X-ray Cobb Angle (XCA) (x) and semi-automatic Ultrasound Cobb Angle (UCA) method (y). **(a)** Thoracic angles; **(b)** thoracolumbar/lumbar angles; **(c)** combined angles of **(a)**&**(b)**.

Fig.4.9 Bland-Altman plots indicate the differences between the pairs **(a)** manual UCA and the proposed semi-automatic UCA method; (b) XCA and the proposed semi-automatic UCA method corrected with the linear regression equations for all angles (combination of thoracic and lumbar angles).

Figure 4.10 Details of the modified Lenke classification system for mild AIS (m-Lenke), adapted from Lenke et al. 2003. The structural criteria for X-ray imaging and ultrasound imaging are provided respectively.

Figure 4.11 Details of the Spinous Characteristic Line (SCL) generation, each set comprises three ultrasound coronal VPI images: standing AP, bending to left and bending to right (from left to right, respectively). (a)raw input; (b) manual annotation, transverse process in thoracic region and lumbar lump in lumbar region; (c) automatic

Figure 4.16 The modified Lenke distribution of mild AIS classification (m-Lenke) results using BAIsp (N=33). Scolioscan 3D ultrasound classification using BAIsp results (Matched cases in orange, mismatched cases in grey) are compared with the gold-standard EOS X-ray classification results (blue). A matched case indicates both ultrasound-based BAIsp method and X-ray ground-truth arrive at identical classification result. The ensemble comprises m-Lenke type 1–6 with a proximal thoracic-dominant variant: PT + L (structural curve in proximal thoracic and lumbar), and the detection of non-structural curves (NSC).

Figure 4.17 The modified Lenke distribution of mild AIS classification (m-Lenke) results using BAItp (N=33). Scolioscan 3D ultrasound classification using BAItp results (Matched cases in orange, mismatched cases in grey) are compared with the gold-standard EOS X-ray classification results (blue). A matched case indicates both ultrasound-based BAItp method and X-ray ground-truth arrive at identical classification result. The ensemble comprises m-Lenke type 1–6 with a proximal thoracic-dominant variant: PT + L (structural curve in proximal thoracic and lumbar), and the detection of non-structural curves (NSC).

Figure 4.18 The modified Lenke distribution of mild AIS classification (m-Lenke) results using BAIsp/BAItp methods (N=33). Scolioscan 3D ultrasound classification using BAIsp results (Matched cases in orange, mismatched cases in grey) and BAItp results (Matched cases in yellow, mismatched cases in cyan) are compared with the gold-standard EOS X-ray classification results (blue), respectively. A matched case indicates both ultrasound-based BAIsp/BAItp method and X-ray ground-truth arrive at identical classification result. The ensemble comprises m-Lenke type 1–6 with a proximal thoracic-dominant variant: PT + L (structural curve in proximal thoracic and lumbar), and the detection of non-structural curves (NSC).

Figure 4.19 An example of left bending ultrasound VPI spine image to illustrate the effect of motion artefact to the BAI method. Red dotted circle in both images highlights the curvature caused by motion artefact) a) BAIsp method, green line: SPL; b) BAItp method, green line: SCL.

LIST OF TABLES

LIST OF ABBREVIATIONS

3D: Three Dimensional

AIS: Adolescent Idiopathic Scoliosis

AUC: Area Under Curve

BAI: Bending Asymmetry Index

BAIsp: Bending Asymmetry Index using Spinous Process

BAItp: Bending Asymmetry Index using Transverse Process Features

BDL: Bending Discrepancy Line

CT: Computed Topography

MAD: Mean Absolute Difference

MRI: Magnetic Resonance Imaging

NSC: Non-structural Curve

PA: Posterior-Anterior

ROC: Receiver Operating Characteristics

SCL: Spinous Characteristics Line

SD: Standard Deviation

SPA: Spinous Process Angle

SPL: Spinous Process Line

SPA: Spinous Process Angle

UCA: Ultrasound Curvature Angle

US: Ultrasound

USSPA: Ultrasound Spinous Process Angle

XCA: X-ray Cobb's Angle

CHAPTER 1. INTRODUCTION

1.1 Adolescent Idiopathic Scoliosis (AIS)

Scoliosis, commonly defined as a lateral curvature of the spine that with a Cobb angle larger than 10° (Lau et al. 2013), affects around 0.47-5.2% of the world's population (Konieczny et al. 2013). Idiopathic scoliosis has multiple causes, possibly include mechanical, metabolic, hormonal, neuromuscular, growth and genetic abnormalities (Do et al. 2001, Wang et al. 2007). It can be further categorized upon the age of onset of the disease: infantile idiopathic scoliosis for patients aged 0-3 years; juvenile idiopathic scoliosis for patients aged 4-10 years; and adolescent idiopathic scoliosis for patients aged 10-19 years; and adult idiopathic scoliosis for patients aged > 19 years (Altaf et al. 2013). Over 70% of Adolescent Idiopathic Scoliosis (AIS) cases develop and progress during or after puberty (Weiss et al. 2008, **Figure 1.1**). As the adolescence growth spurt advances the skeletal maturity of spine (Grave et al. 1976), scoliosis could deteriorate within months in the absence of proper intervention (Negrini et al. 2003). Untreated AIS may lead to chronic back pain and cosmetic impairment (Danielsson et al. 2003), while severe ones may have cardiopulmonary disability or even restricted physical movement (Koumbourlis et al. 2006). Conventional follow-up and treatment options are observation, exercise treatment, bracing, or surgery, depending on the degree of severity and bone maturity of AIS (Weinstein et al. 2008). The latter two options require timely actions to be taken in order to avoid further scoliosis progression (Haher et al. 1999, Julien et al. 2010). Therefore, it is of high importance that AIS subjects (or their guardians) and clinicians could comprehend the conditions and progression factors of scoliosis, and undertake correction measures without delay.

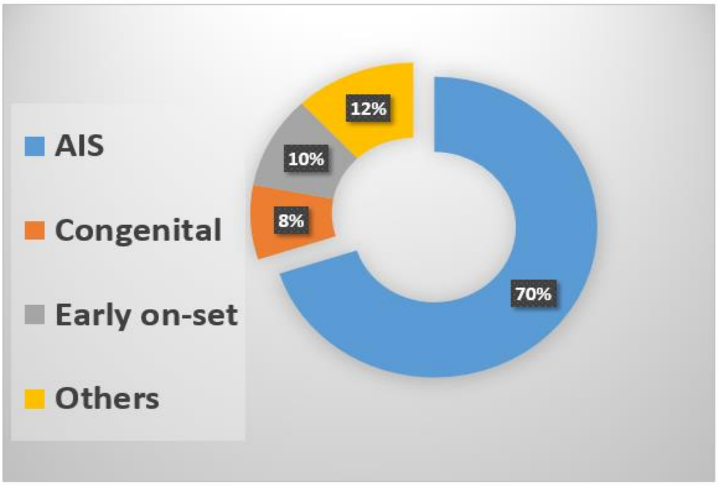

Figure 1.1 A diagram illustrated different categories of scoliosis (Weiss et al. 2008).

1.2 Diagnosis of AIS

1.2.1 Conventional Diagnosis of AIS with Rule-of-thumb X-ray Imaging

On presentation of an AIS subject to primary care, a detailed history, qualitative examination and radiological investigation are generally conducted before referral to specialist (Beausejour et al. 2007). The Adam's forward bend test is conducted to evaluate the degree of rotational deformity associated with AIS (Fairbank 2004).

Quantitatively assessing the conditions of AIS with X-ray imaging remains rule-of-thumb in clinical diagnostics and prognostics for over half a century (Altaf et al. 2013). X-ray imaging provides a lucid manner to obtain one's spinal information in a fast, straightforward and non-invasive way. Upon the radiograph, Cobb angle is measured to characterized the severity of the curve (**Figure 1.2**). However, the virtue that X-ray imaging demonstrated has compromised the risks associated with radiation exposure. Patients receive an effective dose of approximately 140μSv per scanning in traditional scoliosis radiography (Chamberlain et al. 2000), which is equivalent to 8 years of natural background radiation for accumulated imaging episodes in treatment (Loughenbury et al. 2016).

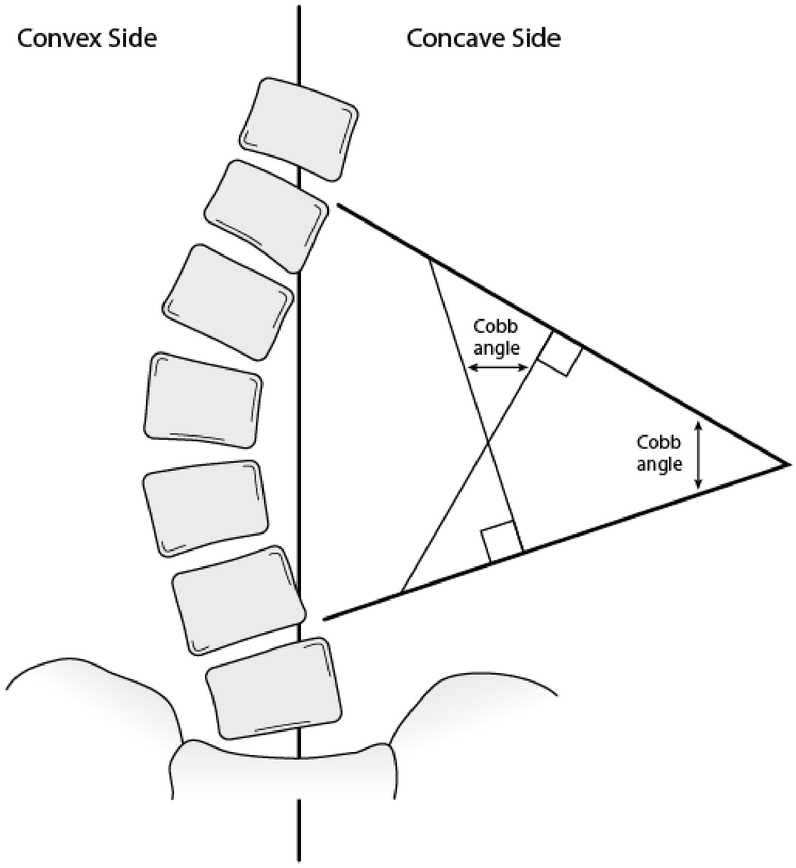

Figure 1.2 Illustration of Cobb angle measurement in X-ray (Altaf et al. 2013).

Human’s adolescence stage is a robust and ever-changing period; studies have demonstrated that teenagers are more sensitive to the radiation abuse (Bolling et al. 2007). X-ray radiation is taken as a high-risk factor for introducing tumor, non-programmed proliferation or organ/tissue malignancies. Himmetoglu et al. (2015) concluded from their research that scoliosis radiography could damage DNA and disturb the 8-OHdG level /SOD activity that promotes tumor development. Regarding that patient may need frequent scanning of spine to keep track with the possible AIS progression, the accumulated radiation absorption could not be simply neglected. Retrospective cohort studies showed that exposure to multiple scoliosis radiography during childhood and adolescence could increase the risk of the development of breast cancer (Hoffman et al. 1989, Doody et al. 2000). In addition, a longitudinal study revealed that AIS patients have a relative risk of 4.8 for developing cancer compared with normal population (Simony et al. 2016).

Efforts have been made to minimize times and region for spinal radiographs in order to achieve radiation reduction for decades (Levy et al. 1996). In addition, the low-dose stereoradiography (EOS) imaging system has been introduced as a technical breakthrough towards optimal radiation reduction in vertebral column visualization (**Figure 1.3**). This slot-scanning radiologic device largely limits the X-ray dose absorbed by the patient by 50%-85% compared with a standardized Digital Radiography or Computed Radiography system (Dubousset et al. 2014). Effective dose of a single micro-dose X-ray (2.6 μSv) in EOS imaging can be less than a day of background radiation, but sacrificing the image quality compared with standard operation (Hui et al. 2016). However, the bottleneck of EOS imaging system lays that it inevitably induces relatively small dose of radiation to the patient and his/her immediate environment. The sword of Damocles is still hung when frequent filming is required for evaluation purpose.

Figure 1.3 An image of the appearance of EOS system (left) and the bi-planar X-ray scanning images (right) (Image courtesy: The EOS Imaging System Website, 2019).

In fact, AIS is a three-dimensional deformity of spine (Weiss et al. 2008). The trend of evaluating AIS in the field is to visualize the patient's spine with an accurate 3D spine model. The EOS imaging system arouses many interests quite recently; its 3D reconstruction of the spine serves as grounds for series of publications in AIS pre-treatment assessment (Sekiya et al. 2018, Pasha et al. 2016). With the 3D modeling workstation (sterEOS) provided by the EOS, users could view the 3D spine model superimposed with EOS X-ray in coronal and sagittal plane, and a pseudo projection from the axial plane (as shown in **Figure 1.4**). However, as stated, EOS imaging system is not radiation-free, accumulated doses of ion radiation still could raise concerns in the planning of follow-up scanning schedules. In addition, the scanning range is limited, as the field-of-view of EOS is difficult for performing lateral bending, especially for performing maximum lateral bending.

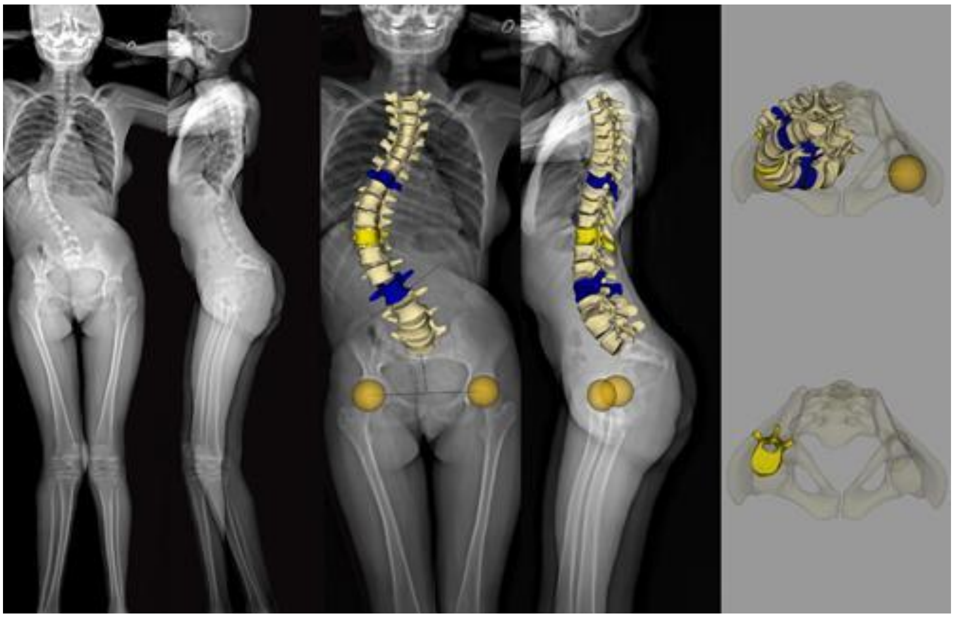

Figure 1.4 An example of EOS imaging system's 3D reconstruction of spine model with superimposing upon the original EOS X-ray films. Three views are provided for AIS assessment: coronal, sagittal and axial (from left to right). (Image courtesy: The EOS Imaging System Website, 2019)

1.2.2 Diagnosis of AIS with Ultrasound Imaging

When searching for radiation-free substitutes; unfortunately, few research has been conducted in the field of whole spinal cord reconstruction and visualization as that of EOS imaging (Solomon et al. 2016). Orthoscan device (e.g. Orthelius 800, Orthelius, Israel) provides a handy radiation-free method for scoliosis assessment in three planes (coronal, sagittal, apical) through electro-magnetic spatial sensing technique, but its effectiveness is hindered by the sampling rate and the primitive 3D reconstruction (in point-form) (Ovadia et al. 2006, **Figure 1.5**). A study also demonstrated that the Orthoscan failed the validity test of AIS evaluation against X-ray gold-standard XCA, and not yet ready to replace the standard radiography (Knott et al. 2005).

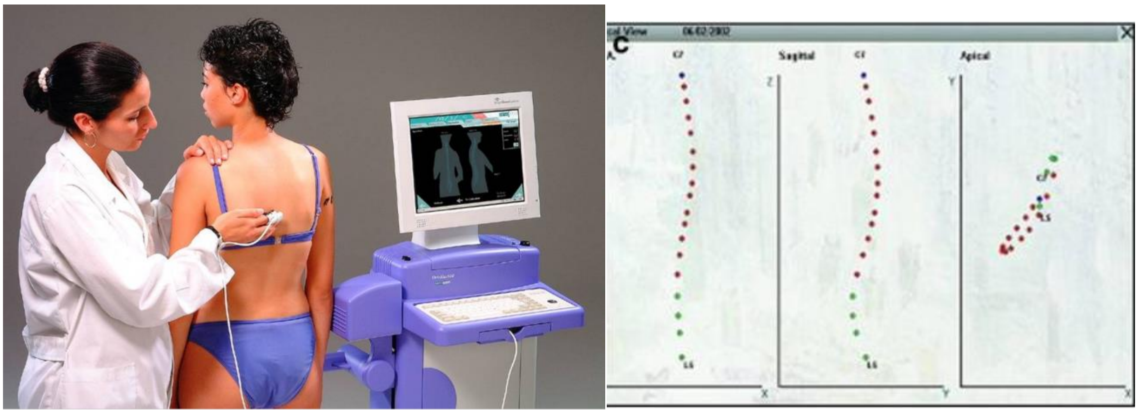

(a) **(b)**

Figure 1.5 (a) The Orthelius 800 imaging device; **(b)** Point-form 3D representation of spine model of Orthelius 800 (Image Courtesy: Ovadia et al. 2005).

In the exploration of other substitute methods to evaluate AIS in a radiation-free manner, ultrasound appeared to be an appropriate candidate. As the fundamental principle of medical ultrasound tells, it cannot penetrate hard surface or highly dense materials, especially the bone. However, from a different perspective, the artifacts (shadow) of the spine can be used to characterize the spinal curve (As shown in **Figure 1.6**). Such idea was first documented and patented by Zheng's group in 2009 (Zheng et al. 2009).

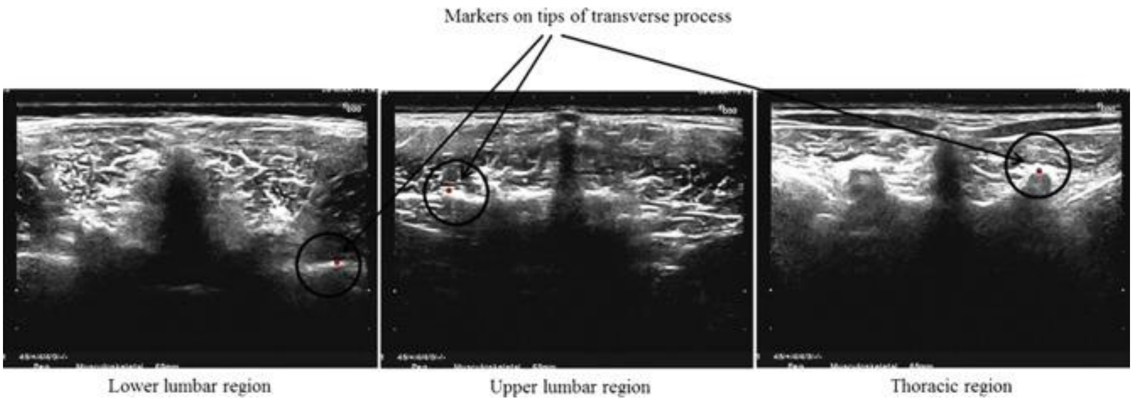

Figure 1.6 Examples of spinal landmarks identification for different regions of spine in 2D ultrasound imaging. (Image Courtesy: Zheng et al. 2009)

In the following years, the use of 3D ultrasound imaging system was frequently reported by other research teams. For instance, Lou's team utilized 3D ultrasound imaging for scoliosis assessment. They started from using ultrasound to visualize the spinal vertebrae in 2012 (Chen et al. 2012) and conducting validity of ultrasound coronal curvature measurement against X-ray film in 2015 (Young et al. 2015) and extending to characterizing spinal features in other planes through a pseudo 3D ultrasound imaging system (SonixTABLET ultrasound unit coupled with SonxiGPS and a C5-2/60 Convex transducer, Ultrasonix, Canada) in 2015 (Wang et al. 2016, as shown in **Figure 1.7**).

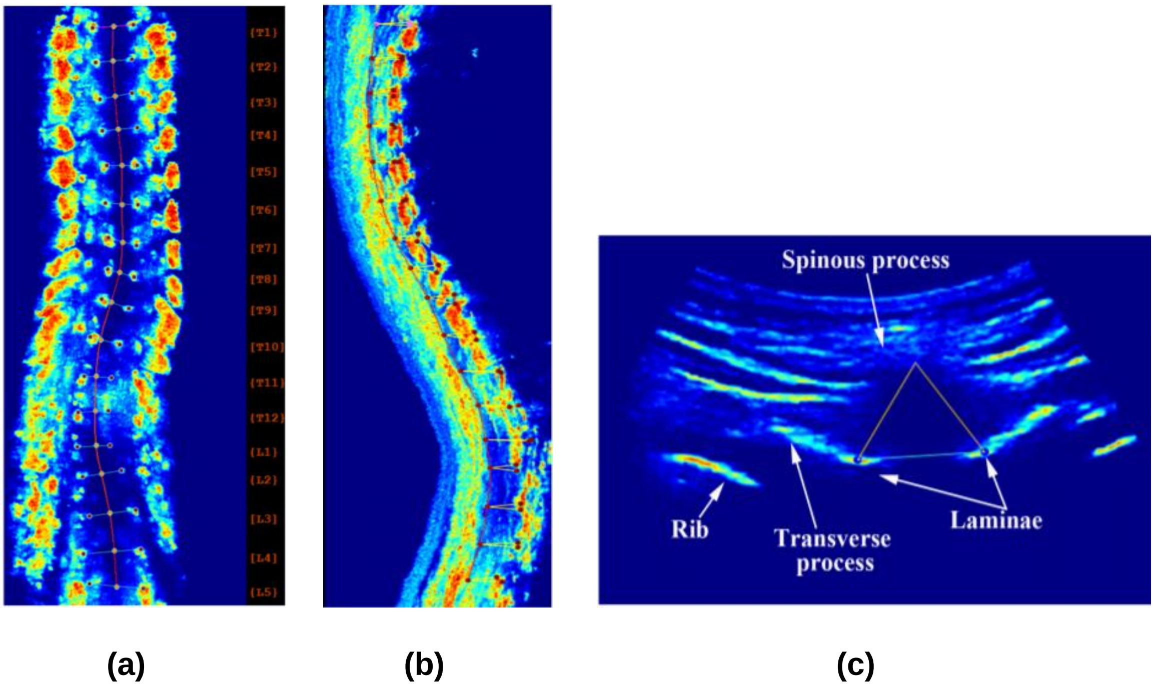

Figure 1.7 The illustrative ultrasound images of three planes from the pseudo 3D ultrasound imaging system by Lou's team. **(a)** Coronal plane; **(b)** Sagittal plane; **(c)** Transverse plane. (Image Courtesy: Wang et al. 2015)

The major limitations of Lou's 3D ultrasound imaging system lay that it required redundant manual input and labelling; the '3D' images were only available in three planes other than a fully 3D rendering of the spine model; and the identifications of spinal landmarks were subjective, side-by-side X-ray reference was preferred.

Scolioscan (Telefield Medical Imaging Ltd, Hong Kong, **Figure 1.8a*)*** has been developed throughout years, it could be regarded as EOS imaging system's radiation-free counterpart in whole volumetric spinal reconstruction (Cheung et al. 2015). In contrast to the traditional 3-D volume rendering approaches (Ungi et al. 2014), Scolioscan directly projects the raw 2-D B-mode ultrasound images to formulate the coronal images, known as volume projection imaging (VPI) method, **Figure 1.8b**, which had been published consecutively in previous years by Zheng's group (Cheung et al. 2015, Jiang et al. 2016, Zhou et al. 2017, Jiang et al. 2019).

(a)

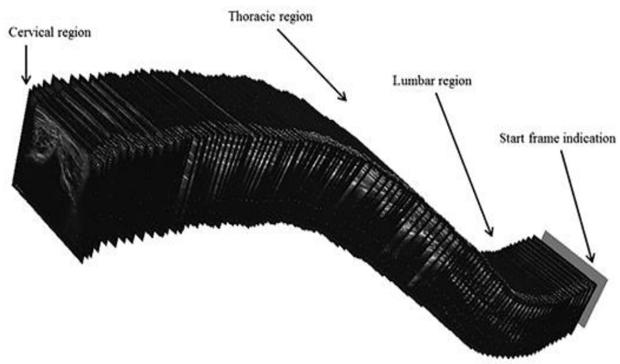

(b)

Figure 1.8 (a) Scolioscan (Model SCN801, Telefield Medical Imaging Ltd, Hong Kong); **(b)** Principle of the volume projection imaging (VPI) method. (Image Courtesy: Zhou et al. 2017)

VPI and the latter improved version fast 3D ultrasound projection imaging (FUPI) method (Jiang et al. 2016) significantly accelerated the visualization of the coronal plane of spine through by-passing the whole volume image reconstruction (Cheung et al. 2015). The spine curve in coronal plane projection, which is formed by the spinous process shadow, could be represented as a polynomial curve (**Figure 1.9**) for the intended scoliosis analysis (Cheung et al. 2015, Jiang et al. 2016, Zhou et al. 2017, Jiang et al. 2019).

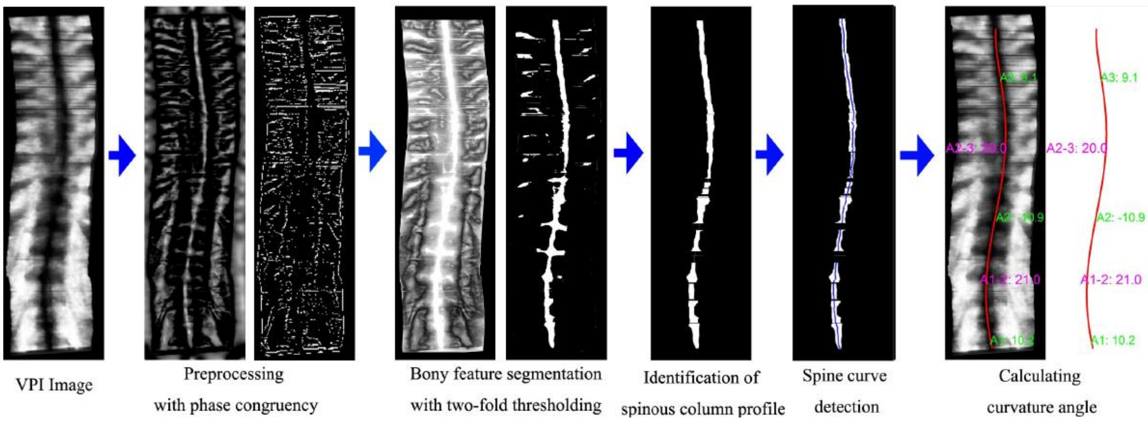

Figure 1.9 The block diagram of Scolioscan's spine curvature extraction and measurement algorithm. (Image Courtesy of Zhou et al. 2015)

Based on these advancements, Scolioscan's VPI technique could be used in coronal plane scoliosis classification and respective features measurement (Cheung et al. 2015, Zhou et al. 2017), which facilitates to evaluating scoliosis both qualitatively and quantitatively. Brink (2017) conducted a reliability and validity study of different coronal angles measurement of Scolioscan against X-ray; and the 3D ultrasound imaging technique had demonstrated satisfactory results (Brink et al. 2018).

Wong's group measured the spinal flexibility to assess the performance of the in-orthosis correction on AIS patients with the quantitative tools provided by the Scolioscan (He et al. 2017, **Figure 1.10**). Spine with a higher degree of flexibility could anticipate a better in-orthosis correction results, which may predict a long-term treatment effectiveness (Buchler et al. 2014).

Figure 1.10 Various posture for spinal flexibility assessment could be achieved by Scolioscan. **(a)** standing PA **(b)** supine **(c)** prone **(d)** sitting with lateral bending **(e)** prone with lateral bending. (Image Courtesy: He et al. 2017)

As for classifying AIS curve, spine morphology and flexibility remains the most important feature to tell structural from non-structural one (Millner et al. 1996, de Araujo et al. 2012). The promising results from the evaluating spine morphology and flexibility using Scolioscan suggest the possibility of using this 3D ultrasound imaging system for the AIS quantitative assessment and pertinent analysis.

1.3 Management for Mild AIS

AIS is divided into three stages, which depends on the severity of the curvature: mild, Cobb< 25°; moderate 25°<Cobb<45°; severe Cobb>45° (Matusik et al. 2020). Observation for AIS is the most common practice for mild AIS patients. Depending on the degree of skeletal maturity, patients are required for clinic assessment every 3-6 months for curve progression monitoring. The objective of bracing for AIS is to halt curve progression. The most widely accepted procedure for brace treatment is for moderate AIS in the most rapidly growing stage (Risser stage 0 or 1) (Altaf et al. 2013). About 10% of AIS will progress to severe AIS that requires consideration of surgery (Lonstein et al. 1984). Such recommendation is derived from studies demonstrated that curves >45° tend to progress slowly after maturity (Ramirez et al .1997).

The rationale for targeting at classifying mild AIS curves for our research are triple-folded: (1) the mild AIS patients could be recruited from large-scale post-screening programs; (2) the mild and skeletal immature AIS patients are perfect subjects to understand the AIS progression risk factors; (3) the mild AIS patients can be managed by non-surgical programs which are aligned with the trend of treating AIS non-invasively (Buchler et al. 2014).

A large population-based (394,401 schoolchildren) cohort study of AIS screening that ran over five years in Hong Kong reported that the prevalence of mild AIS curves were more than that of larger curves (Fong et al. 2015). The annual cohort of mild curve (Cobb<20°) had increased from 1% (F: 1.4%, M: 0.5%) to 2.5% (F: 3.1%, M: 2%) in contrast with larger curve from 1.3% (F: 2.1%, M: 0.5%) to 2.2% (F: 3.2%, M: 1%). (The number can be estimated from two prevalence map in **Figure 1.11**).

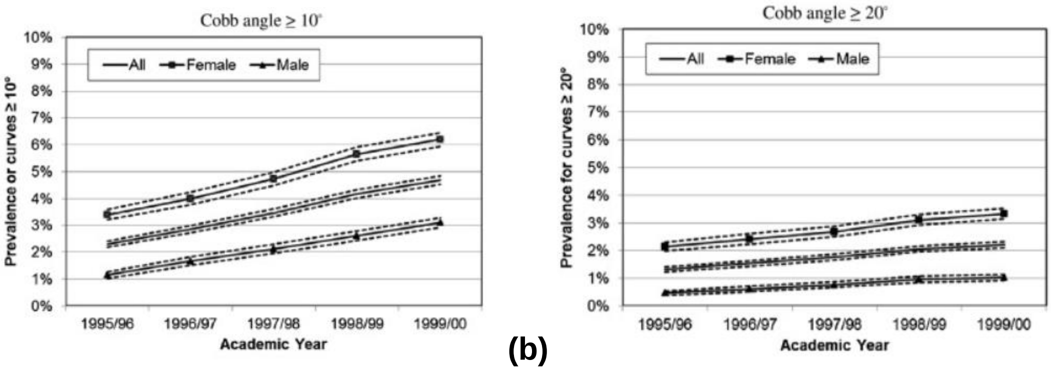

(a) **(b)**

Figure 1.11 Prevalence of patients of AIS with **(a)** Cobb >10° **(b)** Cobb>20°. (Image courtesy: Fong et al. 2015)

As implied by its name, 'AIS' is a kind of idiopathic disease, which means its cause had not been well identified. In order to understand the full 'life cycle' of AIS, studies have been conducted to investigate either the natural course or strategies from the bud stage – that is the mild AIS stage. The risk of progression can be up to 22%, and skyrockets to 68% once passing 20° (Bettany-Saltikov et al. 2015). Skalli's group expressed interest into exploring the progression risk of mild AIS. Drevelle et.al (2010) showed that a combination of several biomechanical parameters: gravity, decreased disc stiffness and anterior spinal growth could induce progress for spines with initial mild curvature. Courvoisier et.al (2013) attempted to study the progression risk of mild AIS from parameters derived from transverse plane: torsion index, apical vertebral rotation (AVR) and intervertebral axial rotation (IAR). In 2017, Skalli's team published deformation phenotype (as shown in **Figure 1.12**) for progression from various planes of assessment (Skalli et al. 2017).

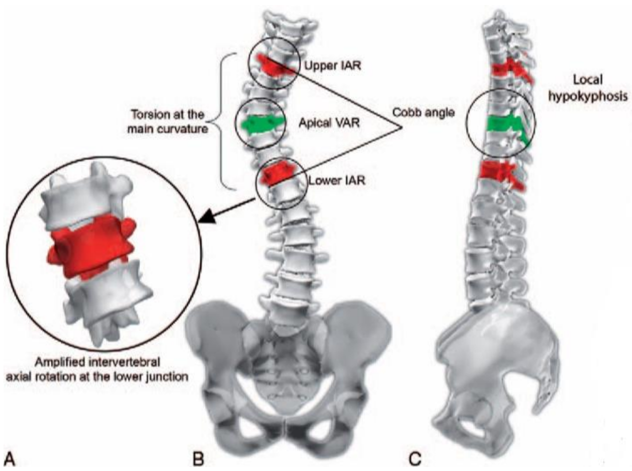

Figure 1.12 The deformation phenotype for progression. **(a)** amplified axial rotation **(b)** coronal view **(c)** sagittal view. (Image Courtesy: Skalli et.al 2017)

Conservative measures to manage non-severe AIS curves are: observation and bracing. Specifically, observation is the option for mild AIS until it progresses (Weinstein et al. 2008). However, the terrain of the mild AIS management is now changing. Other than the passive strategy: observation, several types of exercise programs had been designed to maintain or even alleviate the mild curve.

Schroth therapy is a 3D approach to elongate one’s trunk and correct imbalance of the spine by a subject-aware manner. Kuru et al. (2015) demonstrated that the effectiveness of Cobb reduction (-2.53°, p=0.003) and rotation angle reduction (-4.23°, p=0.000) could sustain at least 24th weeks after the Schroth program. Other auto-correction exercise programs also showed improvement in mild AIS management, including the SEAS program (Negrini et al. 2006), Side shift exercise (den Boer et al. 1999) and Dobomed program (Dobosiewicz et al. 2002).

General exercise could also help prevent mild curve worsening. One popular program is Pilates. Pil-Neo et al. (2016) compared the effectiveness of 12-month Schroth and Pilates exercise of scoliosis correction for mild AIS in paired study. Similar Cobb reduction had been reported: Schroth exercise group (-3.57°, $p<0.05$) and Pilates exercise group (-3.84°, $p<0.05$), respectively.

In light of the effectiveness of these mentioned exercise program for managing mild AIS curves, the classification scheme is necessary for the design or administration of the exercises. Before the commencement of the exercise program, therapists can refer to the classification scheme to prepare treatment for different spinal segments. Take the Schroth program as an example, information of curve type is needed for an effective outcome. As illustrated in **Figure 1.13**, the torso of the subject is divided into four blocks: shoulder, thoracic, lumbar and hip-pelvic. Auto-correction exercise would be customized to manage different types of curves. For a better prior knowledge of curve type in each block, the schroth exercise can achieve cost effectiveness.

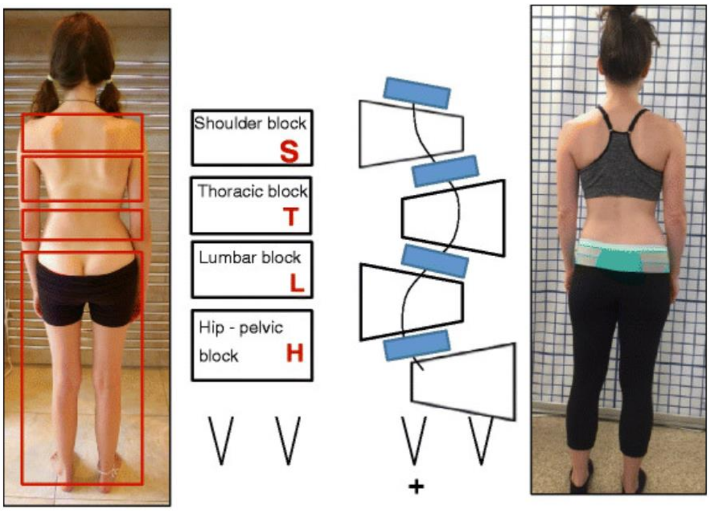

Figure 1.13 The 'body blocks' concept of Schroth program, where information is required to correct curves in the respective region of torso (Lebel et al. 2016).

Above all, for mild AIS treatment, other than observation, there are many exercise programs available to help correct the AIS and showed effectiveness.

1.4 AIS Classification Schemes

Anatomically, AIS curve can be categorized into either structural or non-structural (functional) depends on the skeletal morphology (spine flexibility), which requires distinct treatments. Non-structural scoliosis refers to a type of reversible bent of spine due to muscle spasm, pain or disease that could be corrected in lateral bending; while the structural one refers to a type of irreversible bent caused by congenital defects, infections or neurological-muscular diseases (Millner et al. 1996). As depicted in **Figure 1.14**, the curve that persisted its shape in lateral bending is marked as a structural curve; while the curve that had been corrected is a non-structural one. Some non-structural scoliosis could be levitated by exercise, a study showed that practicing Pilates lessens the degree of scoliosis (de Araujo et al. 2012). Structural scoliosis marks the chronic or permanent change of the normal vertebral column (Elsebaie et al. 2016); and surgery is effective to restore one's normal physical capacity (Millner et al. 1996). The effectiveness of the treatment was very much affected by the type of AIS curve, structural or non-structural. In order to classify structural and non-structural scoliotic curves for mild AIS cases, a clinical group from Prince of Wales Hospital (Hong Kong) extend the Scoliosis Research Society (SRS) standards for defining a scoliotic curve on X-ray imaging as a structural curve if both the upper and lower endplates of the curve have tilt angles > 5° (Upper Tilt Angle, UTA and Lower Tilt Angle, LTA) in practice (Korbel et al. 2014).

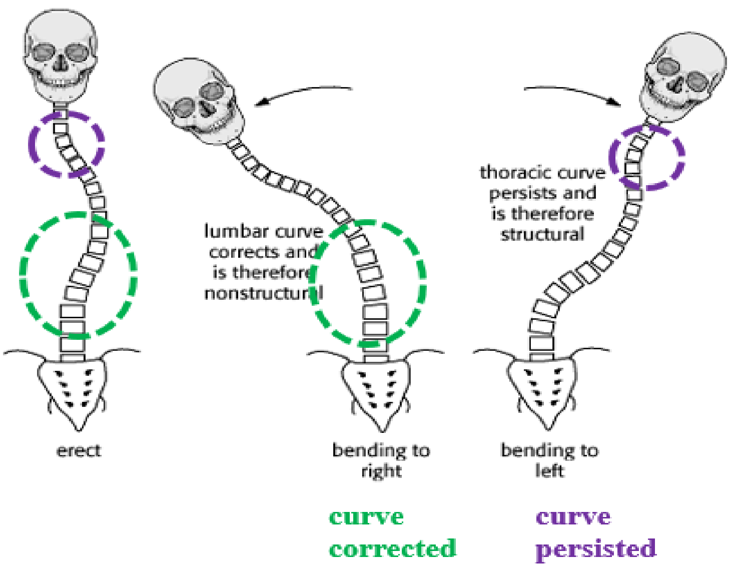

Figure 1.14 Illustration of the fundamental biomechanical difference of structural and non-structural curve [Image courtesy: UW Radiology, 2019].

The classical AIS schemes are primarily used for scoliosis surgery planning: surgeon coded the types of AIS curves based on their structural or non-structural in nature, location in the spine and major/minor curve; and treated the major one in the first-round of surgery and others in the follow-ups. In addition, a common classification scheme is important in evaluating operative approaches in the surgical decision-making process among multiple surgeons or even different surgical unit (Lenke et al. 2001). John Robert Cobb was the first to describe a classification system of scoliosis, and he was also the first to define major and minor curves, structural and non-structural curves, and put guidelines for these deformities treatment (Ovadia et al. 2013). However, this piece of pioneer work of classification did not contain much objective description and could not be communicated with other surgeons effectively.

In 1983, Howard King came up with the first generation of AIS classification system, nowadays known as 'the King Classification' (King et al. 1983). King developed the system based on his experience of Harrington rod instrumentation, which is a stainless steel rod that implanted to straighten the segment that is affected by scoliosis. AIS curves were categorized with specific guidelines given for instrumentation. King, for the first time, drew two critical definitions that are still applicable today: (1) Center Sacral Vertical Line (CSVL): an imaginary line that perpendicular to the sacrum level; (2) Spine lateral flexibility on side bending film help define structural or non-structural (compensatory) curve.

King categorized the AIS curves into five types (as shown in **Figure 1.15**). Of 405 subjects over 33-year period, 99% of the them could be classified according to the scheme.

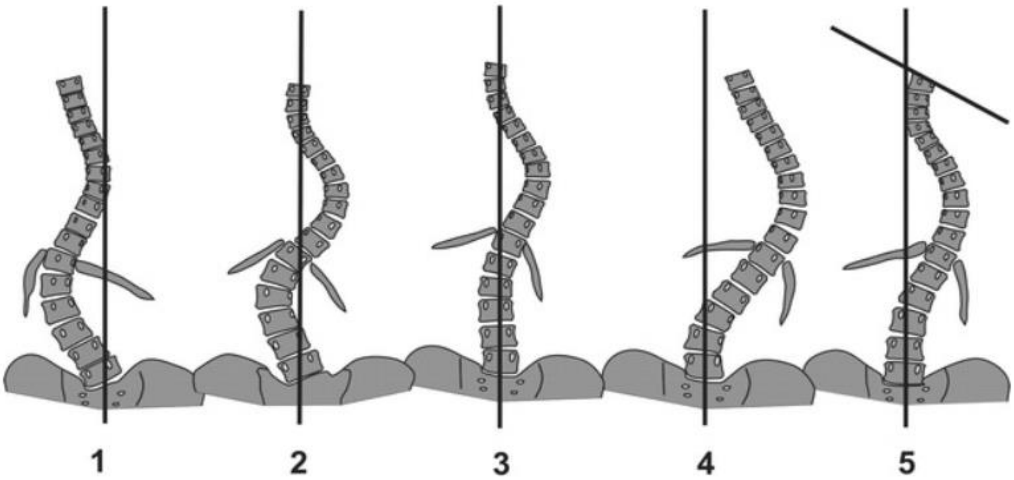

Figure 1.15 The illustrative example of the types of the King classification for AIS (Image Courtesy: King et al. 1983).

- **Type 1**: S-shaped curve in which both thoracic curve and lumbar curve cross CSVL, with the lumbar curve as the major curve and a negative flexibility index (thoracic curve is more flexible that lumbar curve);
- **Type 2**: S-shaped curve in which both thoracic curve and lumbar curve cross CSVL, with the thoracic curve as the major curve and a positive flexibility index (thoracic curve is less flexible that lumbar curve);
- **Type 3**: Major thoracic curve in which only the thoracic curve is structural and crosses the CSVL;
- **Type 4**: Long C-shaped curve in which the L5 is centered over the sacrum and the L4 is tilted into the thoracic curve;
- **Type 5**: Double thoracic curve with T1 tilted into convexity of upper curve.

Since descriptive in nature, peers always had problems to agree on the same type of the King classification result in clinical setting. The King classification has deficiency in communicate the types of AIS efficiently, surgeons are struggling classifying curves in a short period of time. Moreover, in the King classification, there are only five types of curves. The curves cannot be categorized would have to surrender to be sorted. Several articles showed low inter and intra-observer reliability of this system (Cummings et al. 1998, Behensky et al. 2002).

In 2001, Lenke, etc. developed a novel classification system to differentiate structural and nonstructural curves in the proximal thoracic, main thoracic, and thoracolumbar/lumbar region into six curve types (Lenke et al. 2001).

For a comprehensive assessment of the Lenke classification system, not only the curve type shall be identified, but also the lumbar modifier and, for the first time in any previous generation classification scheme, the sagittal profile was taken into consideration. And several related terms had been refined: (1) major curve: the largest curve is always structural (for surgical purpose); (2) minor curve: a smaller curve could be either structural or non-structural; (3) nonstructural curve: a curve which side-bends to less than 25°. The following table (**Figure 1.16**) includes all the Lenke parameters for coding AIS curves, with possible variants of 42.

The Lenke classification system for AIS

Curve type	Proximal Thoracic	Main Thoracic	Thoracolumbar/Lumbar	Description
1	Nonstructural	Structural*	Nonstructural	Main Thoracic
2	Structural×	Structural*	Nonstructural	Double Thoracic
3	Nonstructural	Structural*	Structural×	Double Major
4	Structural×	Structural§	Structural§	Triple Major
5	Nonstructural	Nonstructural	Structural*	Thoracolumbar/Lumbar (TL/L)
6	Nonstructural	Structural×	Structural*	Thoracolumbar/Lumbar-Main Thoracic (TL/L-MT)

***Major curve:** largest Cobb measurement, always structural; ×**Minor curve:** remaining structural curves; §**Type4 – MT or TL/L** can be the major curve

Structural Criteria (Minor curves)

Proximal Thoracic	• Side Bending Cobb ≥25° • T2-T5 Kyphosis ≥+20°
Main Thoracic	• Side Bending Cobb ≥25° • T10-L2 Kyphosis ≥+20°
Thoracolumbar/Lumbar	• Side Bending Cobb ≥25° • T10-L2 Kyphosis ≥+20°

Location of Apex (SRS Definition)

Curve	Apex
Thoracic	T2 to T11-12 Disc
Thoracolumbar	T12-L1
Lumbar	L1-2 Disc to L4

Modifiers

Lumbar Spine Modifier	Center Sacral Vertical Line to Lumbar Apex
A	Between pedicles
B	Touches apical body(ies)
C	Completely medial

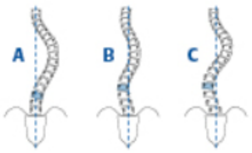

Thoracic Sagittal Profile T5-T12

Modifier	Cobb Angle
- (Hypo)	<10°
N (Normal)	10° – 40°
+ (Hyper)	>40°

Curve Type (1–6) + Lumbar Spine Modifier (A, B, C) + Thoracic Sagittal Modifier (–, N, +) = Curve Classification (e.g. 1B+):

Figure 1.16 The comprehensive Lenke classification system for AIS. (Image courtesy: AO Surgery Reference)

As presented clearly in **Figure 1.16**, there are six major curve types in the Lenke classification system:

- **Type 1**: main thoracic is the only structural curve while others are non-structural;
- **Type 2**: double thoracic in which the main thoracic is the major curve, the proximal thoracic is the minor structural curve and the thoracolumbar or lumbar curves are minor non-structural;
- **Type 3**: double major curve in which the main thoracic is the major curve, the thoracolumbar or lumbar is the minor structural curve and the proximal thoracic curves are minor non-structural;

- **Type 4**: triple major curve in which the main thoracic is the major curve, and all three curves are structural;
- **Type 5**: thoracolumbar/lumbar curve in which the thoracolumbar/lumbar is the only structural curve, with other curves being minor non-structural;
- **Type 6:** thoracolumbar/lumbar-main thoracic curve in which the thoracolumbar /lumbar is the structural curve and the main thoracic being minor structural.

Lenke's classification outperforms King's with a higher inter and intra-reliability (Ovadia et al. 2013). The classification scheme had been verified by the members of the Scoliosis Research Society, and became the popular formula in the research since then. Later classification schemes of AIS were more or less based on the Lenke: Thomas L et.al (2006) defined adult spinal deformity with Lenke as reference; Lin H et.al (2004) applied Lenke in 3D spine model; Phan P et.al (2013) used simplified Lenke in training neural network.

1.5 Overall Objective and Primary Contribution

The overall objective of this study is to investigate the validity and reliability of the measurement parameters originated from the 3D ultrasound imaging: Bending Asymmetry Index (BAI) which reflects the spinal morphology and flexibility of scoliosis from the asymmetrical pattern obtained from bilateral bending and be used for mild AIS classification purposes. Curve type (structural or non-structural) of each scoliotic curvature is determined by the magnitude of BAI value. BAI method is to classify mild

AIS curves for customizing curve-correction exercise design and evaluation, which was unavailable in the current clinical practice. With the AIS curve classification scheme, the efficacy of treatment outcome evaluation and the progression risk monitoring management can be improved in the due course.

The major achievements of this study can be summarized as follow:

1) Application of BAI method using vertebral body centroid from coronal X-ray image (**Figure 1.17a**):

- Vertebral body is one of the most distinct markers to characterize the trend of the spinal curvature;
- Scoliosis curve classification using BAI method computed from vertebral body centroid. This method has been validated on X-ray imaging, as vertebral body is impossible to be visualized on ultrasound imaging.

2) First BAI method derived from spinous process from ultrasound, BAIsp Method (**Figure 1.17b**):

- Application of the BAI concept on projected coronal ultrasound images for mild AIS curve classification, where the profile of spinous process shadow is used as landmark; the BAI value is ultimately evaluated to predict the structural/non-structural pattern of the scoliotic curve;
- AIS screening referrals with BAI and other pertinent ultrasound parameters, where the logistic regression help predict the referral status of individual AIS case.

3) BAI method using transverse process and related features from ultrasound, BAItp Method (**Figure 1.17c**):

- Semi-automatic scoliotic angle measurement using transverse features, where the angle measurement is compared with traditional X-ray Cobb angle measurement;
- Mild AIS curve classification using BAI method computed from transverse process and related features.

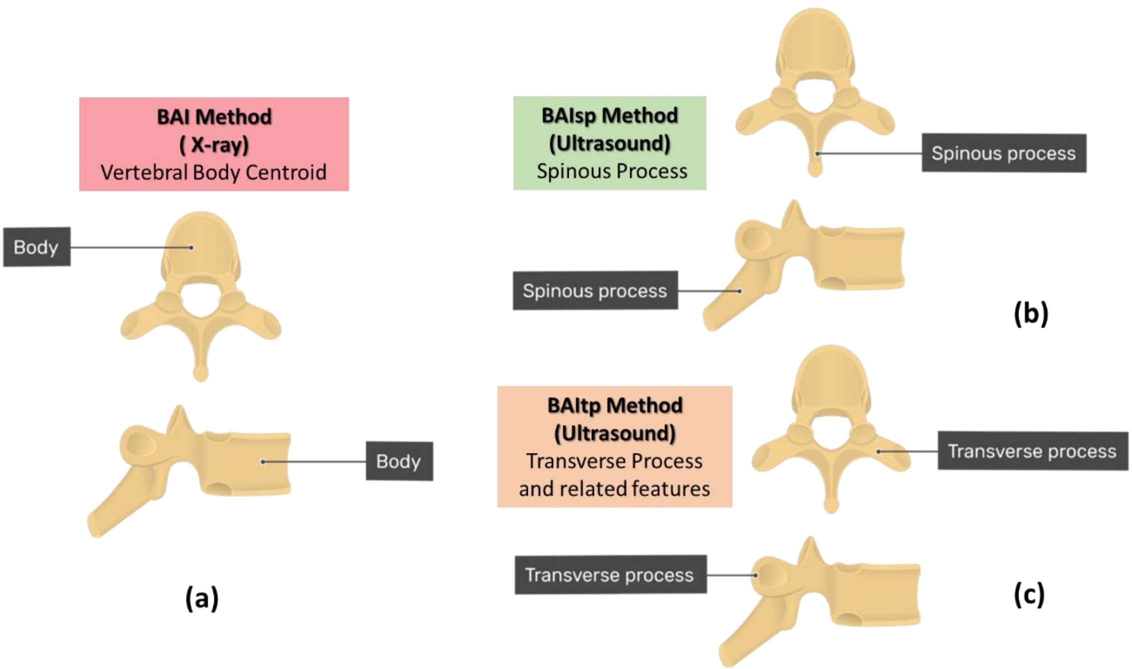

Figure 1.17 Different anatomical landmarks used for proposed bending asymmetry index (BAI) generation. **(a)** vertebral body centroid**;** **(b)** spinous process; **(c)** transverse process.

1.6 Thesis Outlines

This thesis is composed of six main chapters. Chapter 1 introduces the background of the relevant studies, motivation, objectives, primary contribution and overall structure of the thesis. Specifically, these studies serve as a comprehensive literature review, including etiology of AIS, diagnosis of AIS, clinical management for mild AIS and existing AIS classification schemes. No prior studies have demonstrated the use of mild AIS classification for curve-correction exercise design, treatment outcome evaluation and progression monitoring. Chapter 2 to Chapter 4 covers the essence of this thesis: spine morphology/flexibility characterization indicator: bending asymmetry index (BAI)-related studies developed from different spinal landmarks. In Chapter 2, the concept of BAI is firstly discussed and BAI method using vertebral body centroid is developed to observe the scoliosis curve classification performance. Since the vertebral body could not be visualized from acoustic signal, this part of validation study is conducted upon X-ray imaging. In Chapter 3, two studies related to the application of the first BAI concept that originated from ultrasound spinous process (BAIsp method) are included: the first BAI for mild AIS curve classification; BAI accompanies other ultrasound parameters to estimate AIS screening referral decisions. In Chapter 4, two studies related to the use of the BAI method derived from ultrasound transverse process (BAItp method) are involved: the transverse process inspired semi-automatic ultrasound curvature angle (UCA) measurement and mild AIS curve classification based on this variant of BAI method, are elaborated respectively. Finally, in Chapter 5, conclusion from the studies is drawn and recommendations for the future directions of this thesis are provided and elaborated.

1.7 Summary

This introduction chapter gives a review of the etiology, diagnosis, mild clinical management and classification for AIS patients. The cause of AIS has not been clearly identified. Conventional quantitative diagnosis of AIS includes X-ray scans with designated intervals. 3D ultrasound imaging rises as a promising substitute in the AIS assessment, without compromise of unnecessary radiation exposure. Observation is the most common measure for most mild AIS patients; and curve-correction exercise programs are effective supplements. The design of these exercise programs, treatment outcome evaluation and progression management require systematic classification scheme for mild AIS, which was yet to be coded. With the reference of the pre-surgery AIS classification schemes, a new system concerning the curve classification for mild AIS should be proposed to fill the gap. This leads to the overall objective of this study, which is to investigate the validity and reliability of the measurement parameters derived from the 3D ultrasound imaging: Bending Asymmetry Index (BAI) which reflects the spinal morphology and flexibility of scoliosis from the asymmetrical pattern obtained from bilateral bending and be used for mild AIS classification purposes.

CHAPTER 2. AIS CLASSIFICATION USING BENDING ASYMMETRY INDEX (BAI) METHOD

2.1 'BAI' Concept and Its Implications

Scoliotic curves could always be categorized into either structural non-structural/ functional depending on the spine morphology, or spine flexibility. Non-structural scoliotic curve refers to reversible bent of spine due to muscle spasm, muscle pain or subcutaneous disease, and could be greatly reduced or corrected in anti-directionally side-way bending. Structural scoliotic curve refers to irreversible bent of spine because of congenital defects, spinal infections or chronic neurological-muscular complications (Millner et al. 1996). As a re-illustration (**Figure 2.1**) from the **Chapter 1 *(*Figure 1.14)**, the curve that persisted its shape in counter-curve-direction lateral bending is taken as a structural curve; while the curve that could be restored to its normal balance posture is regarded as a non-structural curve.

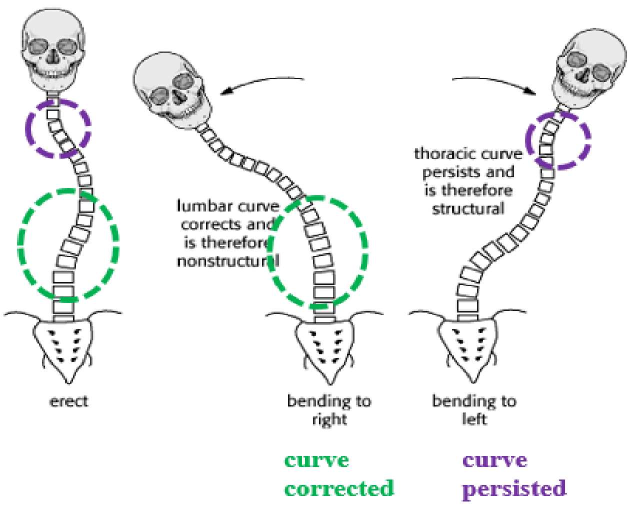

Figure 2.1 Illustration of the biomechanics of different types of scoliotic curves. (Image courtesy: UW Radiology, 2019).

The clinical significance of scoliotic curve classification lies that different curve type requires different clinical management and medical strategies (Majdouline et al. 2007, Weiss et al. 2008, Jada et al. 2017). Depends on the severity or curve morphology, some non-structural scoliosis cases could be levitated by various curve-correction exercise program (Bettany-Saltikov et al. 2015, Romano et al. 2015). Studies also indicated that practicing Pilates reduced the degree of scoliotic angle (de Araugo et al. 2012, Seo et al. 2014). Bracing is frequently applied as a nonoperative scoliosis rectification tool for non-structural AIS patients (Richard et al. 2005, Heary et al. 2008, Julien et al. 2010). Structural scoliosis causes the chronic or permanent change in shape of the normal vertebral column in morphology (Millner et al. 1996); and surgery is commonly practiced to restore one’s normal physical capacity (Elsebaie et al. 2016). Therefore, to understand the nature of respective curve types is crucial to formulate customized treatment strategies, which could benefit the ultimate patient experience. With a blend of structural and non-structural curves on the same individual, the structural one(s) is/are always the primary target for rectification planning (Jada et al. 2017).

The inspiration of developing the Bending Asymmetry Index (BAI) method came from the distinct bilateral bending pattern of structural and non-structure curve. Specifically, as nonstructural curve can be compensated and restored in lateral bending, its left and right bending spinal profiles are most likely symmetrical. On the contrary, structural curve persisted in lateral bending, its left and right bending spinal profiles are asymmetrical in the scoliotic curvature segments. The symmetrical/asymmetrical pattern is more obvious in mild AIS population.

2.2 BAI Method Using Vertebral Body Centroid

The vertebral body is the most straightforward anatomical structure to characterize the scoliosis and spinal curvature. The vertebral body is an anterior anatomical structure from sagittal plane. For invasive ultrasound imaging, the vertebral body could not be visualized from posterior-anterior (PA) scanning, as the posterior spine structures (spinous process, transverse process, lamina etc.) block the acoustic waves (Cheung et al. 2015, Zheng et al. 2016, Zhou et al. 2017); it could neither be seen from anterior-posterior (AP) scanning, as internal organs (lung, stomach, intestine etc.) refract and diffuse the waves (Baka et al. 2017).

In vitro studies reconstruction of the vertebral body through ultrasound imaging has been achieved (Chen et al. 2012, Nguyen et al. 2015); however, the respective implications to clinical practice or scoliosis screening program were very limited. For in vivo studies, vertebral body could be acoustically identified on fetal (Johnson et al.1997, Dyson et al. 2000, Pooh et al. 2005) or new born (Glasier et al. 1990, Lowe et al. 2007, Torres et al. 2014). However, no prior studies had shown similar ultrasonic spine imaging on young adults or adults. The ossification of spine increases the vertebral density, which could not be penetrated by ultrasound anymore (Torres et al. 2014).

In the following section, we would like to explore the anterior surface of the vertebra: the vertebral body itself, to observe whether the BAI method could report promising results. However, the anterior structures of vertebra are difficult to be observed from ultrasound imaging. The anterior fronts of the thoracic and lumbar spine are blocked by various internal organs and fat, which diffuse ultrasound acoustic signal (Wang et al. 2015). With such insights, the BAI method derived from vertebral body would be assessed on bi-lateral bending X-ray imaging. Moreover, the scoliosis subjects involved were pre-surgery cases, as it would be ethically inappropriate to conduct multiple X-ray scanning for mild AIS.

2.2.1 Subjects and data acquisition

This pilot study retrospectively included 30 pre-surgery scoliosis subjects (9 males and 21 females; Cobb: 50.9 ± 19.7°, range 18°-115°), with ethical approvals from the Chinese University of Hong Kong (CREC Ref.No. 2015.463). Each subject underwent X-ray scanning supine on a plain mattress. Specifically, three postures were adopted for the scanning process: Anterior-posterior (AP) supine, bilaterally left and right bending (**Figure 2.2**). The patients were advised to stretch their bodies fully to perform maximum bending on each side; the posture of lower limbs and the pelvis level inclination angles were not constrained by any supporting mechanism (Jalalian et al. 2017).

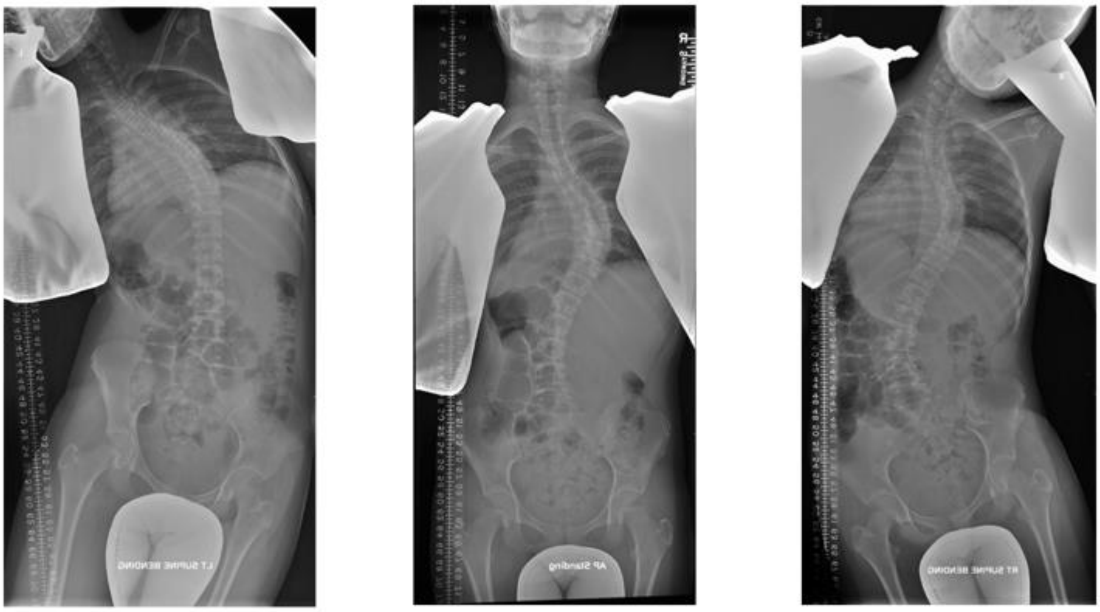

(a) (b) (c)

Figure 2.2 Examples of supine X-ray scanning from a real patient of three postures: **(a)** bending to left; **(b)** AP supine; **(c)** bending to right from posterior-anterior (PA) radiographing.

2.2.2 X-ray BAI method on scoliosis curve classification

The process of X-ray-derived BAI generation is semi-automatic where two major stages are involved: 1) manual annotation and pelvis level inclination adjustment; 2) automatic BAI value generation. BAI method was conducted in semi-automatic manner, as expertise input is important in ultrasound image interpretation. The detailed block diagram is provided in **Figure 2.3**, which shows the respective manual elements (in green color), the automatic procedures (in blue color), the composition of outputs (in brown color) and validation (in purple color)**.**

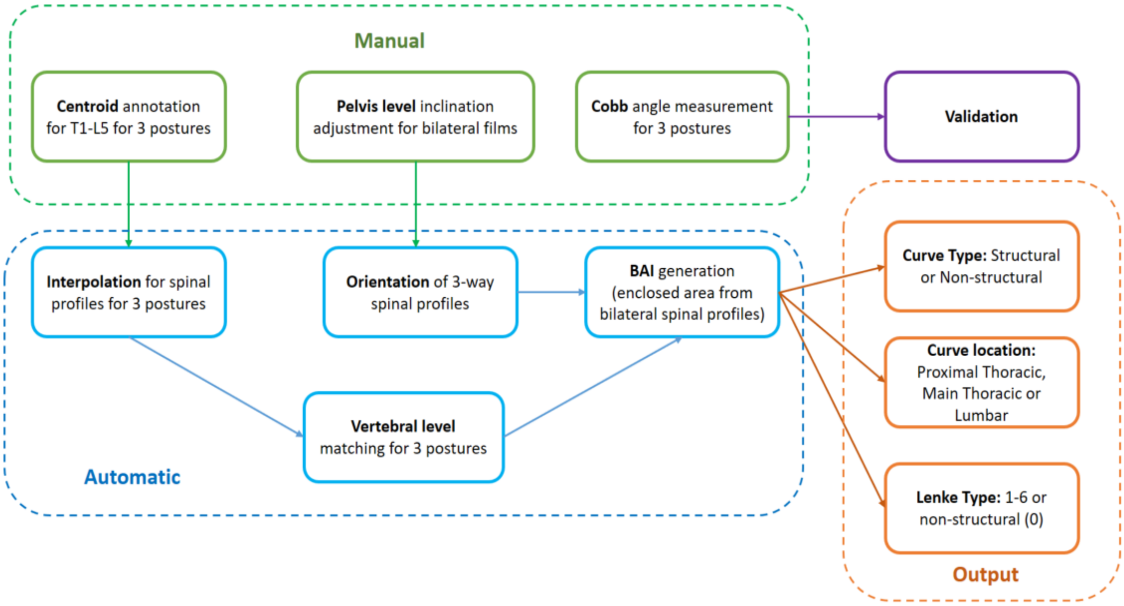

Figure 2.3 Block diagram of the proposed semi-automatic X-ray-based BAI scoliosis curve classification system. The color code for the above diagram is: manual procedure (in green color), automatic processing (in blue color); output components (in brown color) and validation (in purple color).

2.2.2.1 Manual annotation and pelvis level inclination adjustment

In order to characterize the spinal curve on the radiographs, the centroids of each vertebral body from level T1 to L5 (which covers the entire thoracic and lumbar segments of the spine, normally total 17 vertebrae) was annotated manually by an experienced (>2 years) operator (as shown in **Figure 2.4**).

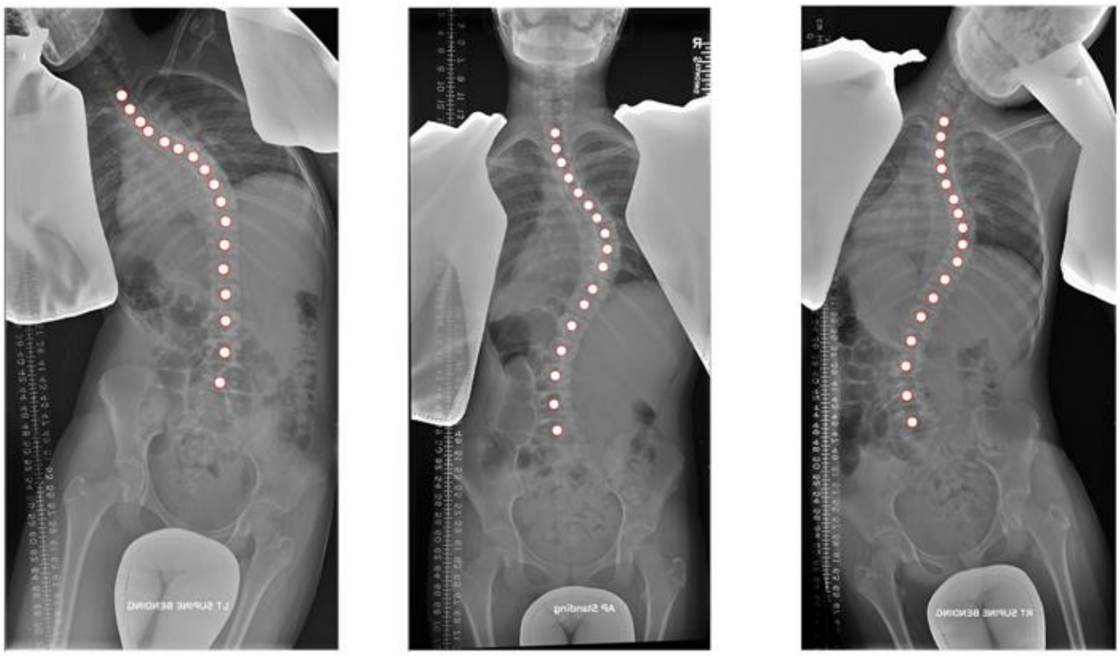

(a) (b) (c)

Figure 2.4 Examples of manual vertebral body centroid annotation from the same subject of three postures: **(a)** bending to left; **(b)** erect (supine front); **(c)** bending to right from posterior-anterior radiographing. The annotation has been conducted from T1 to L5, total 17 vertebrae.

Such process was required for three postures (anterior-posterior (AP) supine and bilateral side-way bending supine) upon X-ray images. The manual annotation was simultaneously saved in the forms of 2D Cartesian coordinates (origin of the coordinate system was set of the top-left corner of the X-ray) with respect to the intended X-ray image. Since the scoliosis patients were scanned in supine position, the lower limbs displaced in side-way bending, which caused the shift of the orientation of the spine with respect to the pelvis among three scans. Manual adjustment of the pelvis level in side-way bending X-ray against the AP supine posture was necessary for an accurate BAI calculation. The operator's manual input included lining up the tips of iliac crest of three postures (AP supine, bending to left and right, **Figure 2.5**) by orientation the three posture x-ray images.

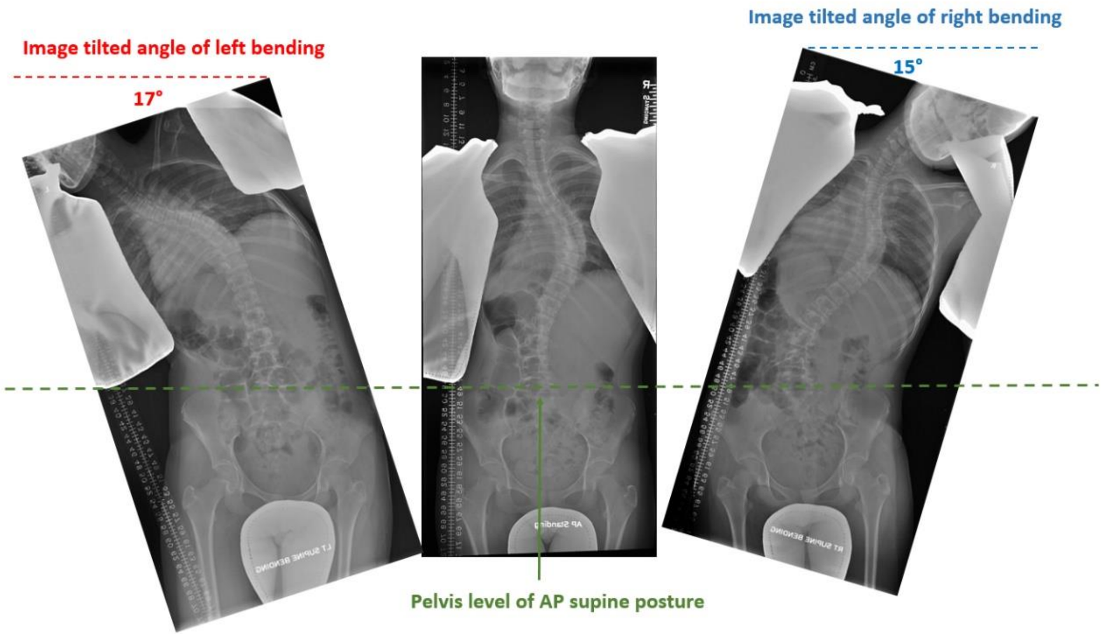

Figure 2.5 Illustration of the principle of pelvis level inclination adjustment. The lateral bending films were tilted to align with the pelvis level indicated by the AP supine front posture.

2.2.2.2 Automatic BAI value generation

After the manual annotation for each vertebral body centroid and bilateral iliac crest of pelvis, the subsequent processes were automatically executed. The coordinates from **Section 2.2.2.1** were passed to the software for spine line interpolation using Matlab spline function (**Figure 2.6a- Figure 2.6c**).

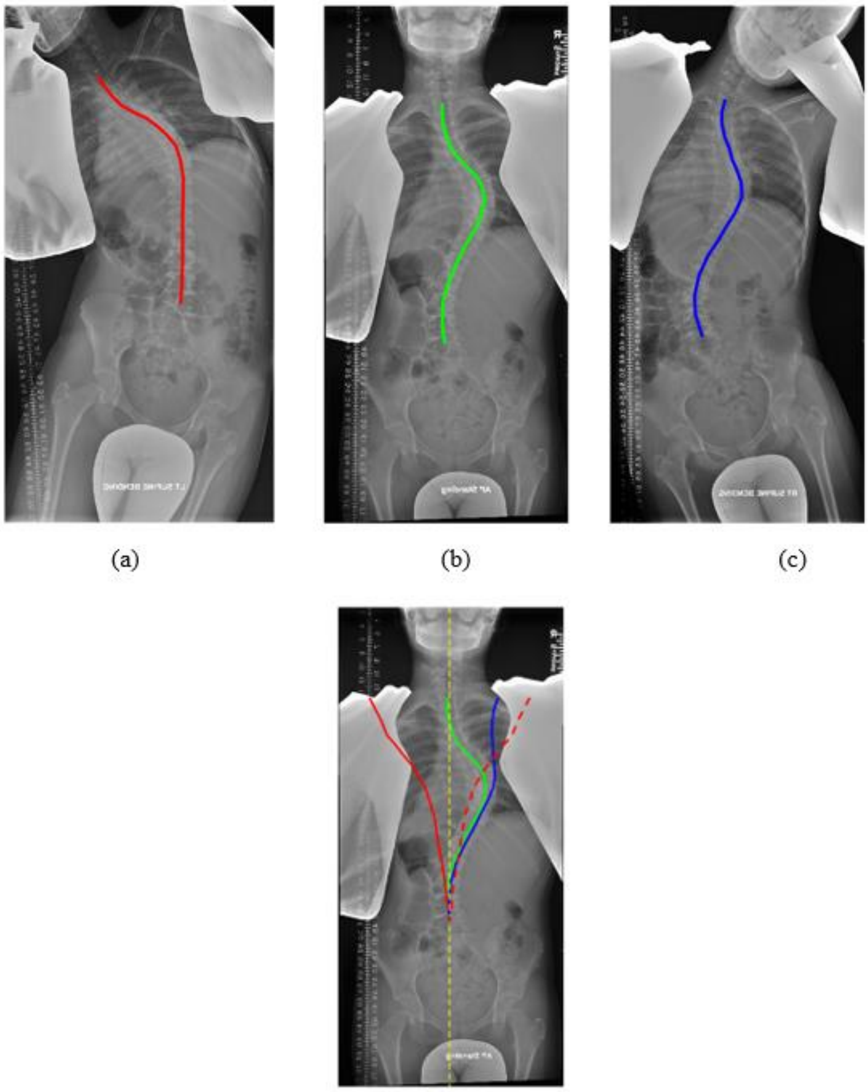

(a) (b) (c)

(d)

Figure 2.6 Examples of automatic interpolation of spinal profiles from the coordinates of the centroids annotated from **Figure 2.4**. The spinal profiles were color-coded as **(a)** bending to left (red color); **(b)** AP supine front (green color); **(c)** bending to right (blue color) from posterior-anterior radiographing. **(a)** and **(c)** were scaled and oriented by the pelvis inclination angle; **(d)** Spinal profiles from **(a)-(c)** were joined at the junction of L5 vertebral body centroid of AP supine film.

The spine profiles from the side-way bending films were them relocated to the AP supine radiograph at the junction of L5 level, with the adjustment of pelvis level inclination of bending profiles (in terms of angle). Then the bilateral bending curves were scaled with respect to individual vertebral level of the AP supine profile to ensure the vertebral matching across different postures (**Figure 2.6d**).

According to the principle of BAI calculation, the left bending spine profile (solid red-color indicated in **Figure 2.7**) was mirrored against the normal passing through the center of L5 vertebra; the intersected area between the mirrored left bending curve (as dotted red-color curve in **Figure 2.7**) and the right bending curve (blue-color indicated in **Figure 2.7**) constituted BAI value(s), denoted in pixel. Each enclosed area represents the apex and upper/lower endplates of a scoliotic curve, where the bilateral symmetrical pattern was deviated. In order to have a fair comparison among the curves in different postures, BAI value was normalized to the length of its respective length of the spinal segment of the curvature before analysis. The threshold of structural/non-structural curves has been intrinsically determined by the clustering of the provided dataset; it might fluctuate with the collected sample. If the self-developed boundary could demonstrate its distinction power among a wide range of severity of scoliosis patients, it could be empirically validated.

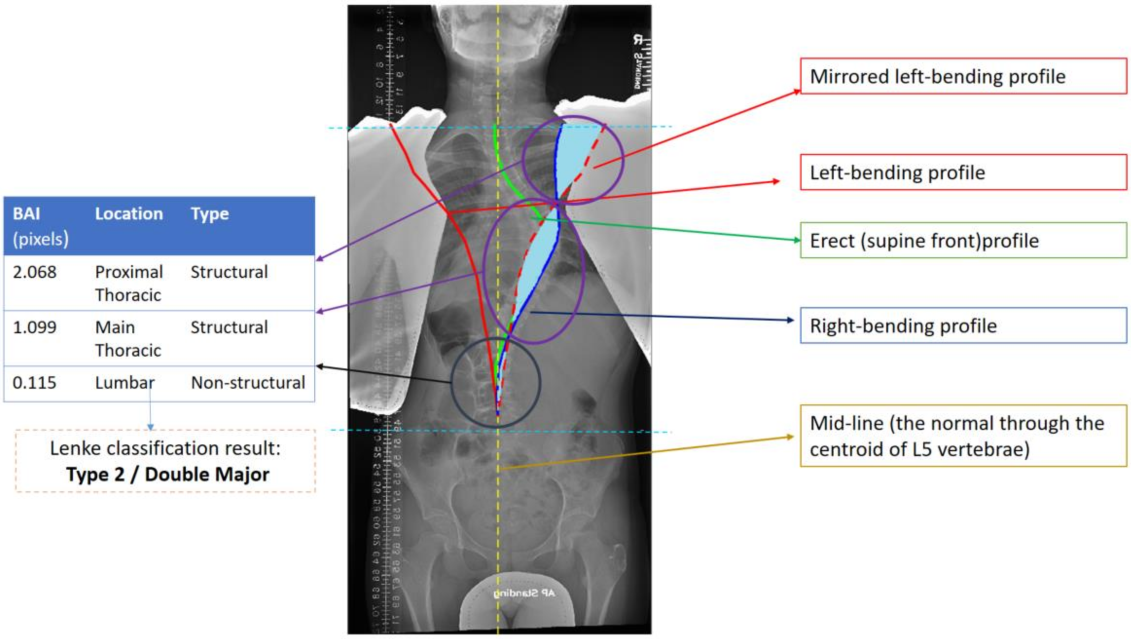

Figure 2.7 An example of the semi-automatic BAI classification result. BAI values were generated by the enclosed area from mirrored left-bending profile (in dotted red color) and right-bending profile (in blue color). Three BAI values were calculated, with 2.068 in proximal thoracic as structural curve; 1.099 in main thoracic as structural curve; and 0.115 in lumbar region as non-structural curve. Lenke classification could be retrieved as Type 2 or 'Double Major' scoliosis.

According to the harvested BAI value(s) of each patient, we could resort to the Lenke classification scheme to sort into different Lenke types of scoliosis (**Figure 2.8**, Lenke et al. 2003). In case of the presence of multiple structural BAI values, the larger BAI value indicates the major curve. The output components of the system include: 1) curve type, which indicates whether the curve is structural or non-structural depending on BAI value; 2) curve location, which classifies whether the curve is proximal-thoracic, main thoracic or thoraco-lumbar/lumbar by the given BAI apex; 3) Lenke type, 1-6 or non-structural (0), which is automatically generated by the results of ***Stage 1*** *and* ***2***.

Curve Type	PT	MT	TL/L	Description
1	NS	S*	NS	Main Thoracic (MT)
2	S	S*	NS	Double Thoracic (DT)
3	NS	S*	S	Double Major (DM)
4	S	S*	S*	Triple Major (TM)
5	NS	NS	S*	Thoracolumbar/lumbar (TL/L)
6	NS	S	S*	Thoracolumbar/Lumbar- MT (TL/L – MT)

Curve Types 1–6 are depicted by the regional structural characterizes of the proximal thoracic (PT), main thoracic (MT), and thoracolumbar/lumbar (TL/L).

Figure 2.8 Description of different curve types (Type 1-6) from the canonic Lenke classification. (Figure is reproduced from Lenke LG et al. 2003, Fig.3.)

On the other hand, an experienced operator was responsible for manually measuring Cobb angles of all curves from the set of three-posture X-ray films. Similarly, the resultant Cobb angles were used to compute the respective Lenke types of scoliosis. The results were used for validating the classification performance of using BAI method. The Cobb angle reduced from the contrary side-bending curve was to compare with 25° for structural or non-structural (Bekki et al. 2018). For example, Cobb angle from the left-bending image was used to judge the type of a dextroscoliotic curve. For the purpose of clarification and ease of explanation, the angle measured during side-bending Cobb was denoted as ‘S- Cobb’ in the following text (**Figure 2.9**).

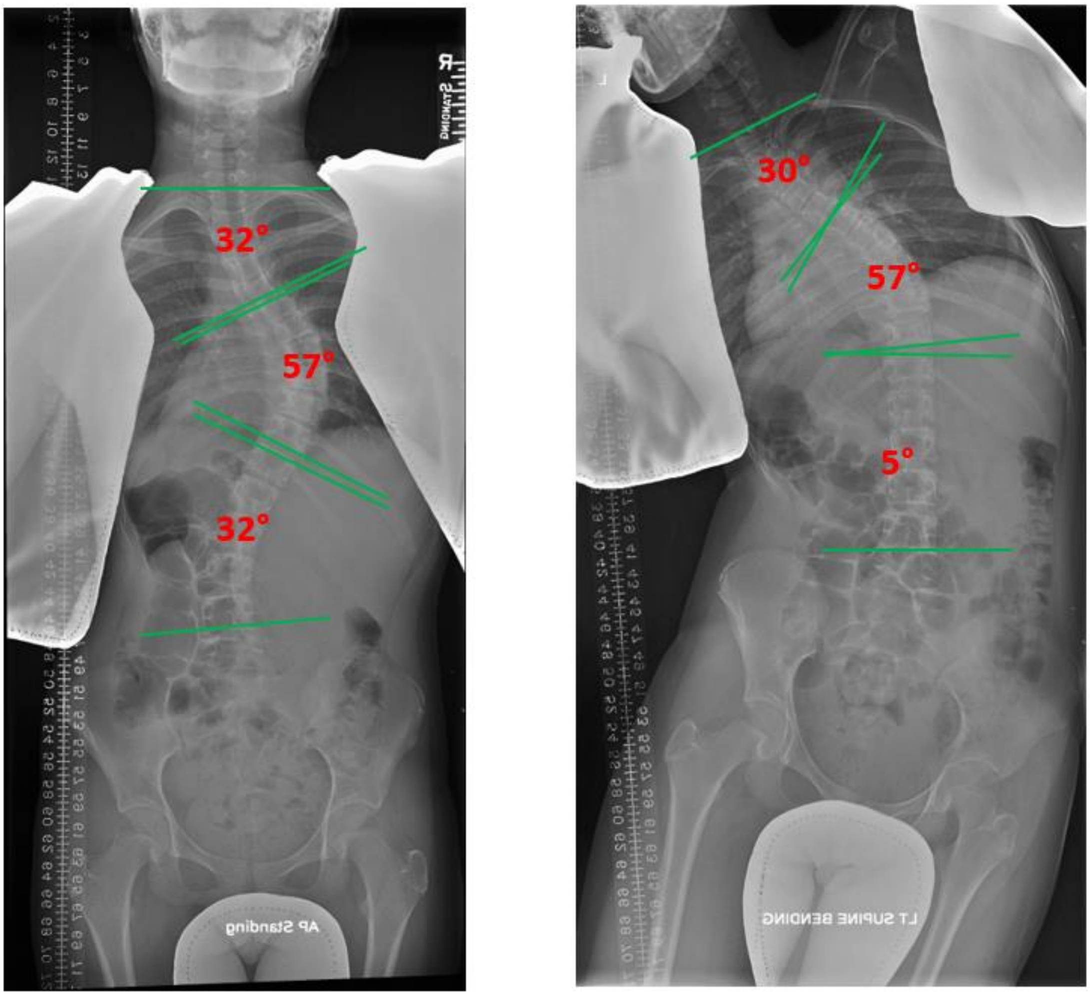

(a) (b)

Figure 2.9 Illustration of side-bending Cobb, denoted as ‘S-Cobb’. **(a)** Anterior-posterior (AP) supine X-ray film shows three angles: proximal thoracic 32°, main thoracic 57° and lumbar 32°; **(b)** With subject performed left bending, leftward curves are reduced in magnitude, which indicated the flexibility of the spine itself. In this example, the side-bending Cobb (S-Cobb) angles are proximal thoracic 30° and lumbar 5°.

2.2.3 Statistical analysis

Statistical analyses were conducted using SPSS 25.0 for Mac (SPSS Inc., Chicago IL, USA). The areas which characterized the type of the scoliotic curves by the proposed BAI method was compared with side-bending Cobb measurements using linear correlation. Linear regression equations with intersections were investigated for this study. Usually, a correlation efficient 0.25 to 0.50 indicates a poor correlation; 0.50 to 0.75 indicates moderate/good correlation; and 0.75-1.00 indicates very good/excellent correlation (Dawson et al. 2004). In addition, a confusion matrix was compiled to examine the precision and specificity of the clusters of structural and non-structural curves (curve-based analysis). False positive and false negative cases were also involved for further investigation. Similarly, another confusion matrix with the above statistical parameters was studied for the Lenke classification of the individual cases (case-based analysis).

2.2.4 Results

82 curves from 30 pre-surgery scoliosis patients were included for the study, with 54/82 (65.9%) structural curves and 28/82 (34.1%) non-structural curves. Very good to excellent correlation was found between the manual S-Cobb angle measurement and the bending discrepancies measured by the semi-automatic X-ray-based BAI method (**Figure 2.10**). Correlation coefficient was $r=0.855 (p<0.05)$ or determination coefficient (R squared) $R^2=0.730$ ($p<0.05$) for all tested curves.

id

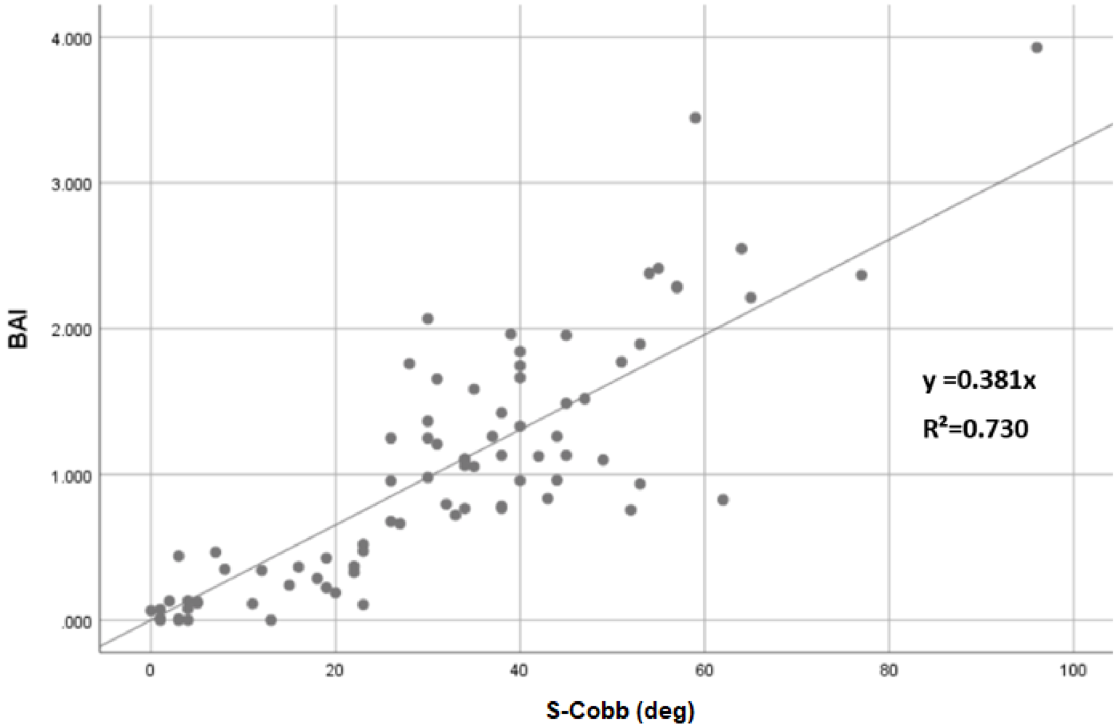

Figure 2.10 Correlation and linear equations between manual measured S-Cobb (x) and the proposed X-ray-based BAI value (y).

The distribution of the clusters of structural curves and non-structural curves could be visualized from **Figure 2.11**. It can be observed that two clusters presented clearly-cut boundaries at around BAI=0.600, which equivalent to S-Cobb=25°. In other words, structural curves and non-structural curves could be conveniently distinguished by the BAI method using vertebral body centroid information for pre-surgery cases.

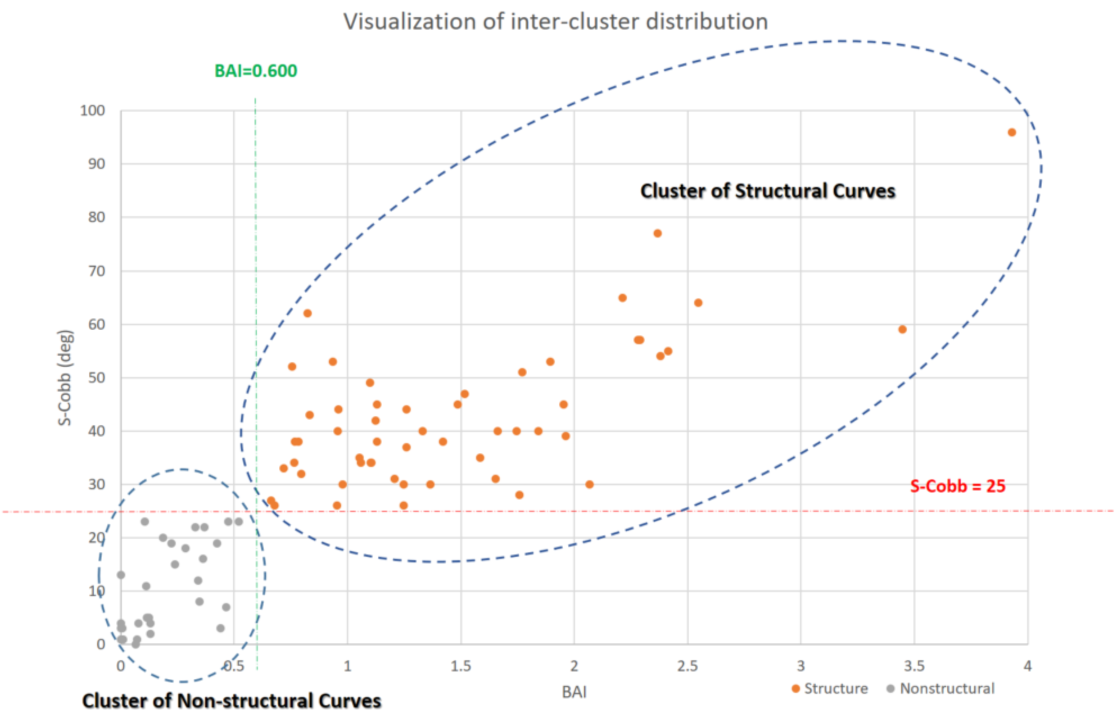

Figure 2.11 Visualization of the inter-cluster distribution. Cluster of Non-structural curves and the cluster of Structural curves have clear-cut boundaries, which indicates that BAI is a powerful discriminator for determining scoliotic curve type. S-Cobb = 25° is the current clinical standard for the curve type while our proposed BAI=0.600 possesses the similar classification power for the intended purpose.

The confusion matrix demonstrated similar finding with no false positive (FP) nor false negative (FN), where all scoliotic curves have been correctly classified (**Table 2.1)**. All structure curves and non-structural curves have been correctly identified by the BAI method using vertebral controids. The nature of such repelling clustering suggested the feasibility of using BAI as a semi-automatic supplementary tool to the S-Cobb manual measurement in clinic.

Table 2.1 Curve-based analysis. The confusion matrix showed the classification results of curve type using BAI method (vertebral body centroid) against the traditional S-Cobb measurement. The threshold of BAI that distinguished structural and non-structural curves was set at 0.600. No false positive or false negative was found.

		Curve Type (Side-bending Cobb)			
		Non-structural	**Structural**	Total	Precision
Curve Type (BAI)	**Non-structural**	28	0	28	1
	Structural	0	54	54	1
	Total	28	54	82	
	Specificity	1	1		

When coding into Lenke classification scheme, the numbers of the Lenke type 1, 2, 3, 4, 5, 6 and nonstructural (marked as '0' in the related description) patients were 6, 15, 2, 3, 1, 2, 1, respectively. Another confusion matrix on case-based analysis with multiple parameters was displayed in ***Table 2.2***, the BAI classification results of the Lenke type 1, 2, 3, 4, 5, 6 and nonstructural were 7, 14, 2, 3, 1, 2, 1, respectively. Out of 30 scoliosis patients, 1 case of Lenke type 2 was misclassified into Lenke type 1; with the rest were precisely classified. It could be judging that BAI method using vertebral body centroids demonstrated very promising classification results from the patient-oriented analysis.

Table 2.2. Case-based analysis. The multi-factorial confusion matrix demonstrated the classification results of BAI in accordance with Lenke classification scheme using traditional S-Cobb method. 1 case of Lenke type 2 was misclassified as Lenke type 1, induced 1 false positive and 1 false negative case into the sample.

		Lenke Classification (BAI)								
		0	**1**	**2**	**3**	**4**	**5**	**6**	**total**	**precision**
Lenke Classification (S-Cobb)	**0**	1	0	0	0	0	0	0	1	**1**
	1	0	6	0	0	0	0	0	6	**1**
	2	0	1	14	0	0	0	0	15	**0.93**
	3	0	0	0	2	0	0	0	2	**1**
	4	0	0	0	0	3	0	0	3	**1**
	5	0	0	0	0	0	1	0	1	**1**
	6	0	0	0	0	0	0	2	2	**1**
total		1	7	14	2	3	1	2	30	
specificity		**1**	**0.86**	**1**	**1**	**1**	**1**	**1**		

2.2.5 Discussion

Using BAI generated from vertebral body centroids to characterize scoliotic curve types and to perform Lenke classification for pre-surgery planning has demonstrated promising results. Structural/non-structural classification for all cases was correctly achieved (**Table 2.1**) in comparison with traditional method and BAI-based Lenke classification also showed accurate results, with only 1 case misclassified (**Table 2.2**). With a closer look at the misclassified case (shown in **Figure 2.12**), we identified that the proximal thoracic curve was not recognized by BAI method.

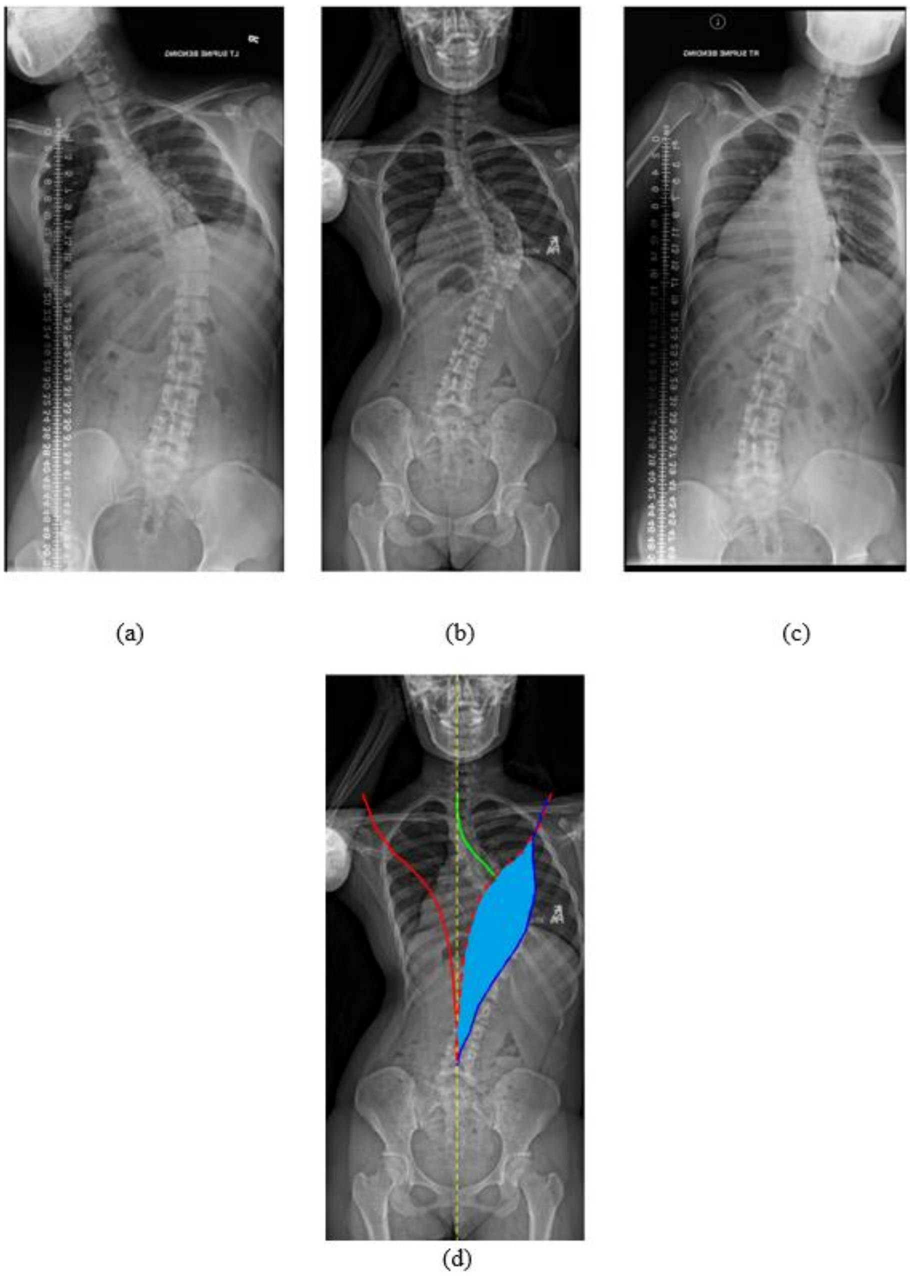

Figure 2.12 The details of the misclassified case. X-ray imaging was taken for **(a)** bending to left, **(b)** erect (supine front) and **(c)** bending to right. **(d)** BAI (vertebral body centroid) was shown in cyan filled area.

Among the 82 curves from 30 subjects, 27 were identified as proximal curves; most of which could be correctly identified except for this captioned case. BAI only processed the single main thoracic curve as a structural type. One possible cause could be the imbalance of the range of motion when performing bilateral bending, which constrained the examination of vertebral flexibility (Wren et al. 2017). In order to reduce the chance that posture imbalance might bring; in our future works, we would instruct the subjects to bend more symmetrically on both sides. Another possible reason could be traced back to the pre-processing part of the X-ray images. Since our dataset was harvested retrospectively, the X-ray images had been cropped to the region of interest manually for surgical assessments. Misalignment across three different postures could also affect the BAI generation process. When validating BAI concepts on X-ray images with a large pool of data, we will incorporate raw full body images into the system for a better data curation.

Lenke types classified by the BAI values calculated from the supine and bilateral bending AP X-ray images showed promising results. This finding illustrated the importance of the symmetrical pattern that observed from the bilateral bending can tell the skeletal morphology suffered from scoliosis, which could be served as a predictive parameter for scoliosis assessment and surgery planning. In addition, we have validated the BAI study with a common Lenke classification scheme, but extended parameter from a comprehensive Lenke codes, such as the sagittal modifier retrieved from the sagittal X-ray film, have not been tested yet.

Depart from the ultrasound spine image, which links the spinous processes from thoracic and lumbar segments T1-L5 in to form spine profile; this study adopted the centroid of each vertebra from T1-L5 to generate the spinal characteristic curve. Although the current scoliosis assessment is based on 2D planar X-ray, scoliosis itself is 3D deformity (Pasha et al. 2019). The primary design of BAI parameter was to investigate mild curves (Cobb < 20°), where rotation of the vertebral body or the skewness of the spinous process is not a concern (Hefti et al. 2013). However, rotation becomes a confounding factor for severe scoliosis subjects (Mohanty et al. 2020), the planar projection of spinous process could deviate from the vertebral body where the canonical Cobb angle measurement was conducted. In light of such consideration, we chose the centroids of the vertebra (projection on the coronal plane) to represent the respective spinal profile for the calculation of the BAI values.

The threshold of BAI value that separated structural curve from non-structural one is drawn by the intrinsic distribution of the 30 subjects (82 curves). This could be one limitation of the study as of a rather small sample size. Similar strategy has been demonstrated by Skalli et.al (2017) that investigated the severity index that computed from a small dataset of 65 subjects (Skalli et al. 2017); and further validated from a larger sample of 205 patients (Vergari et al.2021). Therefore, in order to further validate the functionality of BAI values from X-ray images, we will plan to incorporate a larger pre-surgery cohort to test the parameters that harvested from this exploratory study. The next step shall involve a wider range of pre-surgery scoliosis subjects to understand whether the BAI method derived from vertebral body centroids could be immune to the curves of various degrees of severity.

The BAI method involved manual inputs in the BAI value generation and results validation. Intra-rater and inter-rater reliability test upon the above steps was not conducted, which was a major limitation for this study and will be further investigated in our subsequent studies. In order to suppress the possible human errors, our future direction is to develop a fully automated method; including the step of spinal profile formation and pelvis level inclination adjustment through deep learning approaches. The next-generation of BAI method is expected to assist the clinician better upon formulating pre-surgery plans.

2.3 Summary

This chapter first illustrates the formulation of the idea of BAI method from the biomechanical pattern of spine in bilateral bending: where structural curve preserves the curvature in bilateral bending and non-structural curve reduces or even fully compensates the curvature. Thus, curve types and AIS types could be classified according the assymetrical pattern that presented in side-way bending. To validate the BAI method, the spine profile was generated through the vertebral body centroids from pre-surgery X-ray imaging. The use of pre-surgery X-ray is based on two considerations: 1) vertebral body is the most straightforward anatomical structure to characterize spine curvature, which is invisible in ultrasound; 2) multiple unnecessary X-ray is unethical and not available for mild AIS patients. BAI was calculated semi-automatically with manual annotation of vertebral centroids and pelvis level inclination adjustment. BAI classification was validated with the scoliotic curve type and traditional Lenke classification using side-bending Cobb angle measurement (S-Cobb). In terms of scoliotic curve type classification, all curves were correctly classified; out of 30 subjects, 1 case was confirmed as misclassified when applying to Lenke classification earlier, thus has been adjusted. BAI method has demonstrated its inter-modality versatility in X-ray imaging application. The curve type classification and the pre-surgery Lenke classification both indicated promising performances upon the exploratory dataset. A fully-automated of BAI measurement is surely an interesting direction to continue our endeavor. Deep learning on the vertebral-level segmentation should be involved in further study. Moreover, since BAI method demonstrated satisfactory results with X-ray images, it is worthwhile to explore whether this novel method could be applied for ultrasound images, using other spinous anatomical landmarks that are discernable in ultrasound imaging.

CHAPTER 3. BAIsp METHOD USING SPINOUS PROCESS FROM ULTRASOUND IMAGING

3.1 Ultrasound AIS Assessment Using Spinous Process

Scolioscan, a three-dimensional (3D) ultrasound imaging system, led the trends in providing radiation-free spine imaging solutions (Zheng et al. 2009). Scolioscan was the first medical imaging modality to reconstruct 3D spinal volume through stacking each frame of planar B-mode ultrasound image with its respective spatial and directional information. In order to compare with conventional anterior-posterior standing radiography, the 3D volume data is then projected to the local coronal plane. Such imaging technique is known as volume projection imaging (VPI) (**Figure 3.1a**, Cheung et al. 2015), and had been consistently and steadily improved throughout years (Zheng et al. 2016, Zhou et al. 2017, Jiang et al. 2019). In our previous works, Scolioscan had been demonstrated its validity and reliability for coronal spinal curvature measurement compared against X-ray (Zheng et al. 2016, Brink et al. 2017, Wong et al. 2019). In these previous studies, ultrasound spinous process angle (USSPA), the angle measured based on the medial line that represents the shadow of the spinous processes, was used to evaluate the magnitude of the scoliotic curve (**Figure 3.1b**). This compromise comes from the invisibility of the vertebral body by the nature of ultrasound imaging. It had been observed that USSPA values generally slightly underestimated X-ray Cobb angle measurement (XCA), with coefficients of 0.833-0.866 from the same curve of the same subject (Zheng et al. 2016). The discrepancies are due to the morphological difference between spinous process (vertebra posterior structure) and vertebral body (vertebra anterior structure) (Herzenberg et al. 1990). Such discrepancies implied that USSPA systematically underestimates the gold-standard XCA. USSPA is the pioneered ultrasound-derived scoliotic curve measurement and still encourages various AIS investigations and researches.

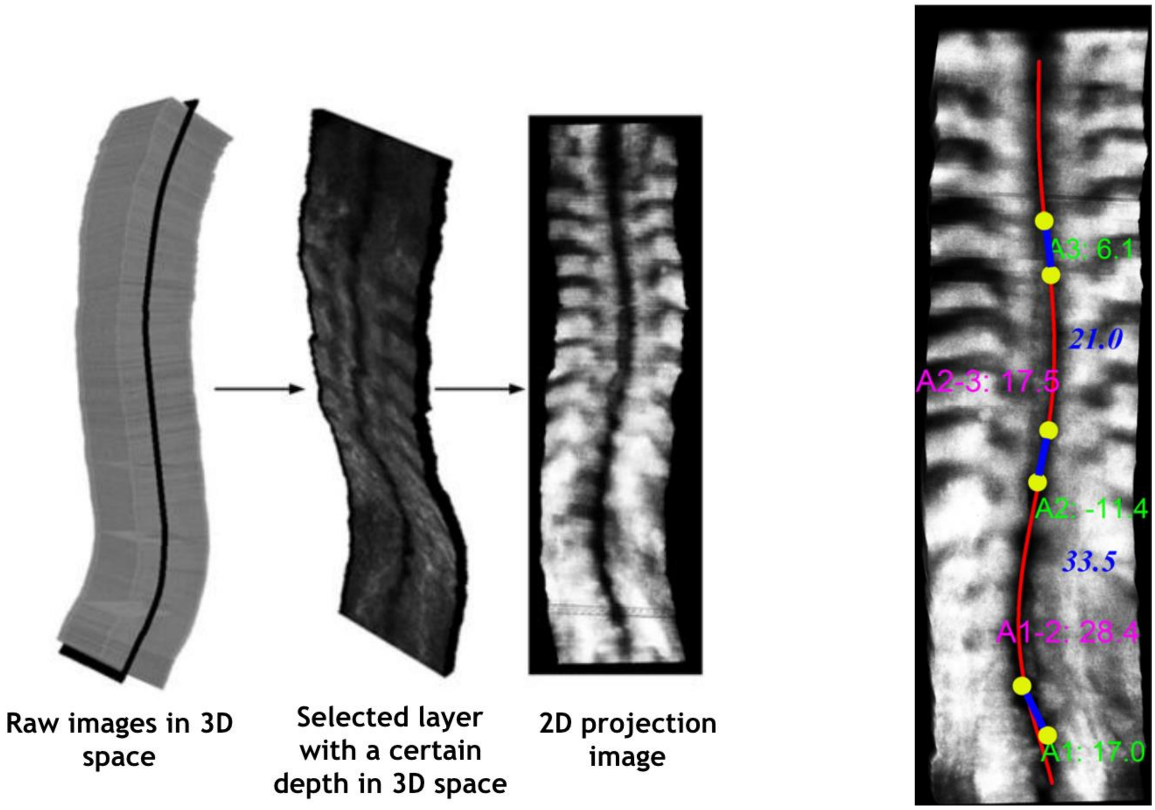

(a) (b)

Figure 3.1 (a) Illustration of the generation process of ultrasound coronal spine image by Scolioscan volume projection imaging (VPI) technique. 3D spinal volume representation is formed by stacks of 2D B-mode ultrasound images with spatial and directional information. 2D coronal projection plane is cut from a customized skin-bone depth. **(b)** An example of conventional Ultrasound Spinous Process Angle (USSPA) measurement by Scolioscan. Both manual and automatic measurement results were presented. Lines in blue are manual drawn along with the medial spinous process shadow; while the curve in red is automatically interpolated by Scolioscan. (Images were reproduced from Cheung et al. 2015)

The following section explains the development of the BAI method obtained through spinous processes with the help of 3D ultrasound imaging.

3.2 Mild AIS Curve Classification Using BAIsp Method (Spinous Process)

3.2.1 Subjects and data acquisitions

This study retrospectively included 90 mild AIS subjects (21 M and 69 F; Age:14.5 ± 1.7 years old; Cobb: 18.2 ± 6.4°) from a schoolchildren screening program in Hong Kong. This batch of cohort was retrospectively recruited from previous Scolioscan validation research (Zheng et al. 2016) with ethical approvals from the Chinese University of Hong Kong (CREC Ref.No. 2015.463). All these patients were recruited and assessed in the Department of Orthopaedics and Traumatology of the Chinese University of Hong Kong. The female to male ratio was around 3:1, which was within the range of gender difference in AIS prevalence (Weiss et al. 2008). The subjects were scanned and clinically assessed in the Department of Orthopaedics and Traumatology of the Chinese University of Hong Kong from October 9, 2017 to September 24, 2018.

Bi-modality assessment was conducted using two systems, involving low-dose X-ray EOS imaging system (EOS Imaging, France) and 3D ultrasound imaging system, Scolioscan (Model SCN801, Telefield Medical Imaging Ltd, Hong Kong) using a linear probe (central frequency of 7.5 MHz and 7.5 cm width). Each subject underwent both 3D ultrasound and X-ray scanning on the same day, including one standing EOS bi-planar X-ray with three ultrasound coronal images obtained under the postures of erect / standing anterior-posterior (AP), left and right bending. To ensure the subjects could fully stretch their arms to perform maximum bending on each side, an adjustable supporter was used in lateral bending to stabilize their postures during scanning. It is important that both the EOS X-ray scanning and Scolioscan ultrasound scanning were conducted on the same day for each individual. Since the development of AIS is a dynamic process, same-day bi-modality data acquisition was conducted to eliminate the variations of the spinal morphology upon scoliosis progression. Information collected from the EOS X-ray imaging was used to verify the results harvested from the ultrasound-derived parameters.

3.2.2 Radiographic assessment on mild AIS curve classification

In order to classify structural and non-structural scoliotic curves for mild AIS cases, a clinical group from Prince of Wales Hospital (Hong Kong) extend the Scoliosis Research Society (SRS) standards for defining a scoliotic curve on X-ray imaging as a structural curve if both the upper and lower endplates of the curve have tilt angles > 5° (Upper Tilt Angle, UTA and Lower Tilt Angle, LTA) in practice (Korbel et al. 2014). Cobb angles from each subject were measured for structural cases. The graphical illustration of the relationships of UTA, LTA and Cobb are shown in **Figure 3.2**. In mild AIS management, structural curves were tended for periodical monitoring for the risks of progression. Intuitively, when multiple curves were identified from the same subject, the largest Cobb measurement was taken as the major curve. The major curve would be given a high priority when evaluating the subsequent treatment options, as it had the largest impact on the spine morphology and flexibility (Jada et al. 2017). Therefore, in the AIS radiographic assessment, the curve types/classification and major curve were documented as gold-standard in ultrasound method validation.

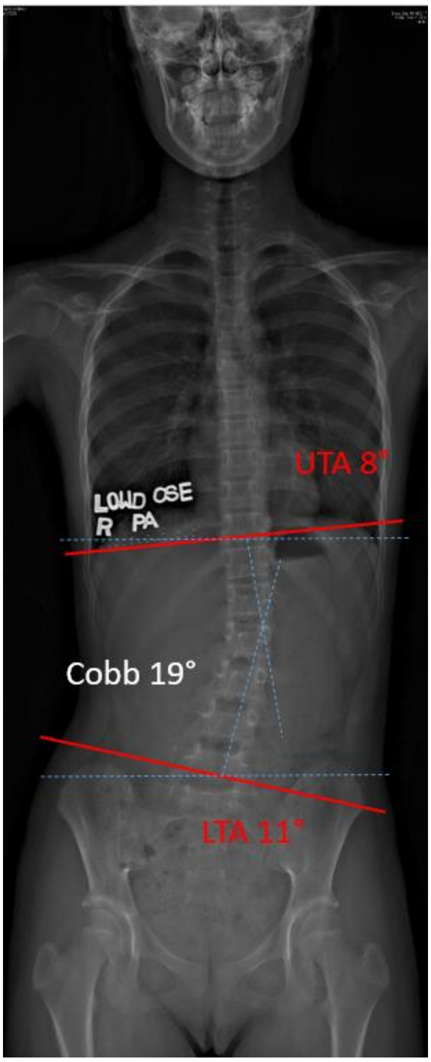

Figure 3.2 Illustration of the concepts and relationships among Upper Tilt Angle (UTA), Lower Tilt Angle (LTA) and Cobb angle.

Patients were further categorized using a modified version of the canonically gold-standard Lenke classification system (m-Lenke) for mild AIS using X-ray. The arrangement was made due to the fact that the Lenke classification had been primarily adopted in scoliosis surgery planning, usually with a Cobb > 40° (Lenke et al. 2003). As our exploratory study attempted to classify mild AIS curves, the numerical criteria were changed according to the above revised structural curve definition (**Figure 3.3**). For a structural curve, both UTA ≥ 5° and LTA ≥ 5°. Similarly, the scoliotic curve was characterized with its location of apex into either proximal thoracic (PT), main thoracic (T) or lumbar/thoraco-lumbar (L) curve. Apex within T2 and T5 represents a PT curve; T6 and T12 disk represents a T curve; and below T12 represents a L curve.

The modified Lenke classification system for mild AIS

Curve type	Proximal Thoracic	Main Thoracic	Thoracolumbar/ Lumbar	Description
1	Nonstructural	Structural*	Nonstructural	Main Thoracic
2	Structural	Structural*	Nonstructural	Double Thoracic
3	Nonstructural	Structural*	Structural	Double Major
4	Structural	Structural*	Structural*	Triple Major
5	Nonstructural	Nonstructural	Structural*	Thoracolumbar/Lumbar
6	Nonstructural	Structural	Structural*	Thoracolumbar/Lumbar – Main Thoracic

* *Major curve, with largest Cobb measurement*

Location of apex

Curve	Apex
Proximal Thoracic	T2-T5
Main Thoracic	T6-T12 Disk
Lumbar	T12-L4

	Structural criteria (X-ray)	Structural criteria (Ultrasound)
Proximal Thoracic	Upper Tilt Angle (UTA) of curve ≥ 5°; Lower Tilt Angle (LTA) of curve ≥ 5°	BAI value; SPA reading from erect ultrasound image
Main Thoracic	Upper Tilt Angle (UTA) of curve ≥ 5°; Lower Tilt Angle (LTA) of curve ≥ 5°	BAI value; SPA reading from erect ultrasound image
Thoracolumbar/Lumbar	Upper Tilt Angle (UTA) of curve ≥ 5°; Lower Tilt Angle (LTA) of curve ≥ 5°	BAI value; SPA reading from erect ultrasound image

Figure 3.3 Details of the modified Lenke classification system for mild AIS (m-Lenke), adapted from Lenke et al. 2003. The structural criteria for X-ray imaging and ultrasound imaging are provided respectively.

For each AIS case, a clinician measured Cobb angles and denoted the major curve from the standing EOS X-ray radiographic as the ground truth. In case of no structural curve was found in a subject, the curve would be labelled as non-structural curve, and 'N/A' for major curve. This is an exception case from traditional pre-operative Lenke classification, which serves severe AIS surgery planning. Non-structural cases were not enumerated in the Lenke classification scheme. However, cases with only non-structure curve(s) are common among mild AIS subjects. Based on the apex location(s) and type(s) of curve(s) identified from each subject, the respective modified Lenke (m-Lenke) type and major curve could be determined and served as the ground truth to validate the corresponding ultrasound results.

3.2.3 Ultrasound-based BAIsp method on mild AIS curve classification

Taking advantage of Scolioscan's radiation-free (Zheng et al. 2009, Zheng et al. 2016) and flexible range of scanning (He et al. 2017), we proposed to locate the structural spinal segment(s) of AIS patients based on the fundamental biomechanics of spine. Nonstructural curves can be restored in lateral bending while structural curves are rigid irreversibly altered in shape (Adams et al. 2005). As shown in the illustration (**Figure 3.1**), the curve maintaining its shape in lateral bending is marked as a structural curve; while the curve being corrected is a non-structural one. The dynamics of spine can be traced and reconstructed from three scanning postures: erect (standing AP), left and right bending. For mild AIS, left and right bending profiles of a non-structural curve shows more or less symmetrical pattern; while structural curve shows an asymmetrical lump in the specific region.

Each subject had taken whole-spine ultrasound scanning by Scolioscan from three postures: standing erect, bending to left and bending to right from posterior-anterior (PA) view (**Figure 3.4**).

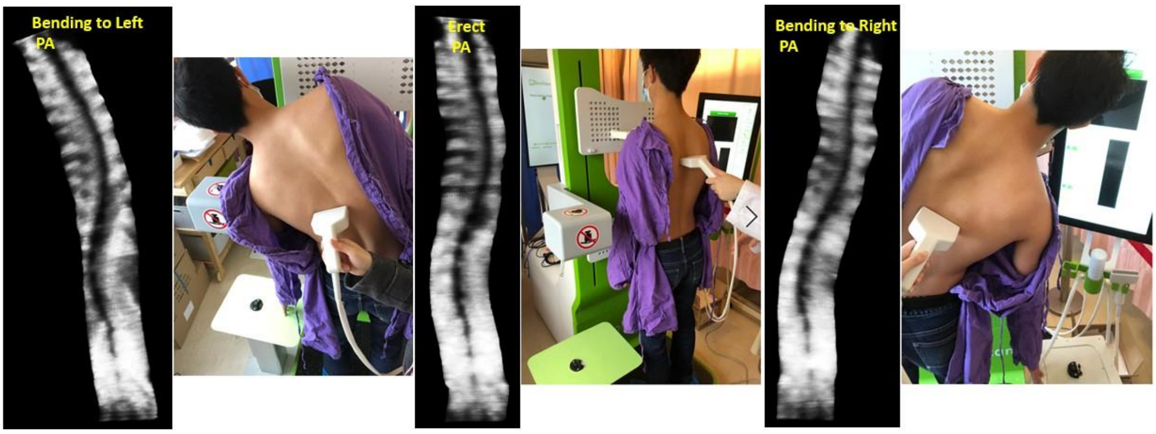

Figure 3.4 Demonstration of ultrasound scanning from three postures (from left to right): bending to left, standing erect and bending to right from PA.

The concept of the bending asymmetry index (BAI) was developed to indicate the presence of a possible location(s) of structural site(s) through the discrepancy of the bilateral spinal profiles, which was constructed from the interpolated ultrasound spinous process shadows observed from the ultrasound coronal spine imaging, from bilateral bending (**Figure 3.5)**. In order to distinguish with other BAI methods, BAI method using spinous process is denoted as BAIsp method. Comparing the spinal profiles from left/right bending ultrasound images, the discrepancies between two directional curves, known as the bending discrepancy line (BDL), can be used to characterize the asymmetrical pattern of the spine: a large discrepancy suggest a rigid deformity of spine. In light of these conditions, we designed parameters that described such discrepancy to represent the possible structural location of scoliotic curve. With such principles, larger BAIsp could implicate a more severe structural curve. To ensure the BAIsp method immune to the noise, statistical control was essential to filter out false positives. In addition, the curvature of the spine under the standing erect posture, i.e. erect spinous process angle (USSPA), was measured automatically by a software developed in our research team previously (Zheng et al. 2016). If BAIsp paired with an USSPA reading in the same level of the spine, the BAIsp value would be used to characterize the structural curve; otherwise, discarded. Similarly, the curve was characterized with its location of apex into either proximal thoracic (PT), main thoracic (T) or thoraco-lumbar / lumbar (L) curve. All these pieces of information could be codified into the table of modified Lenke classification system (m-Lenke) for mild AIS using 3D ultrasound in **Figure 3.3**.

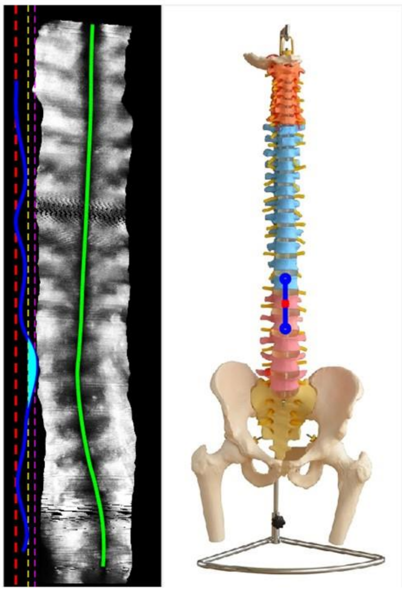

Figure 3.5 Illustration of the representation of BAIsp Method. Line notation: blue line: Bending Discrepancy Line (BDL); red line: pruned mean of the bilateral bending profile; purple line: absolute value of extrema of the bending profile; yellow line: standard error of mean of the bending profile; cyan area: BAIsp.

The block diagram shown in **Figure 3.6** illustrated the detailed process of generating BAI value, which includes the following step:

i. **Pre-processing:** annotate the center of all levels of spine (T1-L5) in the spinous line for three-posture ultrasound images and save all coordinates information; output the spinous process angle in erect stance (USSPA) through the annotation software;

ii. **Image-processing:** interpolate spine curve with the coordinates from previous stage; flip and fuse lateral bending curves and derive the BAIsp through the calculation of the discrepancies of the curves;

iii. **Decision making:** generate the classification result based on the BAIsp and the related position in spine with conform to the modified Lenke classification (m-Lenke) table.

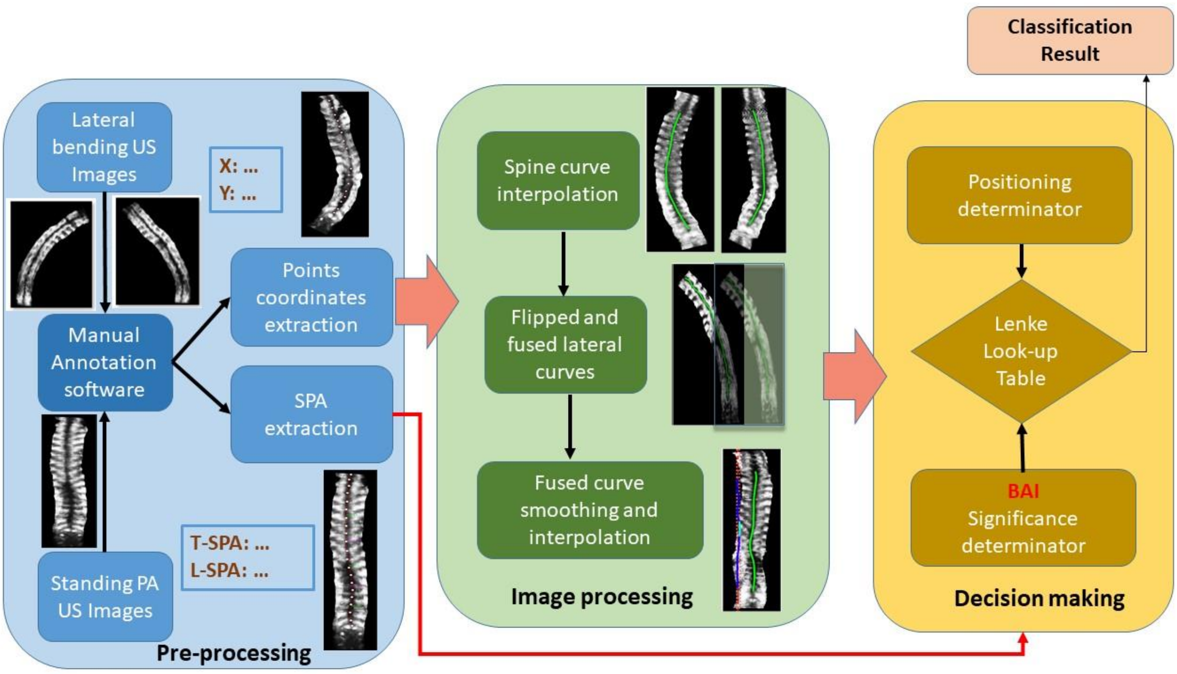

Figure 3.6 Block diagram of the computer-aided BAIsp generation process: pre-processing, imaging processing and decision making (curve classification).

Figure 3.7 and **Figure 3.8** demonstrated that how BAIsp could help identify non-structural and structural curves, respectively. As discussed, for non-structural curves, the curves are corrected during side bending; when mirroring the left/right bending curve, they are more or less matched with each other. For structural curves, the shapes of the curves persist during side bending. When mirroring the left/right bending curve, there would be discrepancies. **Figure 3.7** shows a case with a small curve in the ultrasound coronal image obtained under the erect standing posture, together with two bending curves (**Figure 3.7a**). The extracted spine profiles under the bending postures are shown in **Figure 3.7b**. As it can be observed in **Figure 3.7c**, the two curves are almost identical, leading to a very small discrepancy when subtracting them. Therefore, the case shown in **Figure 3.7** is classified as nonstructural curve. **Figure 3.8** shows a typical case with structural curve. The procedure is the same as that described in ***Figure 3.7***, and the result shown in **Figure 3.8c** indicates that there is an obvious discrepancy between the two curves, and the calculated BAIsp is 269.01 mm^2 (2,330 pixel, 220 ppi for ultrasound scanning), which implies a structural curve. The threshold of structural curve had been determined at 200 pixel or 23.09 mm^2 empirically from a pilot run of the method with X-ray as reference among 33 subjects.

Similar as radiographic assessment, for each case, the measured BAIsp and denoted major curve (the largest BAIsp when multiple curves were presented) exacted from 3D ultrasound imaging analysis would be labelled and stored automatically. In case of no structural curve was found for a subject, the curve would be labelled as non-structural curve, and ‘N/A’ for major curve. Based on the location and magnitude of the structural curves from the same subject, the corresponding m-Lenke type and major curve could be obtained and used to compare with the X-ray findings.

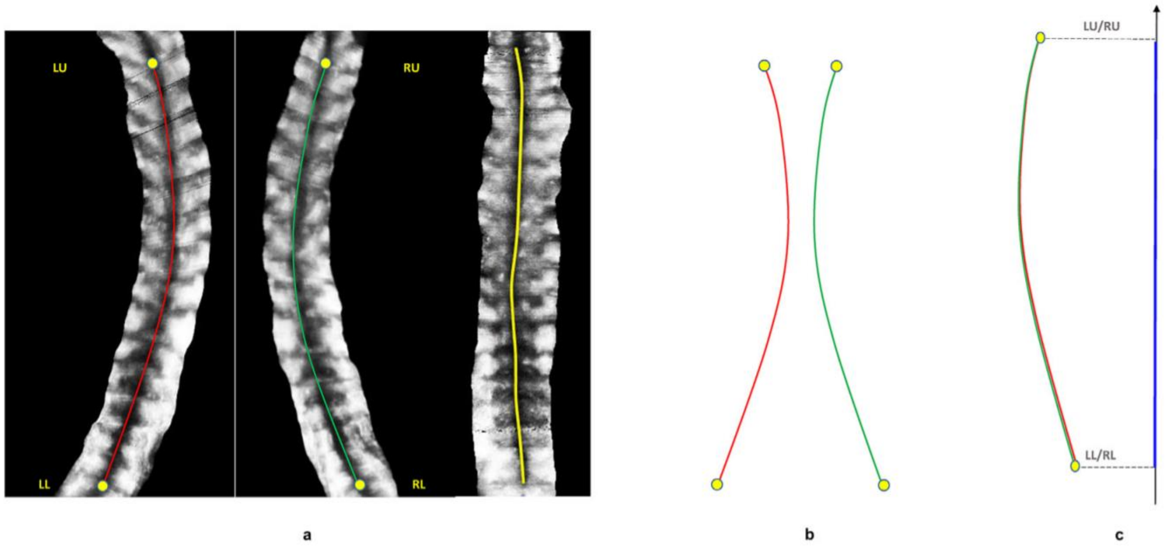

Figure 3.7 Illustration of non-structural curve characterized by BAIsp from a typical subject. **(a)** An example of the three-posture coronal spine images from the same subject with the 3D ultrasound imaging method. The spinous process line, SPL (interpolated by the curve passing through centers of spinous process from all levels, T1-L5) for standing erect (E-SPL, yellow), bending to left (L-SPL, red) and bending to right (R-SPL, green) are super-imposed with the original ultrasound images with end points labelled with (Left/Right Upper/Lower) markers. **(b)** the extracted L-SPL and R-SPL from **(a)** and **(c)** with alignment of end points, L-SPL is flipped to match with R-SPL to examine the asymmetrical pattern. For this curve, the BAIsp value is 90 pixel or 10.39 mm^2, which is smaller than the threshold for structural curve (200 pixel or 23.09 mm^2); it implicates that the thoraco-lumbar curve presented in E-SPL(a) is non-structural. Line notation (also applicable to **Figure 3.8**) – red line: line of the left bending spinous processes (L-SPA); green line: line of right bending spinous processes (R-SPA); yellow line: line of erect spinous processes (USSPA); yellow circle: upper/lower points of line of spinous processes for alignment; blue line: bending discrepancy line (BDL); blue enclosed area: BAIsp.

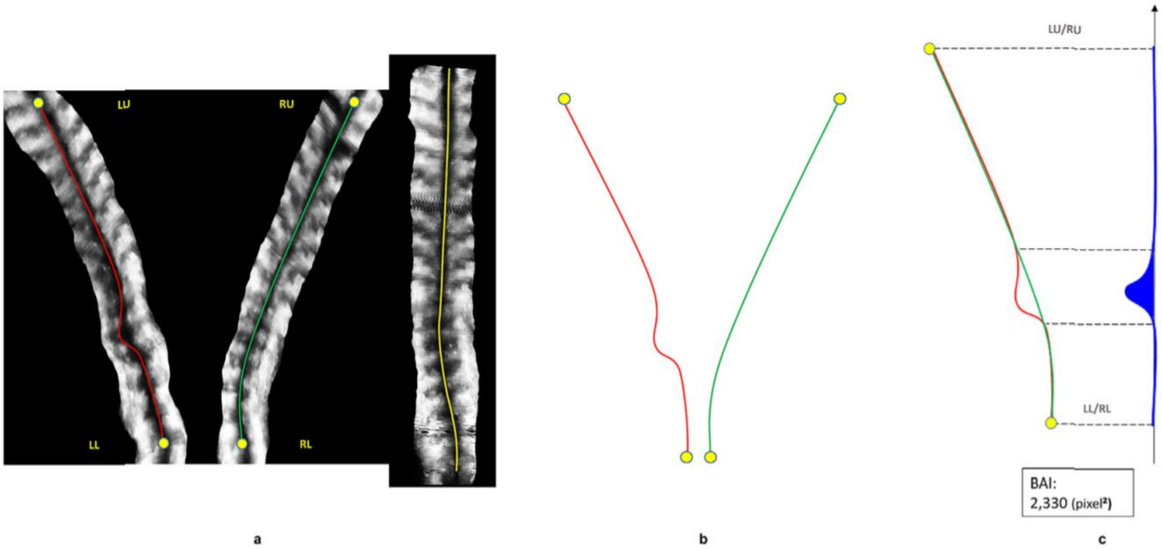

Figure 3.8 Illustration of structural curve characterized by BAIsp from a real subject. **(a)** An example of three-posture coronal spine images from the same subject with the 3D ultrasound imaging method. The spinous process line, SPL (interpolated by the curve passing through centers of spinous process from all levels, T1-L5) for standing erect (E-SPL, yellow), bending to left (L-SPL, red) and bending to right (R-SPL, green) are super-imposed with the original ultrasound images with end points labelled with (Left/Right Upper/Lower) markers. **(b)** the extracted L-SPL and R-SPL from **(a)** and **(c)** with alignment of end points, L-SPL is flipped to match with R-SPL to examine the asymmetrical pattern. For this curve, the BAIsp value is 2330 pixel or 269.01 mm^2 , which is larger than the threshold for structural curve (200 pixel or 23.09 mm^2); it implicates that the thoraco-lumbar curve presented in E-SPL(a) is structural.

3.2.4 Statistical analysis

Various statistical analyses were conducted for this study using SPSS 25.0 for Mac (SPSS Inc., Chicago IL, USA). For mild AIS cases, BAI was proposed to serve as a monitoring tool, as the structural curves involved are too mild for surgery. BAI would be applied to indicate spinal segment(s) required further care or chronic management. The primary statistical tool for this exploratory study included precision (p) and recall (r) for the m-Lenke classification results and major curve identification, respectively. Precision (p) and recall (r) are two important evaluation metrics: precision refer s to the percentage of the harvested which are relevant; recall (r) refers to the percentage of total relevant results correctly classified by the method. As this is the first-ever study in the field to establish the relationship of spinal flexibility (in term of bilateral bending pattern) with scoliotic type, the performance of the classification results could not be compared with prior studies. The statistical results were shown for the study validation and discussion.

3.2.5 Results

During the study period, 87 subjects were subsequently identified as eligible for inclusion. Three of them were dropped due to severe motion artifacts in the ultrasound data acquisition stage, which were difficult for image processing stage of the BAIsp generation process.

Taking the classification results from the EOS X-ray images as gold standard, out of the 87 patients, the number of m-Lenke type 1 to 6 is 8, 2, 10, 12, 23, and 5, respectively. In addition, there were two special categories of curve types could not be codified by the m-Lenke classification scheme: 1 patient had triple curves (similar to m-Lenke type 4), but the major curve was uncommonly located in proximal thoracic region (denoted as PT*); 4 patients had structural curves in proximal thoracic and lumbar regions (denoted as PT+L), and nonstructural curve in main thoracic. Another 21 patients only had non-structural curves and did not possess structural curves (denoted as NSC). The exception cases were frequent, since the spine deformity was light among the mild AIS patients.

Referred to the X-ray classification results, the overall precision (p) of our proposed 3D ultrasound-based BAIsp classification method was 0.70. The detailed m-Lenke classification results were presented in **Figure 3.9** and tabular form **Table 3.1**. From the results we could observe that the proposed method was feasible in characterizing lumbar or lumbar-dominated curve types (m-Lenke type 5 with p=0.91, r=0.91 & m-Lenke type 6 with p=0.80, r=0.80) and nonstructural scoliosis (NSC with p=1, r=0.70). For main thoracic-dominated and without the presence of proximal thoracic curve types (m-Lenke type 1 & 2 & 3), the proposed BAIsp method also displayed certain effectiveness in classification. However, for the curve types that involved proximal thoracic curve (m-Lenke type 4 & variants), the performance of this classifier was under certain challenge.

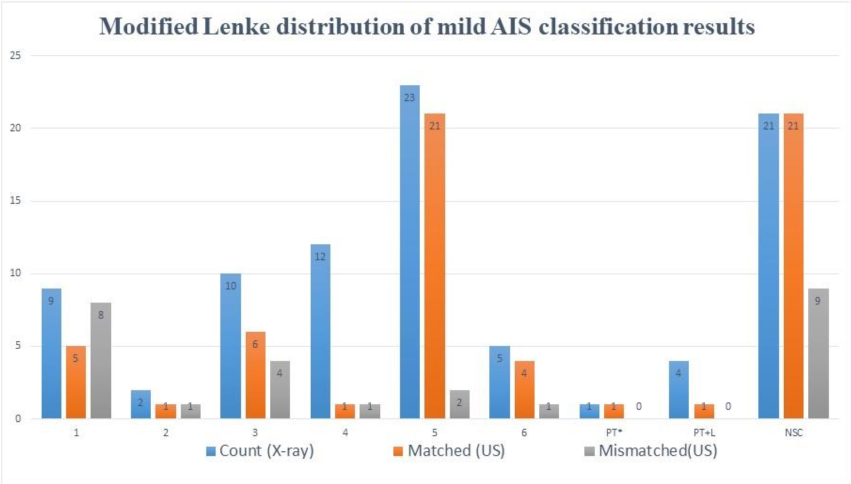

Figure 3.9 The modified Lenke distribution of mild AIS classification (m-Lenke) results (N=87). Scolioscan 3D ultrasound classification results (Matched cases in orange, mismatched cases in grey) are compared with the gold-standard EOS X-ray classification results (blue). A matched case indicates both ultrasound-based BAIsp method and X-ray ground-truth arrive at identical classification result. The ensemble comprises m-Lenke type 1–6 with two proximal thoracic-dominant variants: PT* (structural curve in proximal thoracic) and PT + L (structural curve in proximal thoracic and lumbar), and the detection of non-structural curves (NSC).

Table 3.1 Statistical analysis of the m-Lenke classification results

m-Lenke Type	Count (X-ray)	Matched (US)	Mismatched (US)	Precision (p)	Recall(r)
1	9	5	8	0.56	0.38
2	2	1	1	0.50	0.50
3	10	6	4	0.60	0.60
4	12	1	1	0.08	0.50
5	23	21	2	0.91	0.91
6	5	4	1	0.80	0.80
PT*	1	1	0	1	1
PT+L	4	1	0	0.25	1
NSC	21	21	9	1	0.70

Similarly, the major curve identification results also adopted EOS coronal X-ray imaging as gold standard. Of the 87 patients, 6 patients had proximal thoracic major curves (PT), 23 patients had main thoracic major curves (T), 37 patients had lumbar major curves (L), and 21 patients had no major curves as those were nonstructural (N/A). Compared with the X-ray results, the overall precision(p) of the proposed 3D ultrasound-based BAI method for identifying major curve was 0.72. And the detailed statistics were available in **Figure 3.10** and **Table 3.2**, respectively. The results demonstrated similar trends as that in m-Lenke curve classification. The proposed BAIsp method had distinctive power for lumbar-dominated curves (p=0.70, r=0.90) and non-structural ones (p=1, r=0.70). However, for the curve with main thoracic (p=0.52, r=0.48) or proximal thoracic curve (p=0.50, r=1) as major curve, the results were comparably moderate.

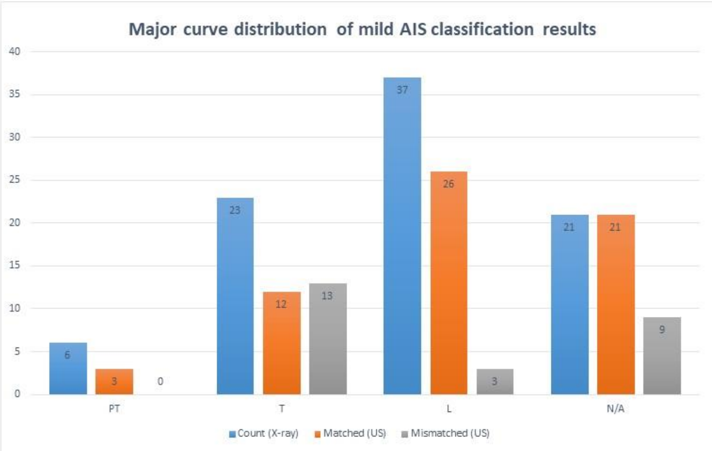

Figure 3.10 The major curve distribution of mild AIS classification results. Scolioscan 3D ultrasound classification results (Matched cases in orange, mismatched cases in grey) are compared with the gold-standard EOS X-ray classification results (blue). A matched case means both ultrasound and X-ray arrive at identical major curve detection result. The ensemble comprises major curve located in proximal thoracic (PT), thoracic (T), lumbar (L) or not detected (N/A, for non-structural curves).

Table 3.2 Statistical analysis of the major curve detection results

Major curve	Count (X-ray)	Matched (US)	Mismatched (US)	Precision (p)	Recall(r)
PT	6	3	0	0.50	1
T	23	12	13	0.52	0.48
L	37	26	3	0.70	0.90
N/A	21	21	9	1	070

3.2.6. Discussion

In this first ultrasound derived scoliotic curve classification study, we reported that a new method based on 3D ultrasound imaging could provide an effective classification for mild AIS, particularly for the cases with lumbar-dominated curves (m-Lenke type 5 with p=0.91, r=0.91 & m-Lenke type 6 with p=0.80, r=0.80). According to a prevalence study of 72,699 schoolchildren, the most common type of mild AIS cases was thoracolumbar curves (40.1%) (Wong et al. 2005). Our cohort of study also displayed similar prevalence of lumbar/thoracolumbar curves (42.4%). It was quite constructive that our proposed BAIsp method could accommodate the majority. From this promising result, the application of the proposed ultrasound BAIsp method could potentially reduce the use of X-ray in clinical management, monitoring and assessment for patients with thoraco-lumbar / lumbar curves. In addition, radiation-free follow-up and chronic tracking programs could be specifically designed for the subjects with thoraco-lumbar / lumbar curves.

The BAIsp method also demonstrated capability in classifying nonstructural curves (p=1, r=0.70). This finding was helpful in post-screening management and cases referrals of mild AIS patients. Non-structural mild AIS cases usually required no follow-ups (Negrini et al. 2003, Weinstein et al. 2008). If these cases could be effectively removed from the lists of clinicians or therapists, the efficacies of the rehabilitation and treatment resources could be further enhanced.

There were some limitations of the BAIsp method upon mild AIS cases. If proximal thoracic curves were presented in the subject, no matter taking the dominant role or not, the curve classification results and major curve identification process may not live up to the expectation. The precision for m-Lenke type 4 classification was 0.08 (1 out of 12), and only 17.6% of the curves that contain proximal thoracic structural curves were correctly assorted. There were 7 failed cases in major curve detection: 3 cases had proximal thoracic as major curve and the other 4 had proximal thoracic as minor curve. This result was due to the physical limitation of the ultrasound scanning around proximal thoracic or cervical region, which has a convex surface and making the ultrasound coupling between the ultrasound probe and the skin be difficult, leading to poor image quality. A clinical study using 3D ultrasound imaging to investigate the measurements on thoracic spine also demonstrated that a comparably lower reliability of measurement was found at upper thoracic segment compared with lumbar spine (Folsch et al. 2012). A proper coupling method for ultrasound scanning for the upper thoracic and cervical region is required to be developed, and flexible ultrasound arrays that could cover the whole spine region may be a good solution for the ‘missing’ curves in the proximal thoracic spinal segments (Shea et al. 2015).

The BAIsp method also showed average classification results towards thoracic curves. The correctness of thoracic curves labelling was slightly above 50-50. Most of the failed cases were misclassifying into NSCs. After carefully reviewing these cases, it was found that the respective UTAs and LTAs were around 5°, which is the threshold value for determining structural or non-structural case from the coronal X-ray imaging. The decision-making process of the system was conducted without human’s discretion, which could result in quite different classification decisions. Additionally, from our previous research (Zheng et al. 2016), we had demonstrated the linear relationship of ultrasound spinous process angle (USSPA) with X-ray's Cobb. The thoracic-lumbar data combined correlation of SPA and Cobb was y=1.1797x, R^2>0.76. This implies that angle measurements in 3D ultrasound images were consistently smaller than that in X-ray, which could also contribute to different decisions made around the threshold value of 5°.

Another concern of the proposed method was raised for the cost-effectiveness of ultrasound scanning. As mentioned, the ultrasound-derived parameter BAIsp required triple times of scanning: extra time and efforts were needed for the practice. Comparably, the benefits were outweighed the time consumption: it was first time to apply side bending ultrasound imaging for scoliotic curve classification. Clinicians could better manage the mild AIS subjects with timely and customized follow-ups.

The cohort of subjects of our study was obtained retrospectively from a government post-screening AIS program. The m-Lenke distribution of subjects was very uneven among different categories. In order to test the distinction power of the proposed method against specific type of AIS, a more even distribution of each class should be included in the further study when subject pool becomes statistically large; and we can understand the landscape of mild AIS classification using BAI methods better.

Last but not least, for this pilot study, one clinical expert was involved for the angle measurement and curve characteristics (start/end of the curve, curve apex) annotation. For our next step, we would like to investigate the intra- and inter-rater reliability of the proposed m-Lenke classification method for mild AIS with a considerably large cohort.

3.3 Mild AIS Screening Referral Decision-Making Using BAIsp Method

AIS screening is essential for young population, as bracing, exercise and other conservative treatment methods can interrupt and slow down scoliotic curve progression (Dunn et al. 2018). Most of the current AIS screening scheme include X-ray scanning for curvature assessment and treatment formulation (Mirtz et al. 2005, Fong et al. 2015, Dunn et al. 2018). As detailly elaborated in **Session 1.3**, the protocols of AIS screening program in Hong Kong involve: 1) Forward bend test, where the angle of trunk rotation (ATR) is measured; and 2) Moire topography, where the contour lines are studied qualitatively. If both ATR ≥ 5 ° and Moire interleaved contour lines ≥ 2, radiographic Cobb assessment is required. For Cobb ≥ 20 °, the subject would be referred to scoliosis specialist care (Fong et al. 2015). The majority of the screening subjects (97.5%) were healthy or mild cases which requires no follow-up from the Hong Kong 10-year scoliosis screening project of 394,401 subjects (Fong et al. 2015). In other words, most of the schoolchildren recruited for AIS screening underwent unnecessary X-ray, which could be risk factors to cancer inducement (Hoffman et al. 1989). Hence, the objectives of this study are: to evaluate whether using ultrasound could play a role similar to X-ray imaging for specialist referral decision making; to reduce unnecessary X-ray exposure in current AIS screening procedure.

3.3.1 Subjects and data acquisitions

This study retrospectively included 80 mild AIS subjects (21 M and 59 F; Age:14.6 ± 1.7 years old; Cobb: 18.3 ± 6.2°) from a schoolchildren screening program in Hong Kong. This batch of cohort was retrospectively recruited (same pool of subject as in **Section 3.2**) from previous Scolioscan validation research (Zheng et al. 2016) with ethical approvals from the Chinese University of Hong Kong (CREC Ref.No. 2015.463). All these patients were recruited and assessed in the Department of Orthopaedics and Traumatology of the Chinese University of Hong Kong. The female to male ratio was around 3:1, which was within the range of gender difference in AIS prevalence (Weiss et al. 2008). The subjects were scanned and clinically evaluated in the Department of Orthopaedics and Traumatology of the Chinese University of Hong Kong from October 9, 2017 to September 24, 2018.

Bi-modality assessment was conducted using two medical imaging systems, including low-dose X-ray EOS imaging system (EOS Imaging, France) and 3D ultrasound imaging system, Scolioscan (Model SCN801, Telefield Medical Imaging Ltd, Hong Kong) using a linear probe (central frequency of 7.5 MHz and 7.5 cm width). Each subject underwent both 3D ultrasound and X-ray scanning on the same day, including one standing EOS bi-planar X-ray with three ultrasound coronal images obtained under the postures of erect / standing anterior-posterior (AP), left and right bending. To ensure the subjects could fully stretch their arms to perform maximum bending on each side and at the same time stabilize the participant's posture during ultrasound scanning; an adjustable supporter was used in bilateral bending. It is important that both the EOS X-ray scanning and Scolioscan ultrasound scanning were conducted on the same day for each individual. Since the development of AIS is a dynamic process, same-day bi-modality data acquisition is to eliminate the variations of the spinal morphology upon scoliosis progression. Cobb angle was measured from the EOS X-ray imaging was used as the ground truth to determine the scoliosis specialist referral status (Cobb ≥ 20 °). The results derived from ultrasound assessment would be compared with the X-ray based decision for validation.

3.3.2 AIS screening referral decision: X-ray and ultrasound methods

As stated in **Section 3.3.1**, each subject was with bi-planar X-ray imaging and three posture coronal view ultrasound imaging (erect/ standing AP, bending to left and bending to right). Cobb angle was measured by an experienced medical imaging expert from coronal X-ray image: if Cobb ≥ 20 °, its scoliosis referral status would be marked as "Yes"; otherwise, 'NO'. The current referral decision was made on a binary discretion basis, and served as ground-truth for the subsequent ultrasound validation.

For ultrasound imaging, spinous process angle (USSPA, Zheng et al. 2016) was measured from the erect coronal spinal image by an experienced ultrasound imaging expert; and BAI was semi-automatically computed from three postures (erect and bilateral bending), as elaborated in **Section 3.2.3** USSPA together with BAI would be used to validate whether the ultrasound-derived parameters could estimate the scoliosis specialist referral decision made by the X-ray Cobb angle measurement. In order to fully understand the predicting power of USSPA and BAIsp, respectively; the following section will estimate the referral decision by: i) USSPA; ii) BAIsp; iii) USSPA and BAIsp. In addition, as USSPA has been reported to predict X-ray referral decision using XCA (Zheng et al. 2016); BAIsp will be tested on how it contribute to the overall prediction.

Besides, in order to test the performance of the ultrasound parameters: curve-based analysis and patient-based analysis would be conducted separately. With such arrangement, we could observe the sensitivity of the proposed method to referral positive or negative decisions.

3.3.3 Statistical analysis

Various statistical analyses were conducted for this study using SPSS 25.0 for Mac (SPSS Inc., Chicago IL, USA). Area under the curve (AUC) was the primary statistical measure for this study, which disclosed the accuracy of a quantitative diagnostic test. A point estimated from the AUC of the empirical ROC curve characterized the Mann-Whitney U estimator (DeLong et al. 1998). The confidence interval for AUC represents the uncertainty of the estimate and uses the Wald Z large sample normal approximation (DeLong et al. 1998). Specifically, a test with fair accuracy than chance has an AUC of 0.5; where a test with perfect accuracy has an AUC of 1. In addition, Poisson regression analysis is studied to test the predictive contribution of BAI for overall referral decision. Specifically, goodness of fit test is to determine how well sample data fits a distribution from a population with a normal distribution; omnibus test is a likelihood-ratio chi-square test of the proposed model with BAI versus the null hypothesis; tests of model effects are studied to understand the effects of other parameters against BAI; and the responsiveness of the parameter estimates from Poisson regression is to demonstrate the effects of BAI prediction (Etier Jr et. Al 2016). The average value of sensitivity for all possible values of specificity; and similarly, the average value of specificity for all possible values of sensitivity (Zhou et al. 2001). The probability that a randomly selected subject with the condition has a test result indicating greater suspicion than that of a randomly chosen subject without such condition (Hanley et al. 1982). Sensitivity and specificity were calculated for the ultrasound-based referral decision upon X-ray ground truth. In addition, positive predictive value (PPV) and negative predictive value (NPV) were calculated to indicate the prevalence of true positives (TP) and true negatives (TN).

3.3.4 Results

During the study period, 79 subjects were subsequently identified as eligible for inclusion (21 M and 58 F; Age:14.6 ± 1.7 years old; Cobb: 18.3 ± 6.1°; scoliosis specialist referral rate: 17.7%). One of them were dropped due to severe motion artifacts in the ultrasound data acquisition stage, which were difficult for image processing stage of the BAI generation process.

For the curve-based analysis, 116 curves were identified from 79 subjects, with 17 curves Cobb ≥ 20 ° (curve-based referral positive) and 99 curves Cobb <20° (curve-based referral negative). The results of ultrasound parameters estimating X-ray Cobb ≥ 20 ° were i) USSPA: AUC=0.784, standard error 0.074, p<0.001; ii) BAIsp: AUC=0.830, standard error 0.058, p<0.001; iii) USSPA and BAIsp: AUC=0.893, standard error 0.049, p<0.001 (**Figure 3.11**).

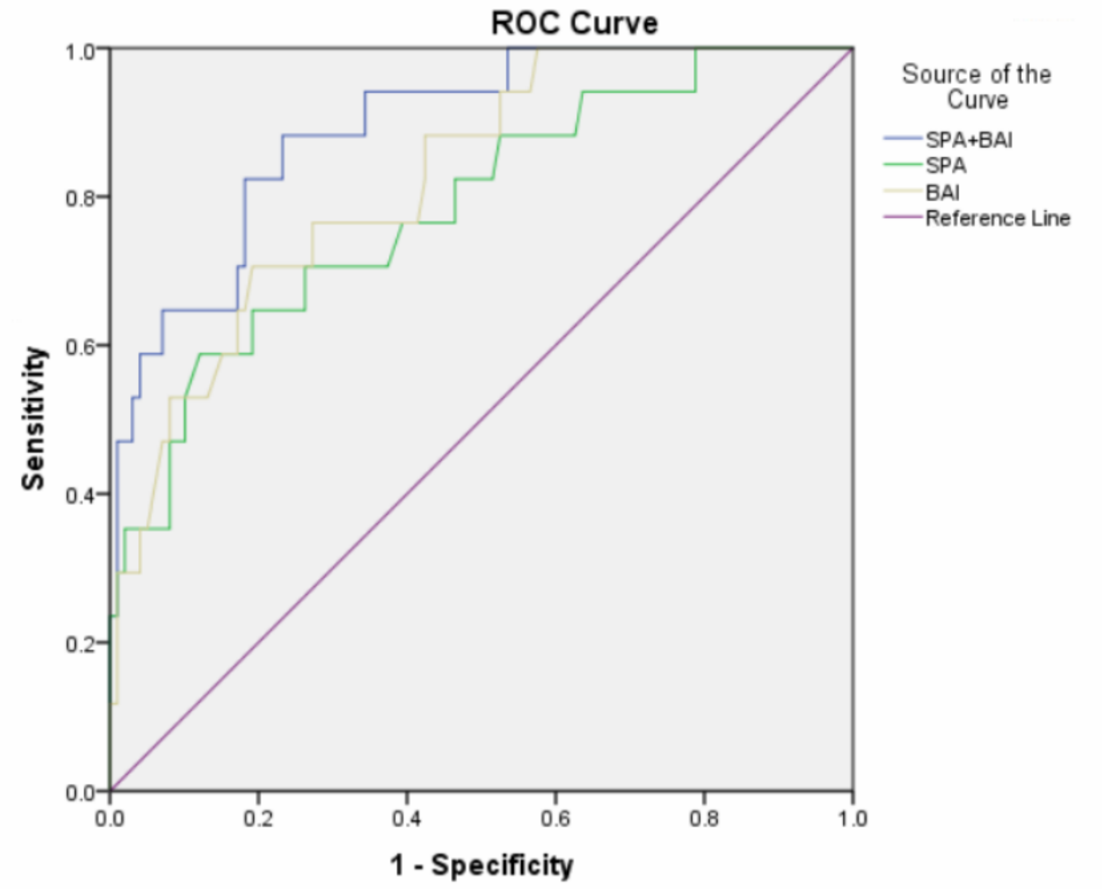

Figure 3.11 Curved-based AUC analysis of ultrasound estimating X-ray Cobb ≥ 20 °. i) green line: using USSPA; ii) yellow line: using BAIsp; iii) blue line: using USSPA and BAIsp together. The purple line is served as a reference line to indicate AUC=0.500.

For the patient-based analysis, 79 subjects, with 14 subjects had 1 or multiple curves Cobb ≥ 20 ° (patient-based referral positive) and 65 subjects had curve(s) Cobb <20° (patient-based referral negative). The results of ultrasound parameters estimating X-ray Cobb ≥ 20 ° were i) USSPA: AUC=0.786, standard error 0.063, p<0.001; ii) BAIsp: AUC=0.824, standard error 0.051, p<0.001; iii) USSPA and BAIsp: AUC=0.892, standard error 0.039, p<0.001 (**Figure 3.12**).

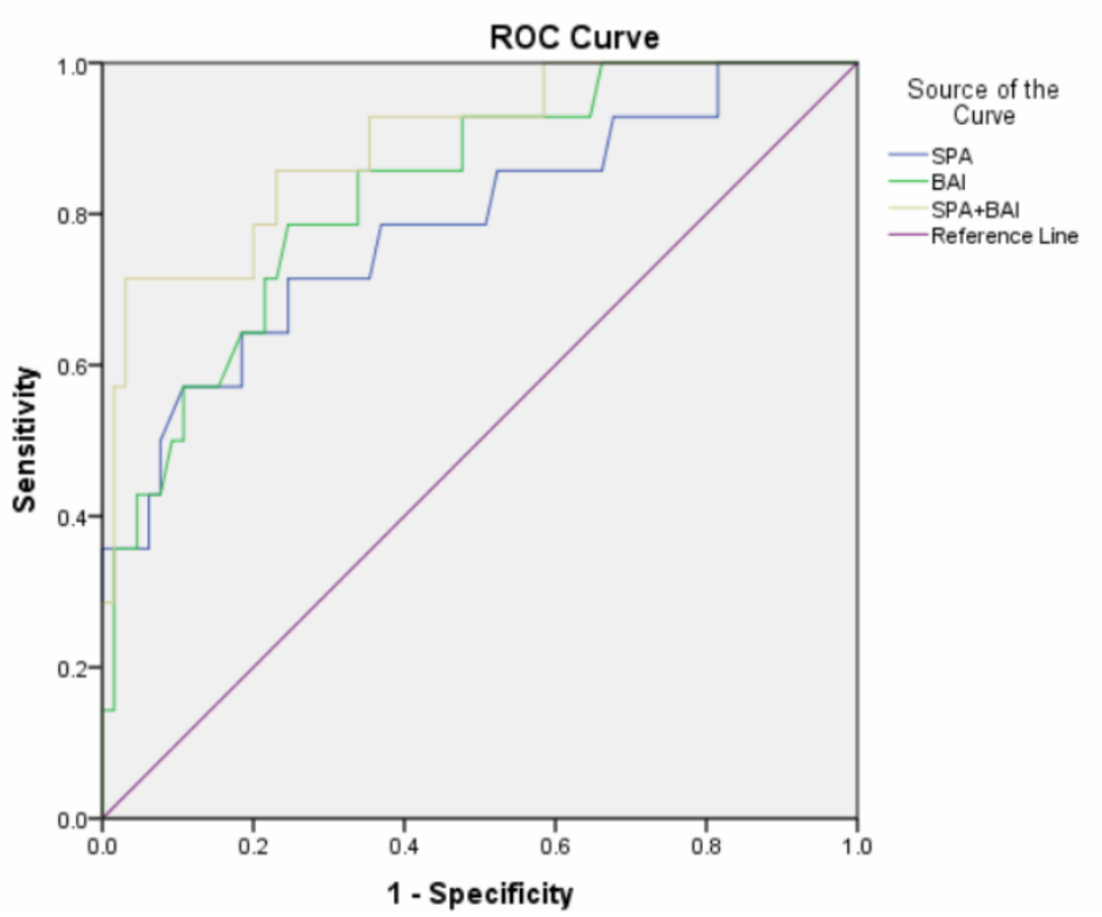

Figure 3.12 Patient-based AUC analysis of ultrasound estimating X-ray Cobb ≥ 20 °. i) green line: using USSPA; ii) yellow line: using BAIsp; iii) blue line: using USSPA and BAIsp together. The purple line is served as a reference line to indicate AUC=0.500.

For the Poisson regression analysis, the BAIsp values were first conducted one-sample Kolmogorov-Smirnov test to confirm the nonparametric Poisson distribution with $p<0.05$. XCA referral decision was selected as factor and USSPA as covariate in the predictors; and BAIsp was selected as the dependent variable in the response. The goodness of fit test was performed, with value/degree of freedom reported of 519.59 in Pearson Chi-square test; which indicated that the distribution of BAIsp values was skewed and not follow normal distribution. Omnibus test reported $p<0.05$, which indicated that the prediction involved BAIsp was significantly different from null hypothesis. Test of model effects reported USSPA $p=0.32$ and XCA referral decision $p<0.05$, which indicated that USSPA has not have significant effect while XCA referral decision have discernible effect on BAIsp prediction. **Table 3.3** showed the details of the parameter estimates for Poisson regression analysis in order to understand the predictive contribution of BAIsp. BAIps reported additional predictive power to referral decision at 0.342 (exponential) with $p<0.05$.

Table 3.3 Parameter Estimates for Poisson Regression Analysis

Parameter Estimates

			95% Wald Confidence Interval		Hypothesis Test				95% Wald Confidence Interval for Exp(B)	
Parameter	B	Std. Error	Lower	Upper	Wald Chi-Square	df	Sig.	Exp(B)	Lower	Upper
(Intercept)	7.240	.0155	7.209	7.270	218189.953	1	.000	1393.643	1351.944	1436.628
[Referral_Decision=0]	-1.072	.0106	-1.093	-1.052	10145.887	1	.000	.342	.335	.349
[Referral_Decision=1]	0[a]	.	.	.	.	.	.	1	.	.
SPA	.001	.0009	-.001	.003	.991	1	.320	1.001	.999	1.003
(Scale)	1[b]									

Dependent Variable: BAI
Model: (Intercept), Referral_Decision, SPA

a. Set to zero because this parameter is redundant.

b. Fixed at the displayed value.

Moreover, the ultrasound and X-ray patient-based scoliosis specialist referral decisions could be investigated using a confusion matrix (**Table 3.4*)***. The performance of the ultrasound-based parameters (USSPA and BAIsp) estimating X-ray: sensitivity 57.1%, specificity 98.5%, PPV 88.9% and NPV 91.4%.

Table 3.4 Confusion matrix of ultrasound-based and X-ray referral status

	X-ray referral status			
Ultrasound based referral status	**Yes**	**No**	**Total**	**PPV & NPV**
Yes	8	1	9	**88.9%**
No	6	64	70	**91.4%**
Total	14	65	79	
Sn & Sp	**57.1%**	**98.5%**		

3.3.5. Discussion

The results of using ultrasound parameters (USSPA and BAIsp) to estimate X-ray scoliosis post-screening specialist referral decision were encouraging, with AUC=0.893 for curve-based analysis and AUC=0.892 for patient-based analysis. A high AUC indicated that the ability of the ultrasound method to distinguish between classes (referral positive and negative). When AUC approximate 1, there is a higher chance that the classifier could distinguish the positive class values from the negative ones; as more true positives (TP) and true negatives (TN) were detected than false positives (FP) and false negatives (FN). The AUC statistics indicated that ultrasound could help formulate the AIS referral decision similar to conventional X-ray-based method (Cobb ≥ 20 °), where referral required cases could be highly likely identified. In addition, the Poisson regression model further proved the predictive power of BAI for XCA decision referral at 0.342 ($p<0.05$); which demonstrated the usefulness of the BAI parameters in the screening analysis.

With sensitivity>50%, specificity>95%, together with PPV=88.9% and NPV=91.4%, the chance of misdiagnosis was comparably low. With such context, the clinician would be very confident (around 90%) that the ultrasound referral positive cases were true positive cases that required further scoliosis specialist consultation; where the ultrasound referral negative cases were true negative cases that no follow-ups needed in the near future. Additionally, the clinician was with high confidence that the patients would not be exposed to unnecessary testing or delay in appropriate therapy. (Cardinal et al. 2016).

Admittedly, the sensitivity from the study is moderate (sn=57.1%). After careful investigation of the false negative (FN, n=6) cases, we have observed that these cases were with Cobb around 20°, with variations less than 3°. Since the referral decision is binary, Cobb<20° curves (e.g., Cobb=18°) would be marked as specialist referral negative, which caused the discrepancy against the X-ray referral decision. However, the intra- and inter-observer variability for Cobb angle measurement was between 4° and 8° (Gstoettner et al. 2007). Such variation did affect our binary ultrasound / X-ray referral decision making process; but it was inevitable to relatively mild AIS cases.

From **Table 3.4**, we can conclude that 88.6% (70 subjects, NPV=91.4%) could avoid unnecessary X-ray. It implied that using ultrasound parameters in AIS screening could reduce the unnecessary X-ray exposure to the vast young population, whose cancer inducement and other risk factors could not be simply neglected (Hoffman et al. 1989). The use of radiation-free ultrasound-based AIS screening supplement is very meaningful for the sake of the health of the schoolchildren.

The limited sample size may be a constraint of the study, the percentiles of the statistics could be more meaningful when validating with a larger cohort. The future work will be focus on retrospectively screening for a considerably large sample among the adolescents / schoolchildren. In addition, admittedly, we had not included the intra- and inter-observer variability in the ground truth measurement of the X-ray Cobb, since such variation could affect the binary decision making of scoliosis specialist referral. In our next step, we will incorporate the intra- and inter-observer reliability in the large cohort of AIS screening study.

3.4 Summary

This chapter focuses on elaborating the validity and application of the BAIsp method derived from spinous process through 3D ultrasound imaging. Previous studies on Scolioscan ultrasound spinous process measurements were reviewed for the validity and reliability. Two sub-sections introduce the performance of using BAIsp to classify mild AIS curves and evaluate the screening referral decisions.

For the curve classification study, 90 mild AIS patients underwent both 3D ultrasound and X-ray scanning on the same day. For each case, a clinician measured Cobbs and denoted major curve as ground truth. The curve classification was coded to a modified Lenke classification for mild cases (m-Lenke). The results of 3D ultrasound classification were evaluated with the X-ray. It was shown that 70.1% of the subjects had identical curve classification results and 72.0% had the correct major curve detection. Lumbar-dominated curves had distinctive performance ($p = 0.91$, $r = 0.91$) against others. The study demonstrated the possibility of a 3D ultrasound-based method for mild AIS curve classification. The discrepancies could be partially explained by the limitations of the ultrasound scanning in proximal thoracic region. Subsequent studies will validate the proposed method with a larger cohort.

For the screening referral study, the main objectives are: to evaluate whether using ultrasound could play a role similar to X-ray imaging for specialist referral decision making; to reduce unnecessary X-ray exposure in current AIS screening procedure. The same batch of mild AIS classification patients were included. Both curve-based analysis and patient-based analysis demonstrated very promising specialist referral decision classification with AUC=0.893, $p<0.001$ and AUC=0.892, $p<0.001$, respectively. With sensitivity>50%, specificity>95%, together with PPV=88.9% and NPV=91.4%, the chance of misdiagnosis was comparably low. 88.6% (70 subjects, NPV=91.4%) could avoid unnecessary X-ray. It implied that using ultrasound parameters in AIS screening could reduce the unnecessary X-ray exposure to the vast young population, whose cancer inducement and other risk factors could not be simply neglected (Hoffman et al. 1989). The use of radiation-free ultrasound-based AIS screening supplement is very meaningful for the sake of the health of the schoolchildren. In our next step, we will incorporate the intra- and inter-observer reliability in the large cohort of AIS screening study.

CHAPTER 4. BAI METHOD USING TRANSVERSE PROCESS AND RELATED FEATURES FROM ULTRASOUND IMAGING

4.1 Semi-automatic Ultrasound Curve Angle (UCA) Measurement for Adolescent Idiopathic Scoliosis

Ultrasound curve angle (UCA) method, which uses transverse process and related features, has demonstrated a closer correlation (Lee et al. 2020) to clinically gold-standard X-ray Cobb angle, compared to the first published spinous process angle (USSPA) (Zheng et al. 2016). Brink et al. (2017) attempted to identify most tilted transverse processes in the coronal spine VPI images to estimate XCA, and demonstrated higher correlation in contrast to USSPA. Lee et al. (2020) extended the concept to a larger cohort, also proved the value of involving spinal transverse process features in the ultrasound imaging. The results of the spinal transverse process feature inspired studies, including Brink et al. 2017, and various earlier validation studies using USSPA are presented in the following table (**Table 4.1,** Zheng et al. 2016, Brink et al. 2017, Wong et al. 2019, Lee et al. 2020, Lee et al. 2021). It could be judged from **Table 4.1** that using spinal transverse process features (manual UCA or equivalent methods) achieved higher correlation with XCA compared with traditional USSPA method (Brink et al. 2017, Lee et al. 2019, Lee et al. 2020, Lee et al. 2021). These observations showed that the orientation of the lines drawn on the bilateral transverse processes on ultrasound images resembled that on the endplates of the vertebrae on radiographs.

Except for the fact that USSPA and XCA measure from different plane, USSPA could suffer from the spinous process distortion and the axial rotation of spine (Goldberg et al. 2008). The interaction between the spinous process and paraspinal muscles could also affect the shape of spinous process, whose acoustic shadow contributes to USSPA. The difference of biomechanical characteristics of the paravertebral muscle on concave and convex side of the scoliotic curve resulted to the skewness of the spinous process, which deviated from its normal position (Liu et al. 2019). On the contrary, the transverse process and pertinent features and vertebral body are in the same anterior-posterior coronal plane for scoliotic curve measurement (Lee et al. 2020, Lee et al. 2021), which reduced the gap as that of USSPA and XCA.

Table 4.1 Summary of the performance (in terms of R square) of ultrasound-based scoliotic angle measurements compared with X-ray Cobb from earlier literature Zheng et al. 2016, Brink et al. 2017, Wong et al. 2019, Lee et al. 2020, Lee et al. 2021). Studies that involved spinal transverse process features (UCA or equivalent*) outperformed USSPA.

* The author revealed no detailed process of identifying transverse process.

Authors	Journal	Number of patients	Pearson's Correlation (r) Thoracic	Pearson's Correlation (r) Lumbar	Ultrasound Angle
Lee et.al(2021)	15th SOSORT	50	0.945	0.940	UCA
Lee et.al(2020)	15th SOSORT	114	0.944	0.933	UCA
Brink et.al(2017)	Spine	33	0.996	0.992	UCA*
Wong et.al (2019)	Ultrasound in Med.& Biol.	952	0.873	0.740	USSPA
Zheng et.al(2016)	Scoliosis and Spinal Disorders	49	0.883	0.849	USSPA

The following image **Figure 4.1** showed how UCA could be derived from respective ultrasound spinal thoracic and lumbar region. Transverse process is identified through different manual object detection process in order to conduct UCA measurement.

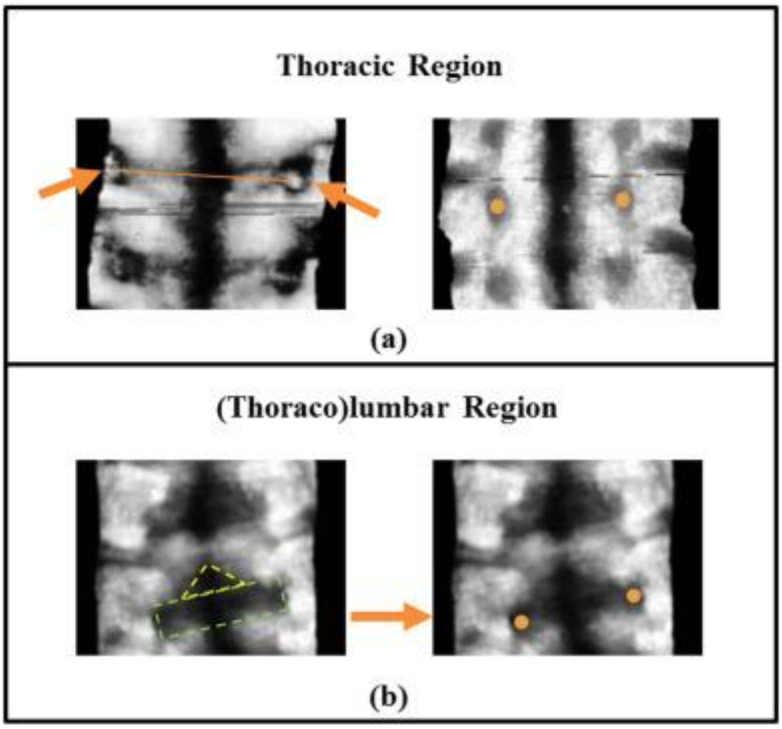

Figure 4.1 Diagrams illustrating how points for line placements were assigned to acquire UCA: **a)** For thoracic region, if a white dot, which corresponded to the echo of a transverse process, could be seen, the center of the white dot will be used to place the point (left); If no white dot could be observed, the center of the black region, which corresponded to the shadow of a transverse process, will be used to place the point (right); **b)** For (thoraco)lumbar region, the lump shadow would be considered as a combination of a triangle (yellow dotted line) and a rectangle (green dotted line) (left). Dots will be placed at locations proximal to the center of the bilateral sides of the rectangle (right). UCA: Ultrasound Curve Angle. (Lee et al. 2021)

The visualization of UCA measurement was drawn by side of XCA for a direct comparison in **Figure 4.2**.

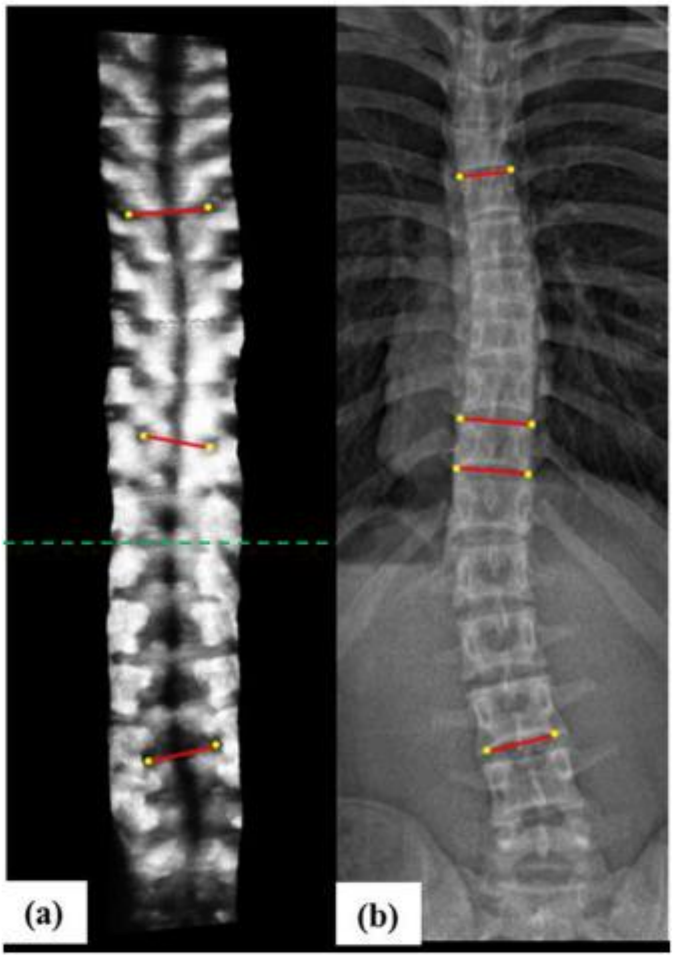

Figure 4.2 Diagram illustrating the **(a)** UCA measured on coronal ultrasound image and **(b)** Cobb angle measured on coronal X-ray images. The pair of T12 ribs was first identified to distinguish the rest of the vertebrae level (green dashed line). For cases with the most tilted vertebrae on T12 or above, line was placed though the center of the bilateral transverse processes echoes or shadows, whereas for cases with the most tilted vertebrae below T12, the line was drawn though the center of the bilateral superior articular processes shadows, which composed of the widest bilateral part of the lump. (Image reproduced from Lee et al. 2021)

This chapter starts with the introduction of a semi-automatic method for UCA measurement from transverse process and pertinent anatomical structures; then explore the performance of BAI calculation from the semi-automatic UCA method and observe the respective implications on the mild AIS curve classification results.

4.2 Semi-automatic Scoliosis Angle Measurement Using Ultrasound Transverse Features

4.2.1 Subjects and data acquisition

This study involved 100 subjects that has been diagnosed with adolescent idiopathic scoliosis (AIS). The demographics of the subjects were 19 males and 81 females, 15.0 ± 1.9 years, average Cobb angle 25.5 ± 9.6°. This batch of cohort was retrospectively recruited from previous Scolioscan validation research (Zheng et al. 2016), with ethical approvals from the Chinese University of Hong Kong (CREC Ref.No. 2015.463). All these patients were recruited and assessed in the Department of Orthopaedics and Traumatology of the Chinese University of Hong Kong. Two spine imaging modalities were used for the study: a low-dose X-ray EOS imaging system (EOS Imaging, France) and a radiation-free Scolioscan 3D ultrasound imaging system (Model SCN801, Telefield Medical Imaging Ltd, Hong Kong) using a linear probe (central frequency of 7.5 MHz and width of 7.5 cm). Each subject underwent both Scolioscan ultrasound and EOS X-ray scanning on the same day in standing posture. The subjects were instructed to stand with arms rested naturally in ultrasound scanning. The average scanning time for ultrasound assessment was 30-40 seconds while around 20 seconds for EOS X-ray scanning. The scoliosis angle measurements of various methods were performed after data acquisition (Zhou et al. 2017, Lee et al. 2020).

4.2.2 Ultrasound curve angle (UCA) and other scoliotic angle measurement methods

In order to validate our semi-automatic method, manual X-ray Cobb measurement together with ultrasound transverse angle measurement were included for a fair comparison. A designated spine imaging analyst was recruited for conducting measurements and providing respective annotations of all stated methods. To facilitate the ease of elaboration in the subsequent text, two terms were used: the X-ray Cobb angle (XCA) method and the ultrasound curve angle (UCA) method. XCA method represented the manual angle measurement using Cobb angle on X-ray image; while UCA method indicated the angle measurement using ultrasound transverse angle on 3D ultrasound volume projection image (VPI) (Lee et al. 2020). To avoid confusion, UCA methods are further divided into manual UCA and semi-automatic UCA depending the levels of labor input. The manual UCA method describes that the UCA measurement are conducted on free-hand while the semi-automatic UCA method (this method) implies that the angle measurement are based on drawn transverse features from 3D ultrasound VPI.

XCA method has been widely practiced and recognized as the gold-standard for quantifying the severity of scoliosis in clinical (Morrissy et al. 1990). XCA method required drawing lines to identify the most tilted vertebras as the on both ends of the curves diagnosed upon the coronal X-ray film of spine (**Figure 4.3a**). Previous works had demonstrated that manual UCA method (**Figure 4.3b)** had better correlation with XCA method than ultrasound spinous process angle measurement (USSPA) (Brink et al. 2017, Lee et al. 2020).

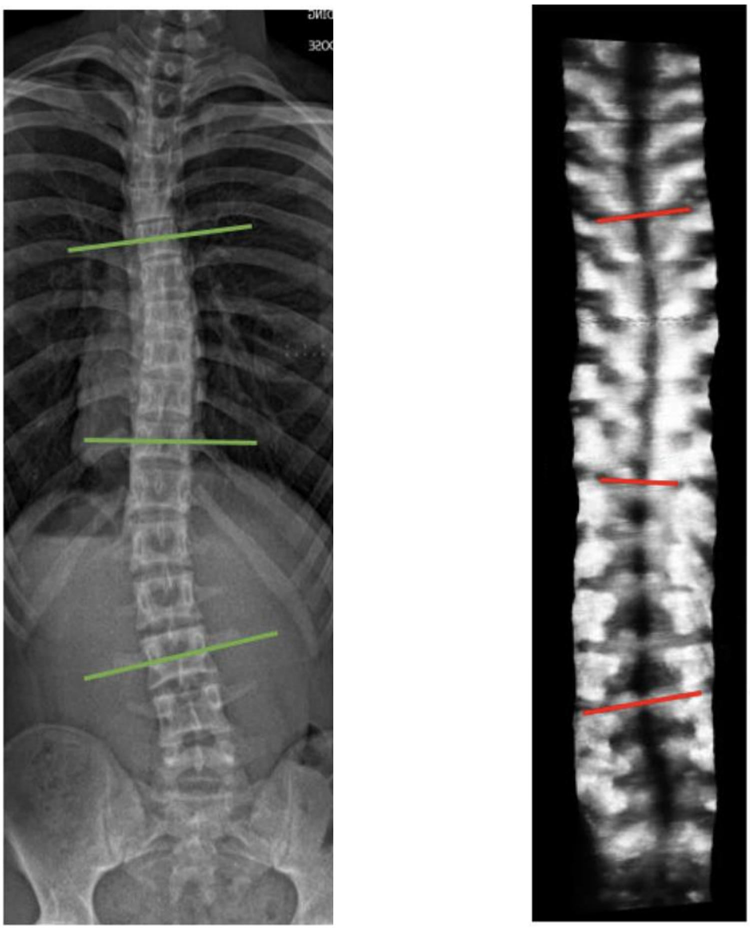

(a) **(b)**

Figure 4.3 (a) An example of X-ray Cobb angle (XCA) method* on coronal X-ray imaging, lines were drawn to cross the middle of the most tilted vertebra to characterize a scoliotic curve. Two curves were presented, thoracic curve (T6-T11) and thoracolumbar curve (T11-L3). * This is a revised XCA method in order to directly compare with UCA method. Lines were drawn passing through the midpoint of each investigated vertebra; **(b)** an example of ultrasound cobb angle (UCA) on ultrasound coronal VPI image, lines were drawn linking the centers of transverse processes in thoracic region and passing through the lower boundary of lumps in lumbar region to characterize a scoliotic curve. Two curves were presented, thoracic curve (T6-T11) and thoracolumbar curve (T11-L3). Both scans were taken on the same subject on the same day.

As the integral vertebral body could not be properly observed in ultrasound imaging, XCA method was impossible to translate its application in the ultrasound setting. Consequently, alternate landmarks were carefully selected to mimic the similar inclination of the tilted end vertebras of scoliotic curves, as in X-ray imaging. Scoliosis mainly deforms the normal thoracic and lumbar curvature of the spine. Since the thoracic region and lumbar region of the spine are distinct from each other, the anatomical features considered for UCA measurement are different. In the thoracic region, lines were drawn passing through the centers of the pairs of the thoracic transverse processes from the upper and lower end-vertebra of the scoliotic curves (**Figure 4.4a** & **Figure 4.4b)**.

As mentioned, the bony features could not be observed from ultrasound imaging; the acoustic signal has less chance to penetrated dense objects. The upper and lower end-vertebra thoracic transverse processes were manually identified by the bony shadow of the respective structures from the coronal ultrasound VPI image.

Distinct from coronal X-ray imaging, the lumps observed from the lumbar region in ultrasound imaging are the combined shadow of the laminae and the inferior articular processes of the superior vertebrae and the superior articular processes of the inferior vertebrae *(***Figure 4.4a** & **Figure 4.4c)**. Commonly, six lumbar lumps could be found in coronal ultrasound VPI images (Lee et al. 2020). Specifically, five lumbar vertebrae together with the T12 laminae and the upper part of the first sacral vertebrae (S1) constitute the lumps. The upmost lumbar lump is formed by stacking the T12 laminae and the L1 articular processes; the last lumbar lump (usually 6th) is formed by combining the L5 laminae and the upper part of the S1 vertebrae; the rest N^{th} lump is formed by the L(N-1) laminae and the articular process of the L(N) vertebrae (N=2-5). For special cases, when subject possesses a 6^{th} lumbar vertebra: an additional lump which comprises of the L5 laminae and the L6 articular processes would be inserted as the second last lump. In the lumbar region, lines were manually drawn passing through the lower boundary of the most titled lumbar lumps to indicate the deformity of the lumbar curvature.

The contours on the mentioned anatomical features that shown in **Figure 4.4a** were not drawn on the ultrasound image by the manual UCA method in practice: they were merely shown as the decision-making process for the image analysts on locating the desirable landmarks in their mindsets. In manual UCA measurement, the investigator simply drew lines from the suspected most tilted transverse features for UCA calculation.

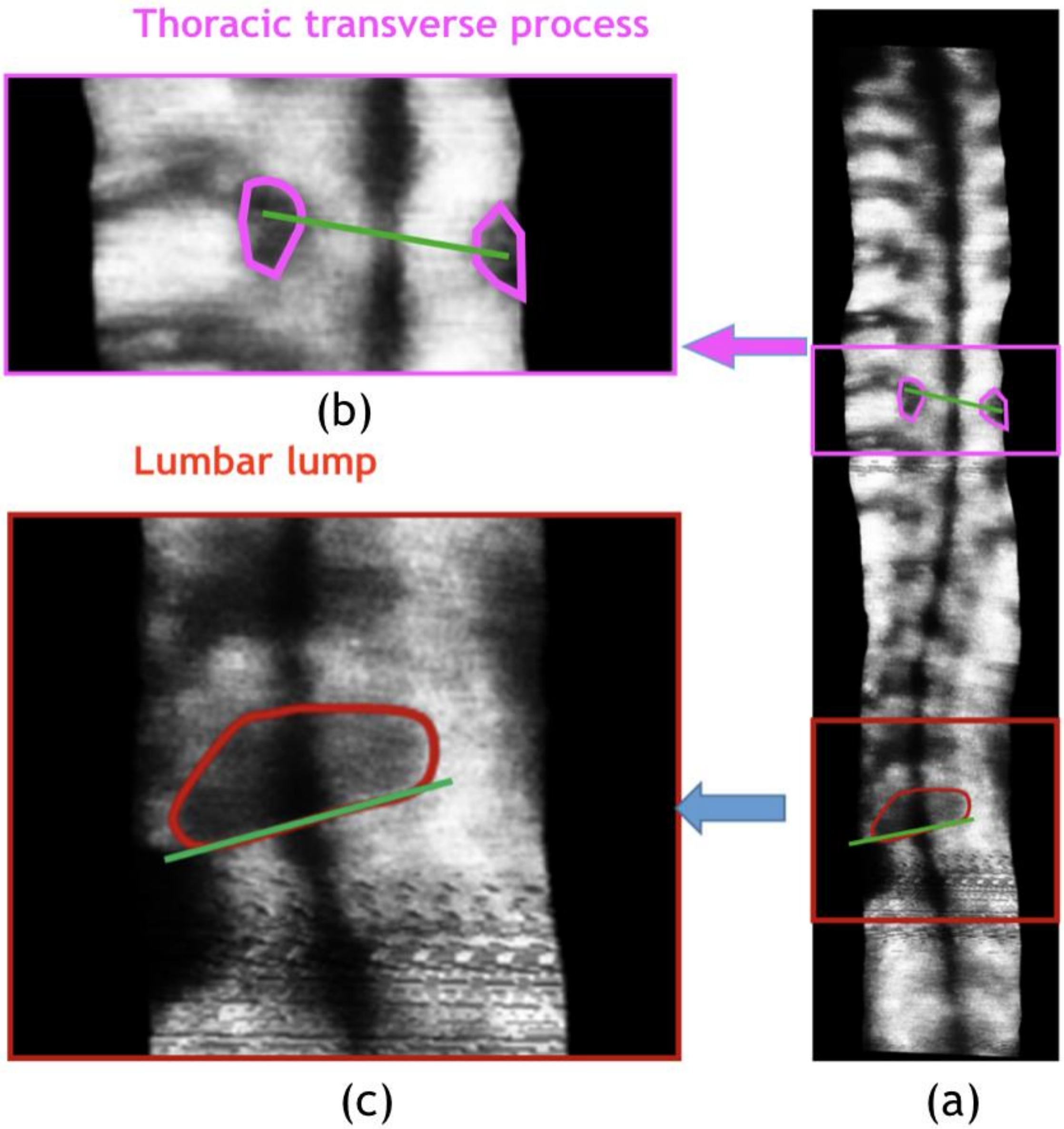

Figure 4.4 (a) Illustration of semi-automatic transverse process-related features used by the Ultrasound Cobb Angle (UCA) method. The contours are used in UCA calculation. **(b)** An example of the contour showing a pair of thoracic transverse process. **(c)** An example of the contour showing a typical lumbar lump (combined shadow of the laminae of the superior vertebrae and the articular processes of the inferior vertebrae). The principle of the manual UCA method is a reiteration from Lee et al. 2020.

In contrast with the XCA method and manual UCA method which are manual procedures, our proposed method is divided into two stages: 1) Manual spinal transverse process-related features identification and contouring; and 2) Automatic angle measurement based on manual contoured masks. In the first stage, inspired by the manual UCA method, the identification of transverse process-related features was similar to manual contouring (**Figure 4.5a** & **Figure 4.5b**). Instead of only locating the most tilted transverse processes pairs, semi-automatic UCA method required drawing all transverse process-related features. This step required clinician's involvement in determining the related important spinal transverse-related features. Prior training for the clinician for identifying relevant features from different depths of the ultrasound VPI images was needed. Similarly, pairs of thoracic transverse processes (in green) were drawn for subsequent comparison of the tilting angles of each pair. Lumbar lumps (in red) were drawn for evaluating the thoracolumbar/lumbar angles. In addition, ribs (in blue) were drawn to provide reference of vertebrae levels. Due to the limitations of ultrasound scanning around the cervico-thoracic region, which may affect the upper thoracic region imaging (Folsch 2012). Ribs are also contoured for vertebrae levels referencing. For example, 12th rib commonly points downwardly in spine ultrasound coronal images; it could be used to navigate through the VPI image. In the second stage, the manual contours were forwarded to the program for automatic filling to create masks for subsequent analysis. The color code for the mask was adhere to the contours: thoracic transverse processes (green), ribs (blue) and lumbar lumps (red) in **Figure 4.5c**. The semi-automatic UCA measurement results would be prompted for each scoliotic curve detected, as the output visualization (**Figure 4.5d)**.

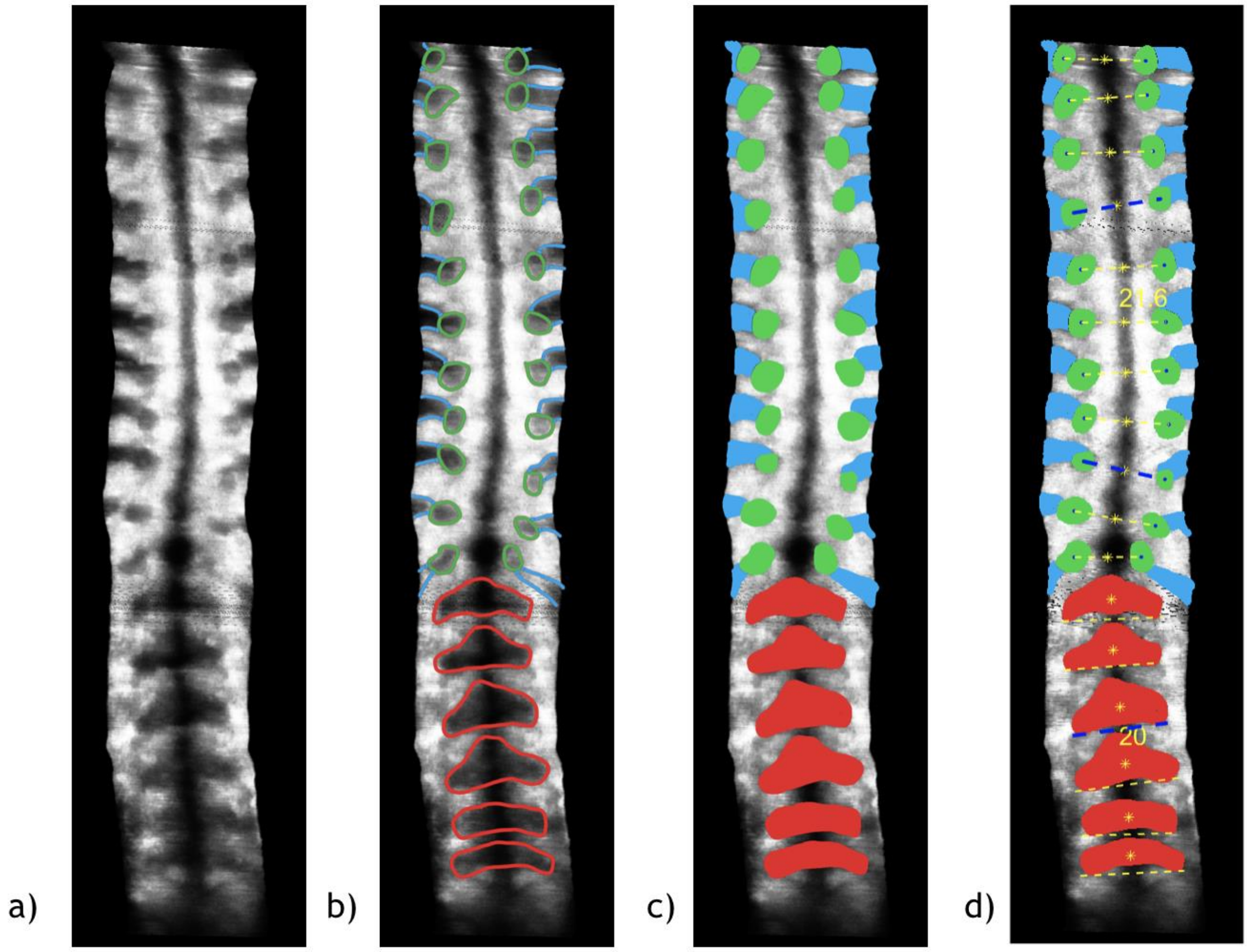

Figure 4.5 Illustration of the process of the proposed semi-automatic UCA method using transverse process-related features. **(a)** Raw ultrasound VPI image; **(b)** spinal transverse process-related features identification (contours were drawn manually): green - thoracic transverse process; blue - rib; red - lumbar lump; **(c)** transverse process-related features mask generation for image processing purpose; **(d)** automatic angle calculation based on the masks.

The program ran in parallel for each mask, and the overall schematic diagram is shown in **Figure 4.6**. After integrating the analysis from different masks, the curve characteristics (number of curves, number of level and start/end level of each curve) could be established; and the transverse process angle could be calculated accordingly.

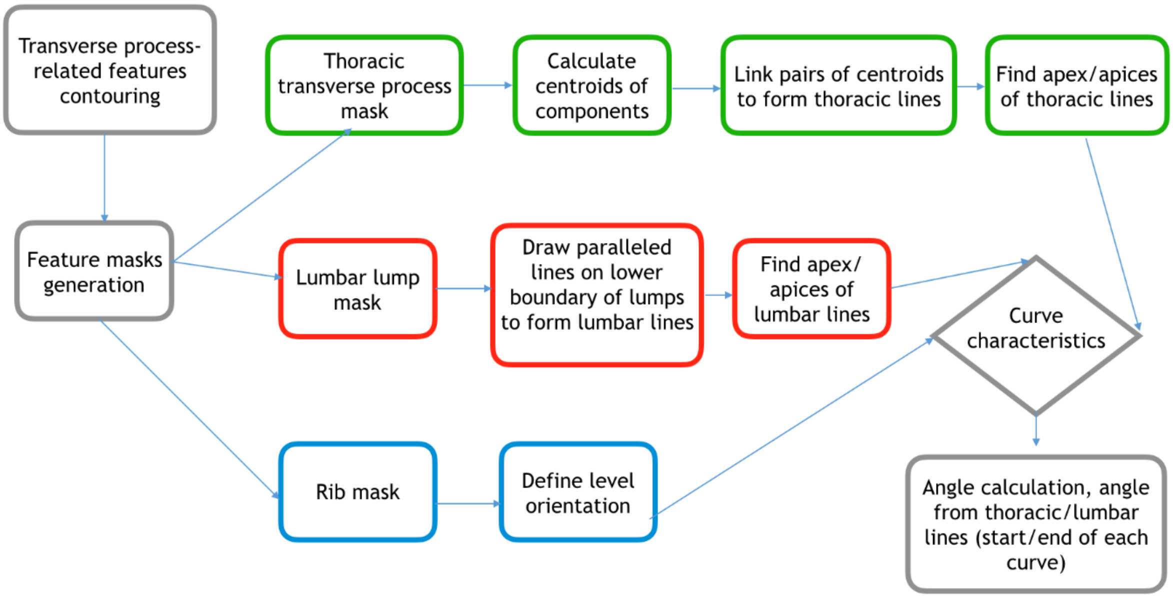

Figure 4.6 Schematic diagram of the automatic program (the proposed semi-automatic UCA method, Stage 2) for computing angles based on transverse process-related features. The block diagrams are color coded according to the respective color of masks (Thoracic transverse process: green; Lumbar lump: red; Rib: blue. Each mask was processed in parallel until the curve characteristics (number of curves, start/end levels) were understood by the program; then the angles were automatically calculated.

4.2.3 Statistical analysis

Various statistical analyses were involved for this study using SPSS 25.0 for Mac (SPSS Inc., Chicago IL, USA). The proposed semi-automatic UCA method were investigated against the manual UCA and conventional XCA methods using linear correlation for thoracic curves, thoracolumbar/lumbar curves and combined curves, respectively. Specifically, Linear regression equations with intersections were studied. Commonly, correlation efficient between 0.25 and 0.50 refers to a poor correlation; 0.50 to 0.75 indicates moderate/good correlation; and 0.75-1.00 demonstrates very good/excellent correlation (Dawson et al. 2004). In order to validate the effectiveness of the proposed semi-automatic UCA method, its correlation with manual XCA should be at least comparable to manual UCA. Bland-Altman method was applied to test the agreement between the semi-automatic UCA and manual UCA or XCA method, respectively. In order to investigate the differences in agreement for the semi-automatic UCA method against other methods, the mean absolute differences (MAD) were computed. The MADs of the mentioned three methods were grouped in pairs for the paired t test. The significance level was set at 0.05.

4.2.4 Results

From the ensemble cohort of 100 AIS subjects (Age: 15.0 ± 1.9 years, Gender: 19 M & 81 F, Cobb: 25.5 ± 9.6°), for the average of thoracic angles: XCA, UCA, and semi-automatic UCA methods obtained results of 25.8 ± 10.9°, 25.6 ± 11.1°, 26.7 ± 11.4°, respectively; for the average of thoracolumbar/lumbar angles: XCA, UCA, and semi-automatic UCA methods obtained results of 25.1 ± 8.4°, 23.2 ± 8.2°, 23.3 ± 8.6°, respectively; for the average of combined thoracic and lumbar angles: they were 25.5 ± 9.6°, 24.3 ± 9.7°, 24.9 ± 10.1°, respectively.

Very good to excellent correlation between the proposed semi-automatic ultrasound-based UCA measurement method and manual UCA / XCA method. For semi-automatic UCA measurement with manual UCA, correlation coefficient R^2=0.866, with thoracic angles R^2=0.921 and lumbar angles R^2=0.780, respectively (**Figure 4.7**); for semi-automatic method with XCA, correlation coefficient R^2=0.815, with thoracic angles R^2=0.857 and lumbar angles R^2=0.787, respectively (**Figure 4.8**).

The results had confidently shown that the performance of semi-automatic UCA method were as good as manual UCA when estimating XCA measurement results. On the other hand, we had observed that ultrasound-based transverse process-related features angle measurements (manual UCA and semi-automatic UCA method) were slightly larger than XCA, the transformation coefficients were between 0.86-0.93. Additionally, the results of the new method were very close to the results of manual UCA, with the transformation coefficient of 0.92.

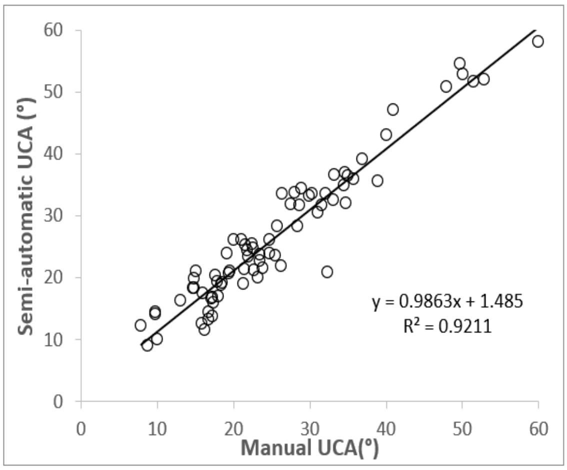

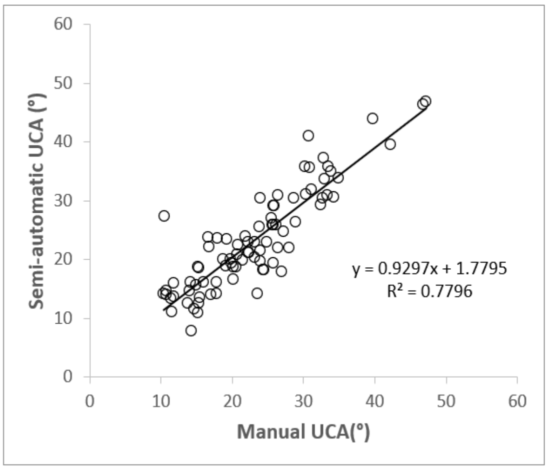

(a) **(b)**

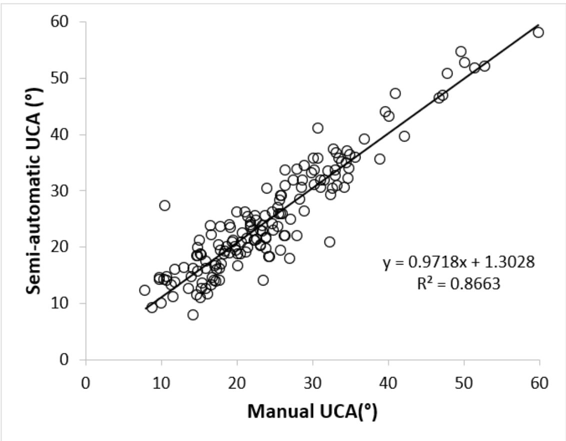

(c)

Figure 4.7 Correlation and linear equations between manual calculated Ultrasound Cobb Angle (UCA) (x) and the proposed semi-automatic UCA method (y). **(a)** Thoracic angles; **(b)** thoracolumbar/lumbar angles; **(c)** combined angles of **(a)**&**(b)**.

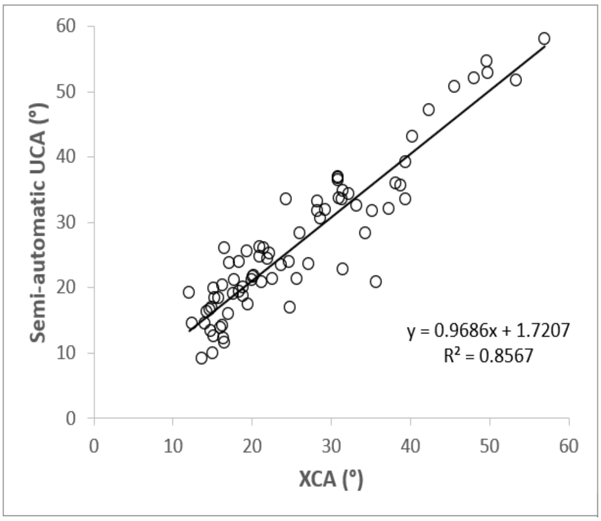

(a)

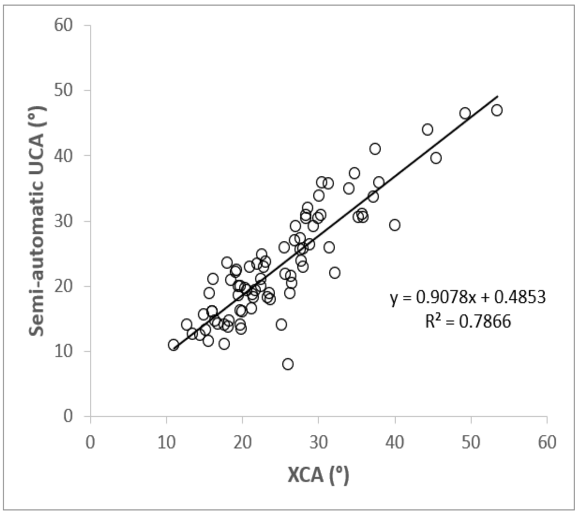

(b)

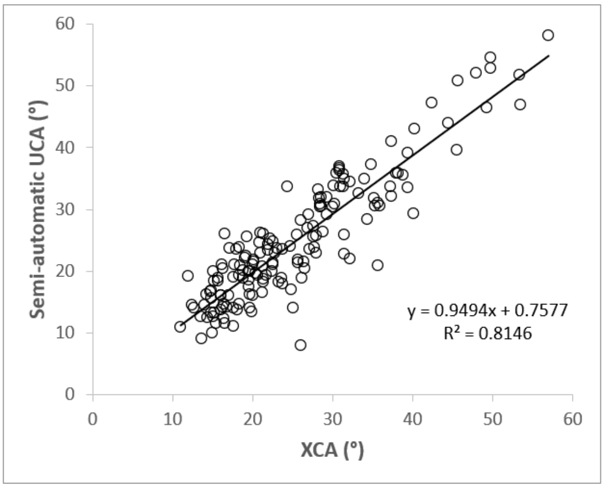

(c)

Figure 4.8 Correlation and linear equations between manual measured X-ray Cobb Angle (XCA) (x) and semi-automatic Ultrasound Cobb Angle (UCA) method (y). **(a)** Thoracic angles; **(b)** thoracolumbar/lumbar angles; **(c)** combined angles of **(a)**&**(b)**.

The Bland-Altman plot also indicated a good agreement between pairs of the semi-automatic method with manual UCA and XCA corrected with the linear regression equations (**Figure 4.9**). Regarding the MADs for measurement results upon validation process, no clinical difference was found. MADs of the semi-automatic UCA method and manual UCA: 2.9 ± 2.4°, range 0-16.8° (thoracic angles: 2.7 ± 2.1°, range 0-11.4°; lumbar angles: 3.0 ± 2.7°, range 0.1-16.8°); MADs of the semi-automatic UCA method and XCA: 3.5 ± 2.7°, range 0-18.1° (thoracic angles: 3.6 ± 2.5°, range 0-14.8°; lumbar angles: 3.4 ± 2.9°, range 0-18.1°).

(a)

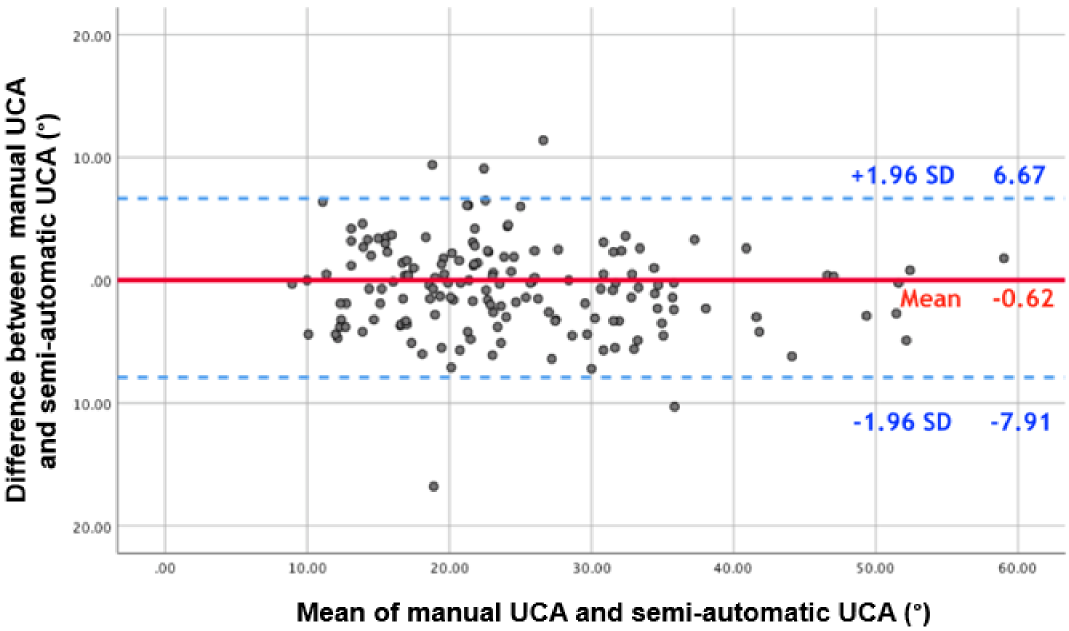

(b)

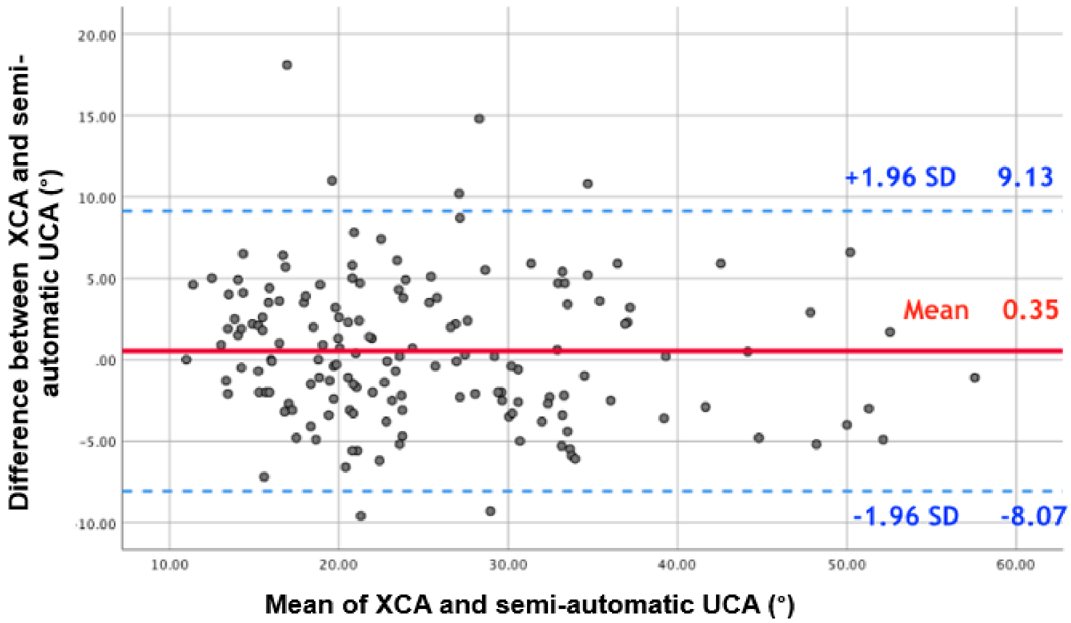

Fig.4.9 Bland-Altman plots indicate the differences between the pairs **(a)** manual UCA and the proposed semi-automatic UCA method; (b) XCA and the proposed semi-automatic UCA method corrected with the linear regression equations for all angles (combination of thoracic and lumbar angles).

4.2.5 Discussion

It had demonstrated promising results using spinal transverse process-related features to estimate scoliotic angles, when compared with XCA from X-ray radiography: ultrasound-based semi-automatic method R^2=0.815, with thoracic angles R^2=0.857 and lumbar angles R^2=0.787, specifically (**Figure 4.8**). MADs were smaller than 5°, which indicates no significant clinical difference between ultrasound and X-ray measurements on the same cohorts. The agreement of the inter-methods of scoliotic angle measurement implied the feasibility of complimentary ultrasound imaging for unnecessary X-ray exposure. These findings validated and further strengthened the results obtained from the pioneer study of manual UCA measurements with main thoracic curve $R^2 \geq 0.892$ and lumbar curve $R^2 \geq 0.872$ (Lee et al. 2020). Strong correlations were established between transverse process-related features-based UCA method and XCA method. Compared with the USSPA method from the cornerstone Scolioscan validation study: R^2=0.760, with thoracic angles R^2=0.780 and lumbar angles R^2=0.721 against XCA (Zheng et al. 2016) and a large-scale Scolioscan research upon 952 subjects with thoracic angles R^2=0.762 and lumbar angles R^2=0.548 against XCA (Wong et al. 2019); transverse process and accompanied landmarks indeed showed a better correlation with XCA. The clinical significance of the UCA method was to make use of the transverse process angle measurements to supplement the conventional Scolioscan USSPA method in AIS management and therefore reduce the use of X-ray in the course of scoliosis development or progression. Also, the reduction of X-ray exposure was very meaningful in scoliosis screening process; as normal subjects could avoid unnecessary radiation exposure, which could be harmful to their health (Lam et al. 2019).

The semi-automatic UCA method also demonstrated comparable results with manual UCA method. These two methods both involved using transverse process-related features from spine ultrasound imaging on the coronal plane. The process of these transverse process-related features identification required labor input and in-field expertise. The training of the users/designated personnel for the labelling procedure involved a brief orientation from an ultrasound expert with essential knowledge of spine anatomy. The angle measurement part could be processed by the software automatically once the user/designated personnel grasp the tactics for contouring transverse process-related features. Bearing such insights, semi-automatic UCA method saved substantial manually intensive efforts in the tedious angle measurements steps, where users only required to circle the relevant transverse process features from the coronal ultrasound imaging; and the program itself would compute and report the results. As previously discussed, the semi-automatic method also showed very good correlation with XCA (R^2=0.815). Since the prior knowledge for the semi-automatic UCA method was given by the same expert who completed manual UCA in parallel, we could understand that the performance of the semi-automatic UCA method was constrained by the manual UCA method. From the comparison with manual UCA results, we can observe that very close correlations R^2=0.866, with thoracic angles R^2=0.921 and lumbar angles R^2=0.780 (**Figure 4.7*).*** MADs were smaller than 5°, which indicates no significant clinical difference between manual UCA and semi-automatic UCA in angle measurements. Therefore, it could be judged that the semi-automatic UCA method was clinically meaningful. It reduced human efforts and possibly lessened human errors in scoliotic angle measurement after manual identification of the transverse process-related features. At the same time, the semi-automatic UCA results were comparable upon manual ones. The semi-automatic method further suggested that as long as the segmentation of the transverse process-related features could be extracted, the angle measurements performance could be guaranteed. The future direction of the UCA method is to generate segmentation of the transverse process-related features in an operator-free manner as of manual contouring.

Results from UCA method appeared to be slightly smaller than XCA from all measurements; with transformation coefficients were between 0.908-0.969 (**Figure 4.8**)*.* XCA were slightly underestimated by the transverse angles from ultrasound imaging. Such consistency indicated that the cause needed to be sought from spinal anatomy. (Lee et al. 2020) Both transverse process and spinous process are posterior structure while vertebra body itself that projected on coronal plane is anterior structure. In light of this difference, UCA and XCA are harvested from distinct bony landmarks of the spine. Hence, linking the tips of a pair of transverse process is differently angulated compared with projecting the vertebra body arc (Louis 2012), which could be partially explained the consistent underestimation of XCA. In our future studies, large-scale validation research would be a good direction to prove the discovery.

Implied from the semi-automatic UCA method, major limitations came from the prefix 'semi-automatic'. The program still required manual input in transverse process-related features identification and labelling, which relied on the subjective expertise of contouring on ultrasound images at Stage 1 of the semi-automatic method. Obviously, manually contouring each pair of transverse process-related features (both in thoracic and lumbar region) can document all necessary features and standardize the protocol, which could lower the risks of arbitrarily defining the transverse process angle (as in manual UCA) from mere observation. However, the performance of the semi-automatic method was still affected by manual UCA, when the two methods were conducted by the same expert. For our next step of the endeavor of UCA measurement, we would focus on intra-operator and inter-operator reliability on the manual contouring part of the semi-automatic UCA method.

Moreover, fully-automated version of the UCA method would be taken as the next milestone. Manual contouring of transverse process-related features still cost human efforts and inevitably suffered from human subjectiveness and errors. As described in **Figure 4.4*,*** transverse process features appear in distinct shapes from thoracic (circular disk) and lumbar regions (aggregated lumbar lump). Hence, the classification and contouring of transverse process-related features could be automated through deep learning (supervised learning). Our group had developed a bone feature segmentation model for the spine coronal ultrasound VPI images using a hybrid U-net; and showed promising possibilities of supervised deep learning in features contouring (Huang et al. 2020). The experience could be used in the fully-automated UCA measurement. With the continuous development of series of imaging processing methods and deep learning approaches, the next-generation of an automatic UCA method can be pervasive on AIS angle measurements and assist clinical decision-making process.

4.3 Mild AIS Curve Classification Using BAItp Method (Transverse Process)

4.3.1 Subjects and data acquisitions

This study retrospectively included 33 mild AIS subjects (16M and 17F; Age:13.2 ±1.5 years old; Cobb: 14.7±3.9) from a schoolchildren screening program in Hong Kong. This batch of cohort was retrospectively recruited from previous Scolioscan validation research (Zheng et al. 2016) with ethical approvals from the Chinese University of Hong Kong (CREC Ref.No. 2015.463). All these patients were recruited and assessed in the Department of Orthopaedics and Traumatology of the Chinese University of Hong Kong. The female to male ratio was half-half. The subjects were scanned and clinically assessed in the Department of Orthopaedics and Traumatology of the Chinese University of Hong Kong from October 9, 2017 to September 24, 2018.

Similar to BAIsp method that derived from spinous process: bi-modality assessment was conducted for BAItp method using two systems, involving low-dose X-ray EOS imaging system (EOS Imaging, France) and 3D ultrasound imaging system, Scolioscan (Model SCN801, Telefield Medical Imaging Ltd, Hong Kong) using a linear probe (central frequency of 7.5 MHz and 7.5 cm width). Each subject was performed both 3D ultrasound and X-ray scanning on the same day, including one standing EOS bi-planar X-ray with three ultrasound coronal images obtained under the postures of erect / standing anterior-posterior (AP), left and right bending. To ensure the subjects could fully stretch their arms to perform maximum bending on each side, an adjustable supporter was used in lateral bending to stabilize their postures during scanning. It is important that both the EOS X-ray scanning and Scolioscan ultrasound scanning were performed on the same day to control AIS progression variable. Information collected from the EOS X-ray imaging was used to verify the results harvested from the ultrasound-derived parameters.

4.3.2 Radiographic assessment on mild AIS curve classification

Since X-ray imaging still remains the gold standard for mild AIS curve classification, we referred to the same modified Lenke classification scheme (**Figure 4.10**), which has been explicitly explained in **Section 3.2.2**.

The modified Lenke classification system for mild AIS				
Curve type	Proximal Thoracic	Main Thoracic	Thoracolumbar/ Lumbar	Description
1	Nonstructural	Structural*	Nonstructural	Main Thoracic
2	Structural	Structural*	Nonstructural	Double Thoracic
3	Nonstructural	Structural*	Structural	Double Major
4	Structural	Structural*	Structural*	Triple Major
5	Nonstructural	Nonstructural	Structural*	Thoracolumbar/Lumbar
6	Nonstructural	Structural	Structural*	Thoracolumbar/Lumbar – Main Thoracic

** Major curve, with largest Cobb measurement*

Location of apex	
Curve	Apex
Proximal Thoracic	T2-T5
Main Thoracic	T6-T12 Disk
Lumbar	T12-L4

	Structural criteria (X-ray)	Structural criteria (Ultrasound)
Proximal Thoracic	Upper Tilt Angle (UTA) of curve ≥ 5°; Lower Tilt Angle (LTA) of curve ≥ 5°	BAI value; SPA reading from erect ultrasound image
Main Thoracic	Upper Tilt Angle (UTA) of curve ≥ 5°; Lower Tilt Angle (LTA) of curve ≥ 5°	BAI value; SPA reading from erect ultrasound image
Thoracolumbar/Lumbar	Upper Tilt Angle (UTA) of curve ≥ 5°; Lower Tilt Angle (LTA) of curve ≥ 5°	BAI value; SPA reading from erect ultrasound image

Figure 4.10 Details of the modified Lenke classification system for mild AIS (m-Lenke), adapted from Lenke et al. 2003. The structural criteria for X-ray imaging and ultrasound imaging are provided respectively.

4.3.3 Ultrasound-based BAItp method (Transverse Process) on mild AIS curve classification

Similar to the data acquisition in **Section 3.2**. The dynamics of spine can be traced and reconstructed from three scanning postures: erect (standing AP), left and right bending. For mild AIS, left and right bending profiles of a non-structural curve shows symmetrical pattern; while structural curve shows an asymmetrical lump in the specific region. Two BAI methods were called for comparison: 1) BAIsp method derived from spinous process and 2) BAItp method derived from transverse process and related features. In order to avoid redundancy, the description of the details of method 1) is omitted, which could be referred to in **Section 3.2**.

For the transverse process derived BAI method (BAItp), was also developed to indicate the presence of a possible location(s) of structural site(s) through the discrepancy of the bilateral spinal profiles, which was constructed from the interpolated midpoints of transverse process (in thoracic region) and lumbar lumps (in lumbar region) from the ultrasound coronal spine imaging, from bilateral bending. The development of the idea was inspired by the semi-automatic UCA calculation (**Section 4.2**), where UCA demonstrated a closer relationship with XCA against USSPA. This led to our curiosity whether BAI method using transverse process could outperform the one using spinous process.

The spinous characteristic line (SCL) was used to replace the spinous process line (SPL), as in the spinous process derived BAI method. The process of the formulation of the SCL is illustrated in **Figure 4.11**.

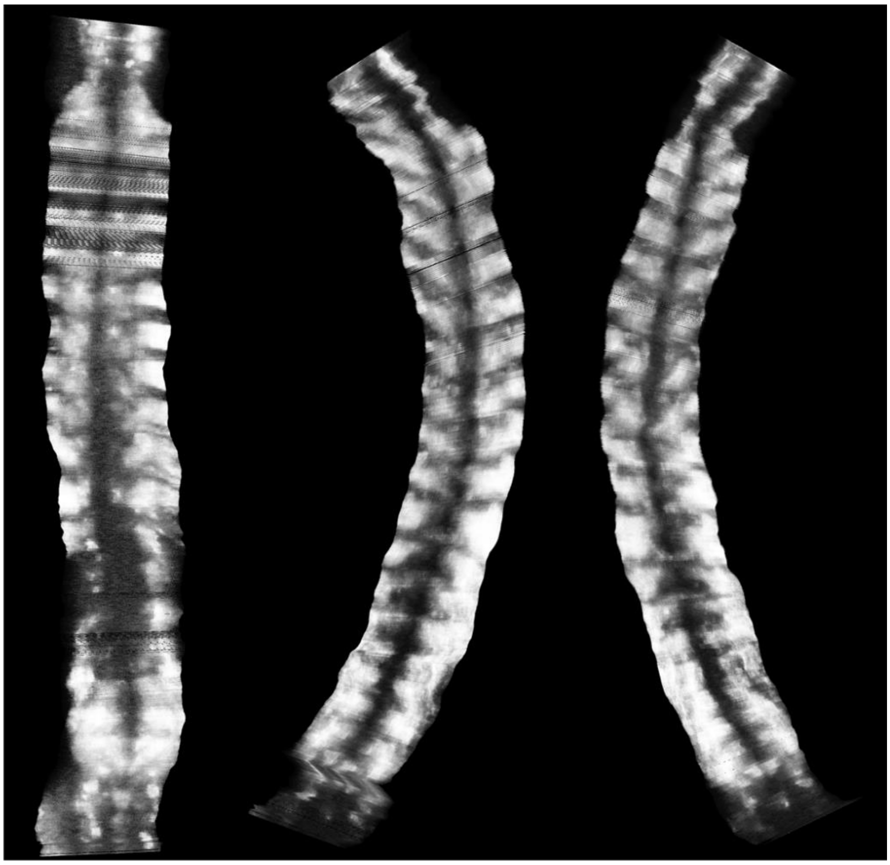

(a)

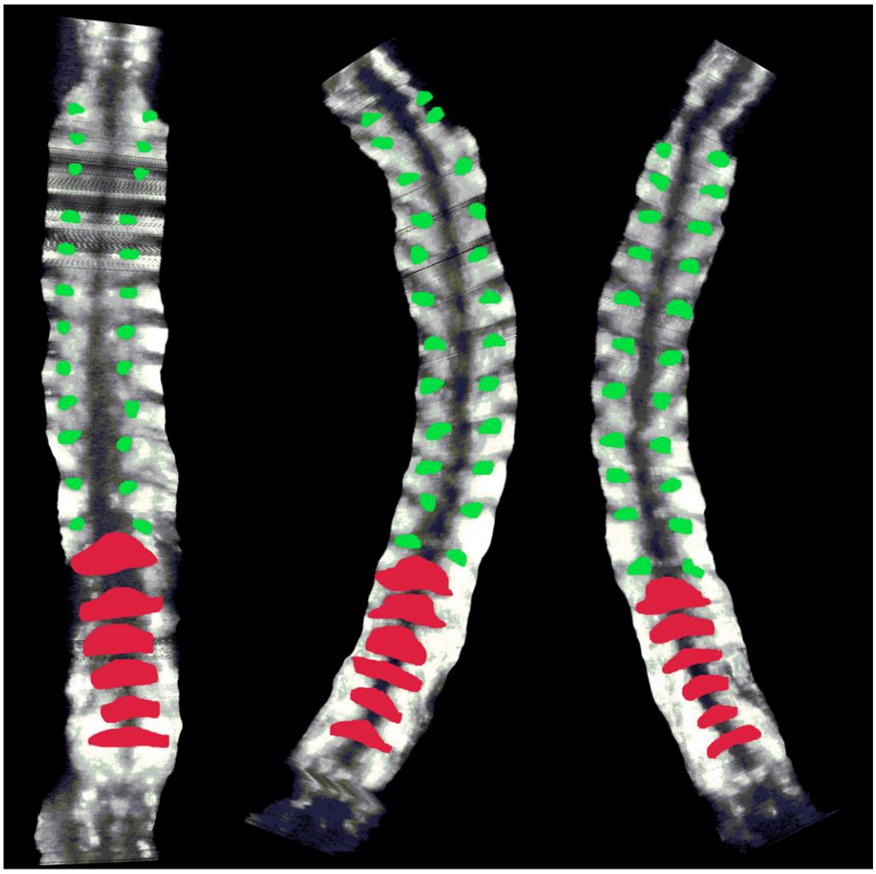

(b)

(c)

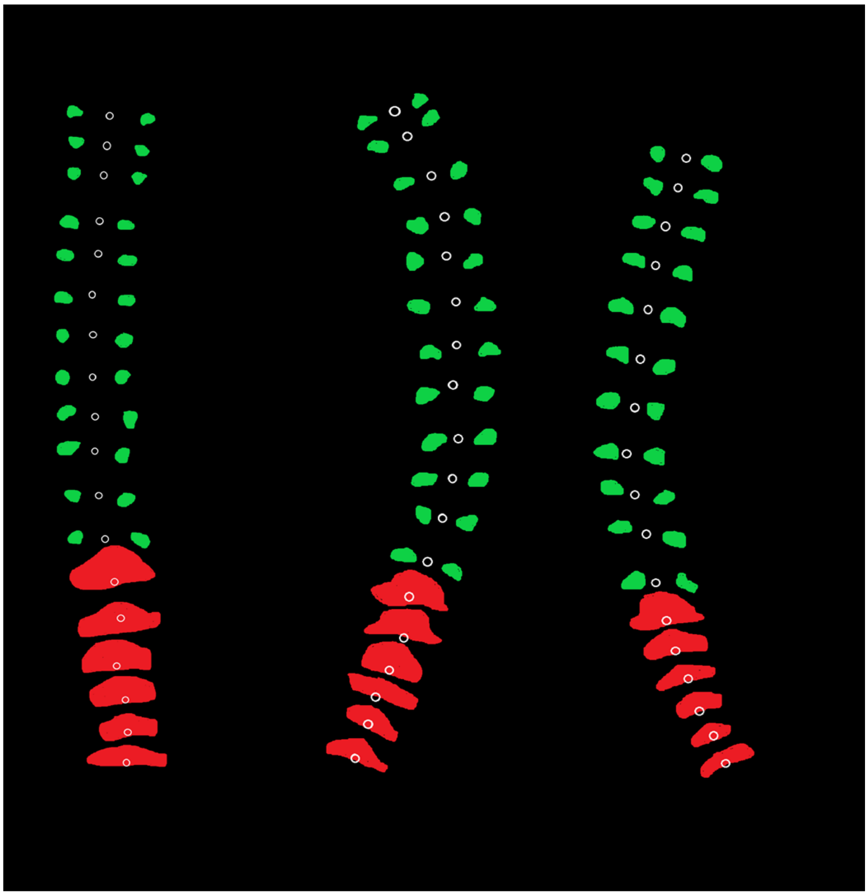

(d)

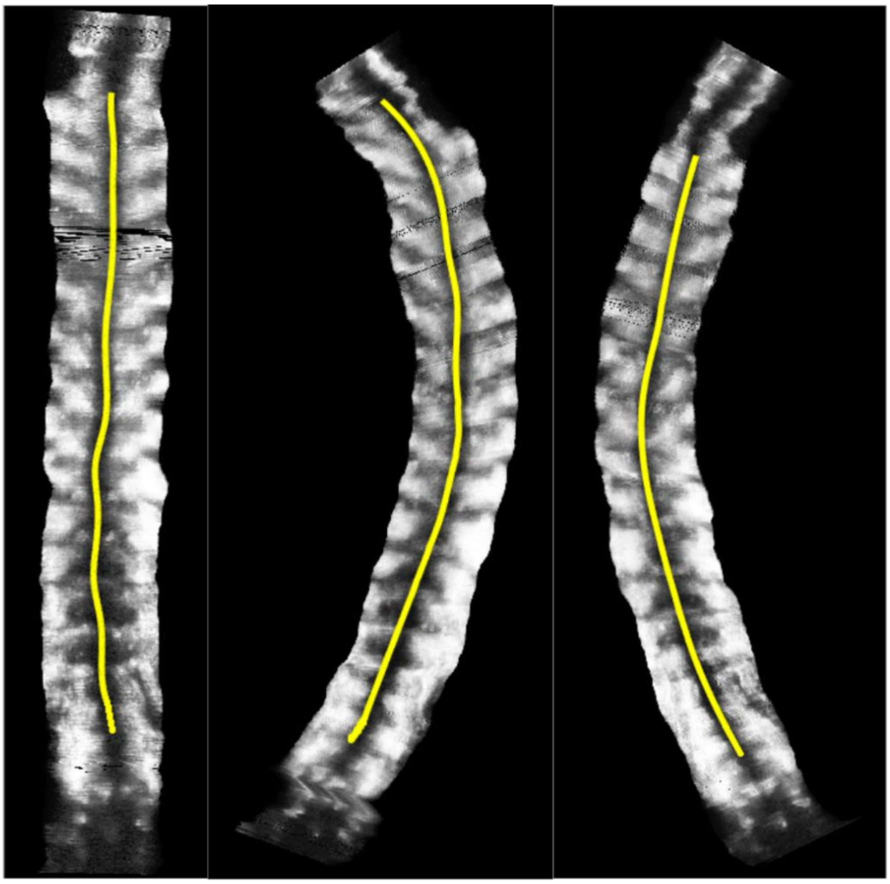

Figure 4.11 Details of the Spinous Characteristic Line (SCL) generation, each set comprises three ultrasound coronal VPI images: standing AP, bending to left and bending to right (from left to right, respectively). (a)raw input; (b) manual annotation, transverse process in thoracic region and lumbar lump in lumbar region; (c) automatic segmentation and characteristic point identification; (d)SCL generation through interpolation of characteristic points.

Different from SPL, which was interpolated through the manually identified spinous process shadow for all levels (T1-L5) from the coronal ultrasound VPI image; SCL was interpolated through the semi-automatically calculated characteristic points. Raw inputs included three postures of ultrasound scanning: standing AP, bending to left and bending to right (**Figure 4.11a**). Then manual annotation of the transverse related features was performed, according to the principle introduced in **Section 4.1** and **Section 4.2.2**. For thoracic region (T1-T12), bilateral thoracic transverse processes were contoured; and for lumbar region (lower part of T12 and L1-L5), lumbar lumps were contoured (**Figure 4.11b**). Followed by an automated procedure, which extracted and segmented the manual annotated labels; and computed the level-by-level (T1-L5) spinous characteristic points (**Figure 4.11c**). Specifically, the midpoints of the centroids of each pair of thoracic transverse process were identified for the thoracic region (T1-T12). And the midpoints of the lower boundary of each lumbar lump were used for the lumbar region (lower part of T12 and L1-L5). Such idea was identical to the semi-automatic UCA measurement discussed in **Section 4.2**. Subsequently, with the coordinates of these characteristic points, the spinal curvature representation: SCL could be automatically computed with interpolation at 6th order polynomial (***Figure 4.11d***). SCL deviated from SPL, as SCL preserved transverse process information and they were mutually aligned. With the help of SCL, transverse process derived BAI could thus be automatically calculated, identically as that with SPL. Similarly, comparing the spinal profiles from left/right bending ultrasound images, the discrepancies between bilateral curves, known as the bending discrepancy line (BDL), could be used to characterize the asymmetrical pattern of the spine: a large discrepancy suggested a rigid deformity of spine. In light of these conditions, larger BAItp could implicate a more severe structural curve. To ensure the BAItp method immune to the noise, statistical control was essential to filter out false positives caused by motion artefacts in the lateral bending scanning. UCA was measured from standing AP ultrasound image. If BAItp paired with an UCA reading in the same location, the BAItp value would be used to characterize the structural curve; otherwise, discarded. In addition, the curve was categorized depending on its location of apex: proximal thoracic (PT), main thoracic (T) or thoraco-lumbar / lumbar (L) curve. With the above information, such subject could be codified into the table of modified Lenke classification system (m-Lenke) for mild AIS using 3D ultrasound in **Figure 4.10**.

The block diagram shown in **Figure 4.12** illustrated the detailed process of generating transverse process derived BAI value, which includes the following:

i. ***Pre-processing:*** *semi-automatically generate the SDLs (as explained in* ***Figure 4.11****); output the UCA from standing AP ultrasound VPI image through the semi-automatic UCA measurement software (***Section** ***4.2****);*

ii. ***Image-processing:*** *input SDLs from previous stage; flip and fuse lateral bending curves and derive the BAItp through the calculation of the discrepancies of the curves;*

*iii. **Decision making:** generate the classification result based on the BAItp and the related apex location in spine with respect to the modified Lenke classification (m-Lenke) table.*

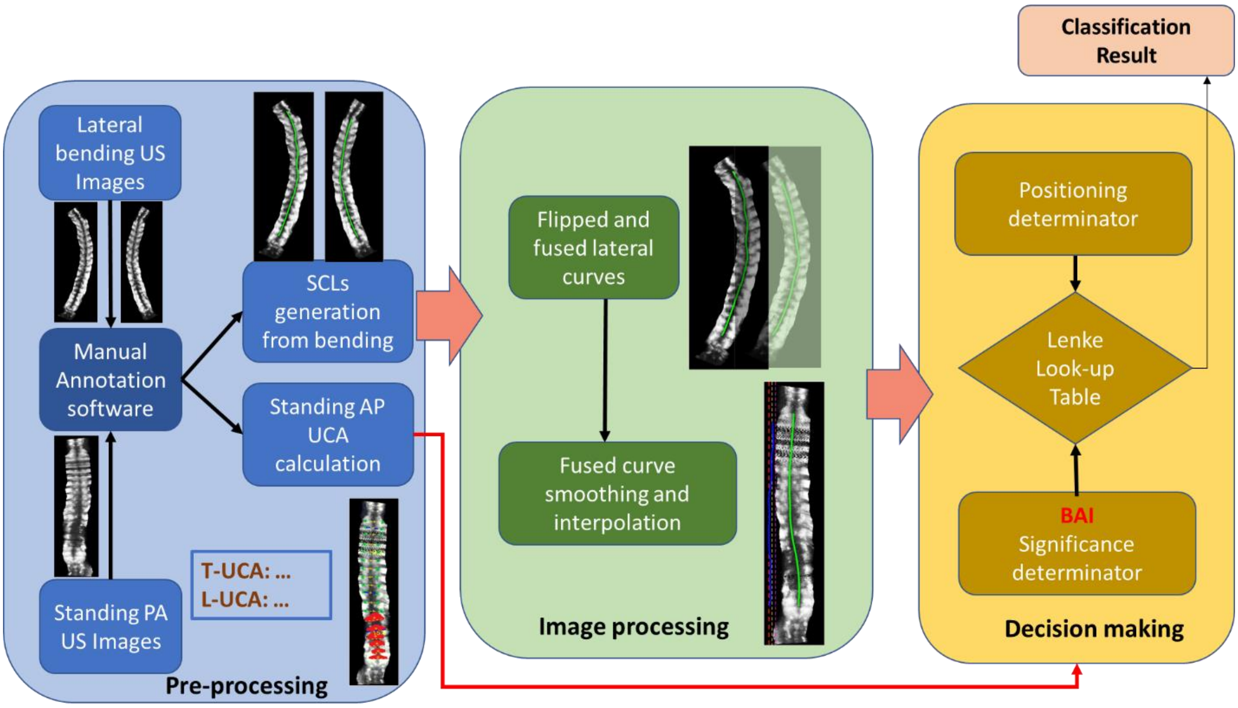

Figure 4.12 Block diagram of the computer-aided transverse process-based BAItp generation process: pre-processing, imaging processing and decision making (AIS curve classification).

Figure 4.13 and **Figure 4.14** show that how BAI could help classify non-structural and structural curves for mild AIS curves, respectively. As discussed, for non-structural curves, the curves are restored under side bending; when mirroring the left/right bending curve, they are more or less matched with each other for mild AIS cases. For structural curves, the shapes of the curves persist during side bending. When mirroring the left/right bending curve, there would be considerable discrepancies.

Figure 4.13 showed a case with a small curve in the coronal ultrasound VPI image obtained from the standing AP posture, together with two bilateral bending curves; all curves presented are characterized by SCL (**Figure 4.13a**). The extracted SCLs under the bilateral bending postures are shown in **Figure 4.13b**. As it can be observed in **Figure 4.13c**, the two curves were almost identical, leading to a very small discrepancy and could be cancelled off. Therefore, the case shown in **Figure 4.13** was classified as a nonstructural curve.

Figure 4.14 showed a typical case with structural curve. The process was the same as that described in **Figure 4.13**, and the result shown in **Figure 4.14c** suggests that there is an obvious discrepancy between the two curves, and the calculated BAItp was 221.67 mm^2 (1920 pixel, 220 ppi for ultrasound scanning), which indicated a structural curve. The thresholding value of structural curve was determined at 200 pixel or 23.09 mm^2 empirically from a pilot run of the spinous process derived BAIsp method. Since the image pixel density was identical in the ultrasound scanning process, the empirical defined cut-off value was exchangeable between BAIsp and BAItp methods. In case of no structural curve was found for a subject, the curve would be labelled as non-structural curve. Based on the location and magnitude of the structural curves from the same subject, the corresponding m-Lenke type could be obtained and collected to compare with the X-ray gold-standards.

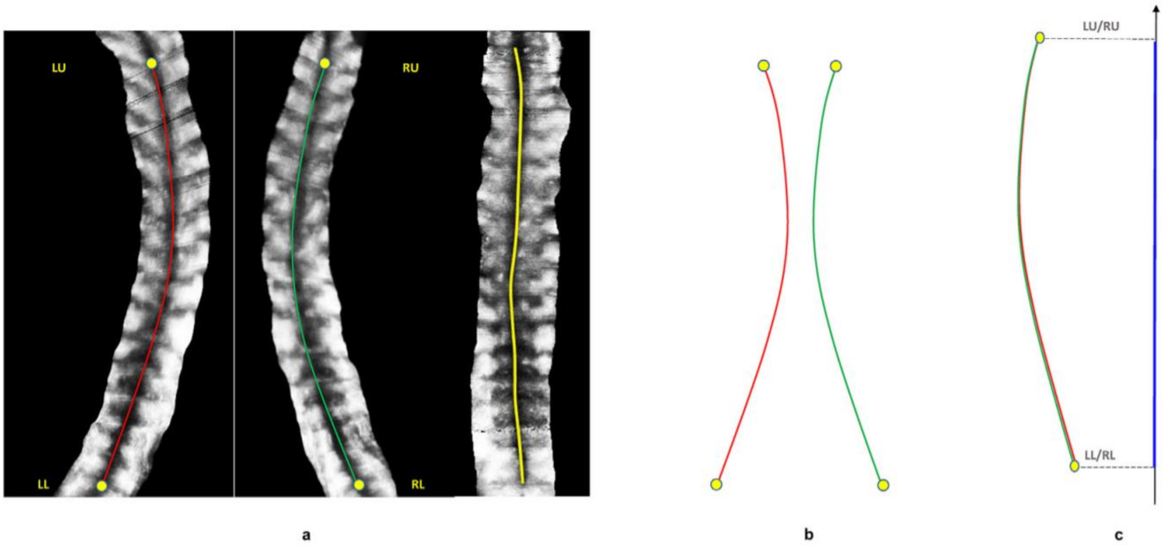

Figure 4.13 Illustration of non-structural curve characterized by BAItp from a typical mild AIS patient. **(a)** An example of the three-posture coronal spine images from the same subject with the coronal ultrasound VPI method. The SCLs for standing AP (E-SCL, yellow), bending to left (L-SCL, red) and bending to right (R-SCL, green) are combined with the original ultrasound images with end points annotated with (Left/Right Upper/Lower) markers. **(b)** the extracted L-SCL and R-SCL from **(a)** to **(c)** with alignment of end points, L-SCL is flipped to match with R-SCL to examine the asymmetrical pattern. For this curve, the BAItp value is 90 pixel or 10.39 mm^2, which is smaller than the threshold for structural curve (200 pixel or 23.09 mm^2); it indicates that the thoraco-lumbar curve presented in E-SCL**(a)** is non-structural. Line notation (also applicable to **Figure 4.13**) – red line: L-SCL; green line: R-SCL; yellow line: E-SCL; yellow circle: upper/lower points of line of SCLs for alignment; blue line: bending discrepancy line (BDL); blue enclosed area: BAItp.

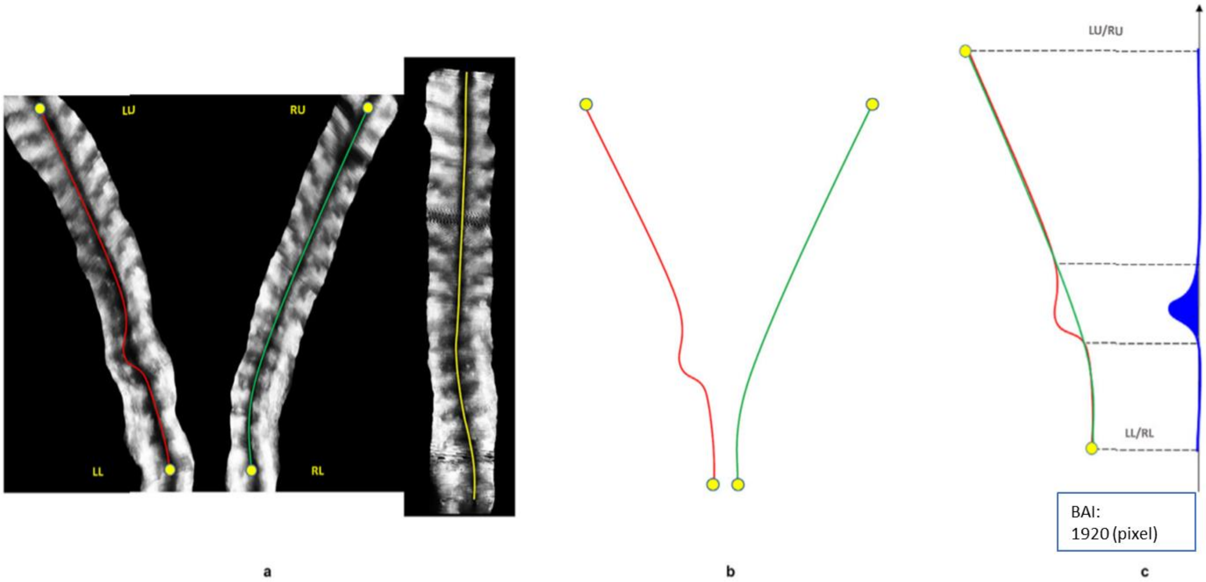

Figure 4.14 Illustration of structural curve characterized by BAItp from a real mild AIS subject. **(a)** An example of the three-posture coronal spine images from the same subject with the coronal ultrasound VPI method. The SCLs for standing AP (E-SCL, yellow), bending to left (L-SCL, red) and bending to right (R-SCL, green) are combined with the original ultrasound images with end points annotated with (Left/Right Upper/Lower) markers. **(b)** the extracted L-SCL and R-SCL from **(a)** to **(c)** with alignment of end points, L-SCL is flipped to match with R-SCL to examine the asymmetrical pattern. For this curve, the BAItp value is 1920 pixel or 221.67 mm^2 , which is larger than the threshold for structural curve (200 pixel or 23.09 mm^2); it indicates that the thoraco-lumbar curve presented in E-SPL(a) is structural.

4.3.4 Statistical analysis

Various statistical analyses were conducted for this study using SPSS 25.0 for Mac (SPSS Inc., Chicago IL, USA). For mild AIS cases, BAI was proposed to serve as a monitoring tool, as the structural curves involved are too mild for surgery. BAI would be applied to indicate spinal segment(s) required further care or chronic management. BAIsp and BAItp would be performed to compare the classification performance. Area under the curve (AUC), which disclosed the accuracy of a quantitative diagnostic test is conducted to examine the performance of single curve type classification (curve-based analysis). A point estimated from the AUC of the empirical ROC curve characterized the Mann-Whitney U estimator (DeLong et al. 1998). The confidence interval for AUC represents the uncertainty of the estimate and uses the Wald Z large sample normal approximation (DeLong et al. 1998). Specifically, a test with fair accuracy than chance has an AUC of 0.5; where a test with perfect accuracy has an AUC of 1. Statistical tool included precision (p) and recall (r) for the m-Lenke classification results (patient-based analysis). Precision (p) and recall (r) are two important evaluation metrics: precision refer s to the percentage of the harvested which are relevant; recall (r) refers to the percentage of total relevant results correctly classified by the method.

4.3.5 Results

For the included 33 mild AIS subjects (16M and 17F; Age:13.2 ±1.5 years old; Cobb: 14.7±3.9), total 44 curves were identified: with 32 structural curves and 12 non-structural curves. For the curve-based analysis, the results of BAI classifying individual curve types were i) BAIsp (BAI derived from ultrasound spinous process): AUC=0.823, standard error 0.071, p<0.001; ii) BAItp (BAI derived from ultrasound transverse process): AUC=0.905, standard error 0.045, p<0.001 ***(Figure 4.15)***.

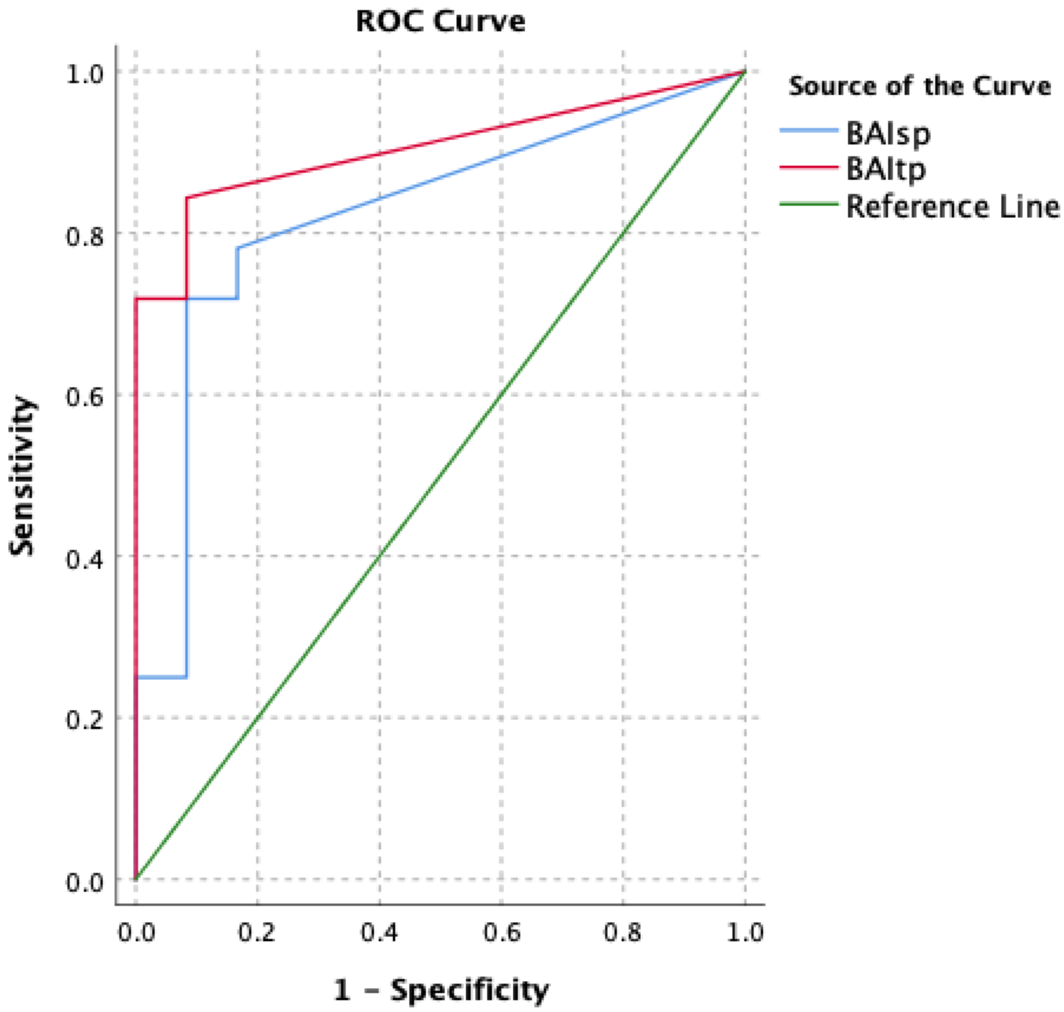

Figure 4.15 Curve-based AUC analysis of BAI classification of individual curve types i) blue line: using BAIsp (BAI derived from ultrasound spinous process); ii) red line: using BAItp (BAI derived from ultrasound transverse process). The green line is served as a reference line to indicate AUC=0.500.

With respect to the m-Lenke classification look-up table ***(*****Figure 4.10*****);*** out of the 33 patients, the number of m-Lenke type 1 to 6 is 7, 2, 3, 1, 10, and 1, respectively. In addition, there was 1 special curve type could not be codified by the existing m-Lenke classification scheme: 1 patient had structural curves in proximal thoracic and lumbar regions (denoted as PT+L), and nonstructural curve in main thoracic. Another 8 patients only had non-structural curves and did not possess structural curves (denoted as NSC). The non-structural cases were frequent, since the spine deformity was not severe among the mild AIS patients, and the spine flexibility was large before bone maturity.

Referred to the X-ray classification for mild AIS results as ground truth, the overall precision (p) of ultrasound spinous process based BAI classification method (BAIsp) was 0.73. The detailed m-Lenke classification results were presented in **Figure 4.16** and tabular form **Table 4.2**. From the results we could observe that the performance of the method diverges for different curve types: m-Lenke type 1 p=0.71, r=0.83; m-Lenke type 2 p=0, r=0; m-Lenke type 3 p=1, r=0.50; m-Lenke type 4 p=0, r=0; m-Lenke type 5 p=1, r=0.91; m-Lenke type 6 p=0, r=0; m-Lenke type variant (PT+L) p=0, r=0; non-structural curves p=0.75, r=0.75;

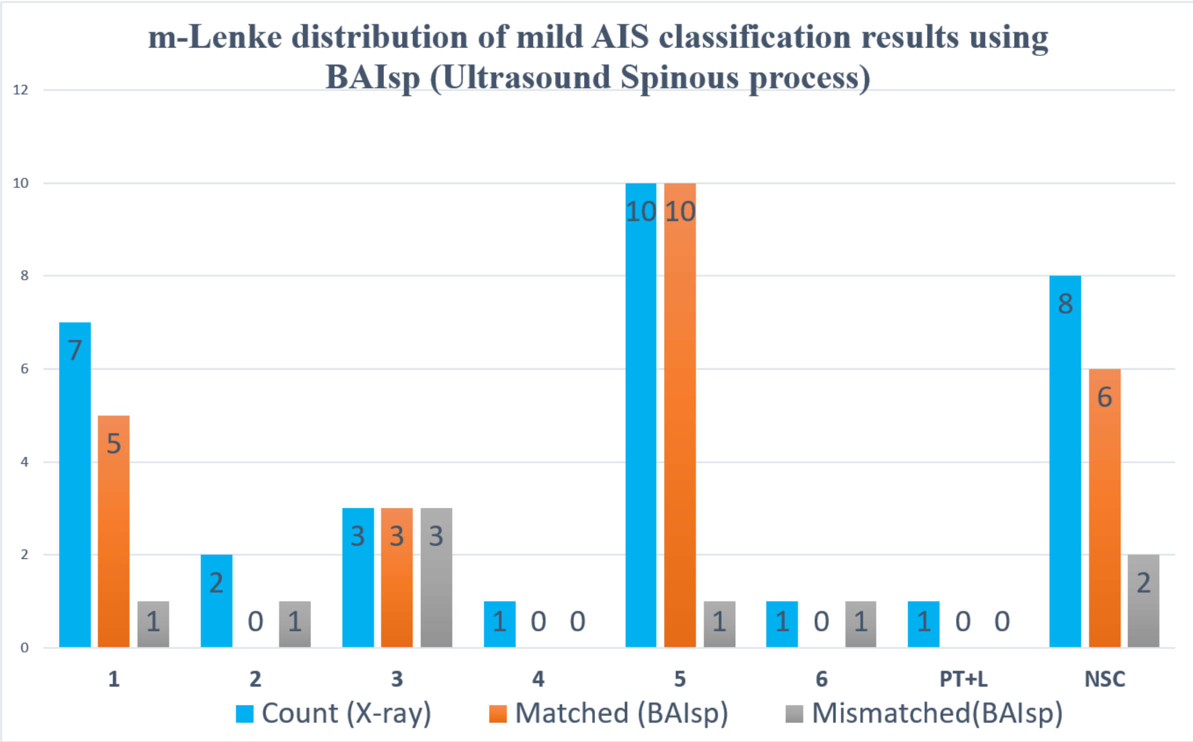

Figure 4.16 The modified Lenke distribution of mild AIS classification (m-Lenke) results using BAIsp (N=33). Scolioscan 3D ultrasound classification using BAIsp results (Matched cases in orange, mismatched cases in grey) are compared with the gold-standard EOS X-ray classification results (blue). A matched case indicates both ultrasound-based BAIsp method and X-ray ground-truth arrive at identical classification result. The ensemble comprises m-Lenke type 1–6 with a proximal thoracic-dominant variant: PT + L (structural curve in proximal thoracic and lumbar), and the detection of non-structural curves (NSC).

Table 4.2 Statistical analysis of the BAIsp (ultrasound spinous process) m-Lenke classification results

m-Lenke Type	Count (X-ray)	Matched (BAIsp)	Mismatched (BAIsp)	Precision (p)	Recall(r)
1	7	5	1	0.71	0.83
2	2	0	1	0	0
3	3	3	3	1	0.50
4	1	0	0	0	0
5	10	10	1	1	0.91
6	1	0	1	0	0
PT+L	1	0	0	0	0
NSC	8	6	2	0.75	0.75

Similarly, referred to the X-ray classification for mild AIS results as ground truth, the overall precision (p) of ultrasound transverse process based BAI classification method (BAItp) was 0.85. The detailed m-Lenke classification results were presented in **Figure 4.17** and tabular form **Table 4.3**. From the results we could observe that the performance of the method diverges for different curve types: m-Lenke type 1 p=0.86, r=0.86; m-Lenke type 2 p=0, r=0; m-Lenke type 3 p=1, r=1; m-Lenke type 4 p=0, r=0; m-Lenke type 5 p=1, r=0.91; m-Lenke type 6 p=1, r=0.50; m-Lenke type variant (PT+L) p=0, r=0; non-structural curves p=1, r=0.80;

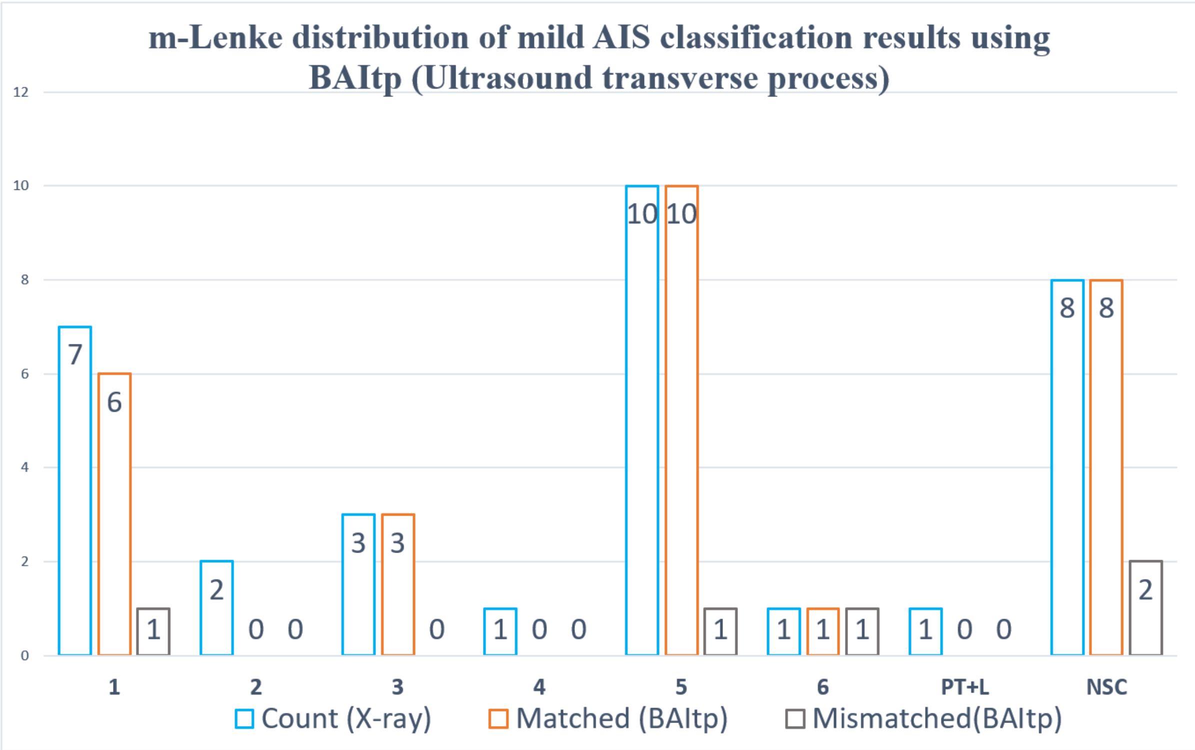

Figure 4.17 The modified Lenke distribution of mild AIS classification (m-Lenke) results using BAItp (N=33). Scolioscan 3D ultrasound classification using BAItp results (Matched cases in orange, mismatched cases in grey) are compared with the gold-standard EOS X-ray classification results (blue). A matched case indicates both ultrasound-based BAItp method and X-ray ground-truth arrive at identical classification result. The ensemble comprises m-Lenke type 1–6 with a proximal thoracic-dominant variant: PT + L (structural curve in proximal thoracic and lumbar), and the detection of non-structural curves (NSC).

Table 4.3 Statistical analysis of the BAItp (ultrasound transverse process) m-Lenke classification results

m-Lenke Type	Count (X-ray)	Matched (BAItp)	Mismatched (BAItp)	Precision (p)	Recall(r)
1	7	6	1	0.86	0.86
2	2	0	0	0	0
3	3	3	0	1	1
4	1	0	0	0	0
5	10	10	1	1	0.91
6	1	1	1	1	0.50
PT+L	1	0	0	0	0
NSC	8	8	2	1	0.80

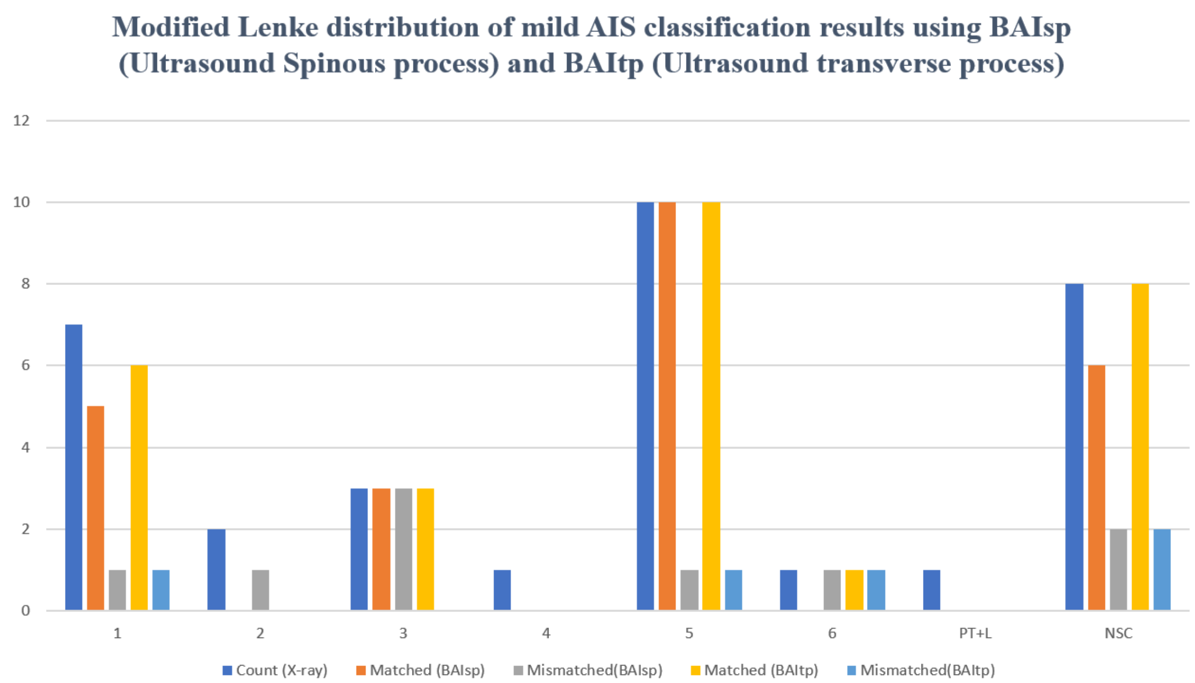

Figure 4.18 The modified Lenke distribution of mild AIS classification (m-Lenke) results using BAIsp/BAItp methods (N=33). Scolioscan 3D ultrasound classification using BAIsp results (Matched cases in orange, mismatched cases in grey) and BAItp results (Matched cases in yellow, mismatched cases in cyan) are compared with the gold-standard EOS X-ray classification results (blue), respectively. A matched case indicates both ultrasound-based BAIsp/BAItp method and X-ray ground-truth arrive at identical classification result. The ensemble comprises m-Lenke type 1–6 with a proximal thoracic-dominant variant: PT + L (structural curve in proximal thoracic and lumbar), and the detection of non-structural curves (NSC).

4.3.6 Discussion

The overall performance of ultrasound BAI method is promising for classifying mild AIS curves, which has not been systematically investigated in previous studies. For identifying structural or non-structural curves, BAIsp method achieved AUC=0.823, standard error 0.071, $p<0.001$; and BAItp improved further with AUC=0.905, standard error 0.045, $p<0.001$. This finding proves the BAItp method (transverse process features) outperformed BAIsp method (spinous process) when estimating the conventional Cobb measurement (XCA), as illustrated in **Section 4.1** and **Section 4.2**. One advantage of using transverse process is that it suffers less when presenting motion artifacts in the ultrasound scanning (especially in lateral posture bending, where subject is required to hold the designated posture for a few minutes). As an example of left-bending ultrasound VPI spine image shown in **Figure 4.19**, motion artefact results in a curvature (the region highlighted by dotted red circle) with apex at T10. BAIsp method captures this curvature by following the tips of spinous process shadow. On contrary BAItp method improves the performance when the motion artefact presented, as it is generated by transverse process features. Motion artefact is inevitable in ultrasound dynamic scanning; therefore, BAItp method is more robust compared with BAIsp method, which achieved a better classification performance against the latter method.

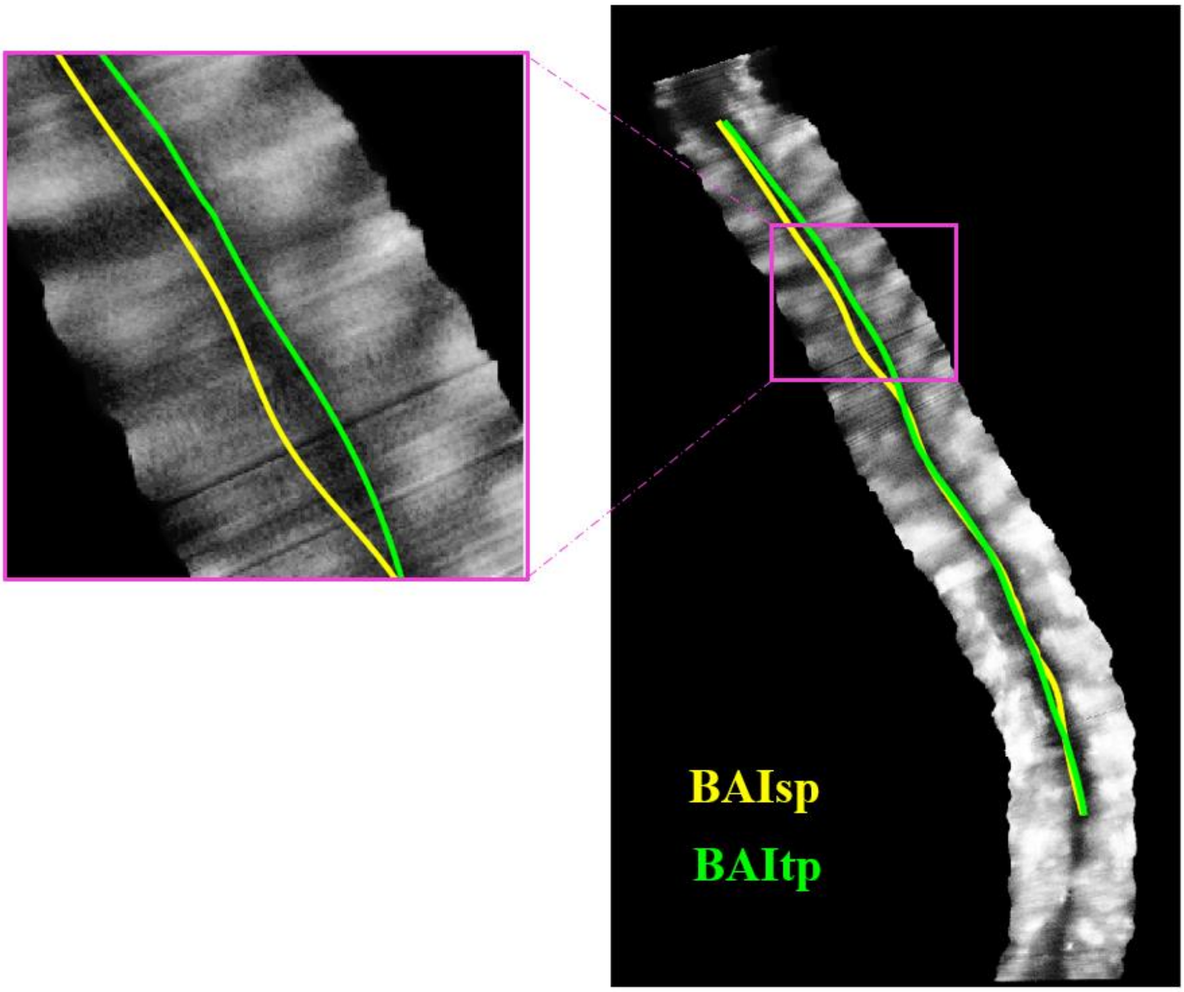

Figure 4.19 An example of left bending ultrasound VPI spine image to illustrate the effect of motion artefact to the BAI method. Pink rectangle window in the image highlights the curvature caused by motion artefact. BAIsp method, yellow line: SPL; BAItp method, green line: SCL. The discrepancy of BAIsp method and BAItp method is illustrated.

From **Table 4.2** and **Table 4.3**, we can observe that the performances for different m-Lenke types of curves for both BAI methods are distinct. From m-Lenke type 5, which is thoraco-lumbar/lumbar curve, both BAI methods demonstrated extremely high classification capacity, with BAIsp method p=1, r=0.91 and BAItp method p=1, r=0.91. According to a prevalence study of 72,699 schoolchildren, the most common type of mild AIS cases was thoracolumbar curves (40.1%) (Wong et al. 2005). It was quite constructive that our proposed BAI method could accommodate the majority. From this promising result, the application of the proposed ultrasound BAI method could potentially reduce the use of X-ray in clinical management, and monitoring for patients with thoraco-lumbar / lumbar curves. In addition, radiation-free follow-up planning and chronic tracking programs could be specifically designed for the patients with thoraco-lumbar / lumbar curves.

Both BAI methods demonstrated capability in classifying nonstructural curves, with BAIsp method p=0.75, r=0.75 and BAItp method p=1, r=0.80. This finding was helpful in post-screening management and cases referrals of mild AIS patients. Non-structural mild AIS cases usually required no follow-ups (Negrini et al. 2003, Weinstein et al. 2008). Especially for using BAItp method, labor could be saved when removing these subjects without the need of follow-ups for cost effectiveness in clinical management practice.

For m-Lenke type 3, double major curve, BAItp method had a perfect classification result of p=1, r=1 than BAIsp method p=1, r=0.50. After carefully examining the mismatched cases for BAIsp method, we identified the discrepancies were derived from motion artefact as discussed. For m-Lenke type 1,3,5, which covered the whole span of thoracic curve and thoraco-lumbar/ lumbar curve, both BAI methods demonstrated satisfactory results, especially the BAItp method. In short, curve types within thoracic and lumbar region all received considerably excellent classification performance.

However, the m-Lenke curve types included proximal thoracic region (curve apex within T2-T5) were underperformed. Specifically, both BAI methods upon m-Lenke type 2, 4 and variant PT+L have p=0, r=0. This result was due to the physical limitation of the ultrasound scanning around proximal thoracic or cervical region, which had a convex surface and making the ultrasound coupling between the ultrasound probe and the skin be difficult, leading to poor image quality. The proximal thoracic could be visualized clearly in X-ray imaging while barely seen in respective ultrasound imaging. Thus, the performance of BAI was hindered by the proximal thoracic spine scanning. A clinical study using 3D ultrasound imaging to investigate the measurements on thoracic spine also demonstrated that a comparably lower reliability of measurement was found at upper thoracic segment compared with lumbar spine (Folsch et al. 2012). A proper coupling method for ultrasound scanning for the upper thoracic and cervical region is required to be developed, and flexible ultrasound arrays that could cover the whole spine region may be a good solution for the ‘missing’ curves in the proximal thoracic spinal segments (Shea et al. 2015). On the other hand, proximal thoracic curves are the least important curve types in curve-correction exercise, as they impact less to the overall loading of the biomechanics in mild AIS treatment (Negrini et al. 2015).

The cohort of subjects of our study was obtained retrospectively from a government post-screening AIS program. The m-Lenke distribution of subjects was very uneven among different categories. In order to test the distinction power of the proposed method against specific type of AIS, a more even distribution of each class should be included in the further study when subject pool becomes statistically large; and we can understand the landscape of mild AIS classification using BAI better.

Another concern of BAI methods (both BAIsp and BAItp) was raised for the cost-effectiveness of ultrasound scanning. As mentioned, the ultrasound-derived parameter BAI required triple times of scanning: extra time and efforts were needed for the practice. And the generation of BAI methods are semi-automatic, manual labor is required for the pre-processing stage of BAI. BAIsp method needs manual annotation of spinous process on the ultrasound coronal VPI spine image; and BAItp method needs manual identification and contouring of transverse process features from the ultrasound coronal VPI spine image. However, the benefits were still outweighed the time consumption: management and monitoring of mild AIS subjects with timely and customized radiation-free follow-ups. For the further development of BAI method, deep learning approaches should be applied to liberate the manual input towards a fully-automated practice, which could be more clinically meaningful.

4.4 Summary

This chapter focuses on elaborating the validity and application of the BAItp method derived from transverse process through 3D ultrasound imaging. Previous studies on Scolioscan transverse process feature measurements were reviewed for the validity and reliability. Two sub-sections separately introduce the semi-automatic UCA measurement method and performance of using BAI methods to classify mild AIS curves types.

This semi-automatic UCA method aimed at analyzing and measuring scoliotic angles through a novel semi-automatic UCA method. This is an important intermediate step for the development of BAItp method, which uses ultrasound transverse process features. 100 AIS subjects underwent both 3D ultrasound and X-ray scanning on the same day. Scoliotic angles with XCA and UCA methods were measured manually; and transverse process-related features were identified/drawn for the semi-automatic UCA method. The semi-automatic method measured the spinal curvature with pairs of thoracic transverse processes and lumbar lumps in respective regions. The new semi-automatic UCA method showed excellent correlations with manual XCA ($R^2 = 0.815$: thoracic angles $R^2 = 0.857$, lumbar angles $R^2 = 0.787$); and excellent correlations with manual UCA ($R^2 = 0.866$: thoracic angles $R^2 = 0.921$, lumbar angles $R^2 = 0.780$). The Bland–Altman plot also showed a good agreement against manual UCA/XCA. The MADs of semi-automatic UCA against XCA were less than 5°, which is clinically insignificant. The semi-automatic UCA method had demonstrated the possibilities of estimating manual XCA and UCA. Further advancement in image processing to detect the vertebral landmarks in ultrasound images could help building a fully automated measurement method.

For the AIS curve classification study, 33 mild AIS patients underwent both 3D ultrasound and X-ray scanning on the same day. For each case, an experienced clinician (with >2 years' experience in the field) measured Cobbs and denoted major curve as ground truth. The curve classification was coded to a modified Lenke classification for mild cases (m-Lenke). In terms of curve-based analysis, BAItp method with AUC=0.905, standard error 0.045, $p<0.001$ outperforms BAIsp method AUC=0.823, standard error 0.071, $p<0.001$. When considering patient-based analysis, it was shown that 73% and 85% of the mild AIS patients achieve accurate classification from BAIsp and BAItp methods respectively. BAItp method outperforms BAIsp method by preserving immune to motion artefacts. Specifically, BAItp method demonstrated extremely high classifying capacity in categorizing main thoracic, thoraco-lumbar/ lumbar and non-structural curves. However, the limitation of the BAI methods is the unsatisfactory 3D ultrasound imaging scanning around the proximal thoracic (with apex T2-T5). Considering the limited sample size, a large cohort should be included for future studies. For the further development of BAI method, deep learning approaches should be applied to liberate the manual input towards a fully-automated practice, which could be more clinically meaningful.

CHAPTER 5. CONCLUSIONS AND FUTURE WORKS

In this thesis, the feasibility and validity of using BAI methods to conduct mild AIS classification for clinical management through radiation-free 3D ultrasound imaging, have been investigated. Ultrasound-based BAI methods were demonstrated to be valid and applicable for classifying different types of scoliotic curves in the early stage of curve progression (mild AIS, Cobb<20°). Ultrasound BAI methods not only classify mild AIS curves, but also take an important role in AIS screening referrals. Especially, BAItp method (BAI method using ultrasound transverse process features) outperforms BAIsp method (BAI method using ultrasound spinous process), which echoes the UCA value is closer to X-ray Cobb angle compared with USSPA measurement. Further studies are worthwhile to investigate whether deep learning approaches could liberate the manual procedures for the current semi-automatic BAI method(s). Due to the radiation-free nature of ultrasound, it will also be very meaningful to conduct follow-up investigation of patients with AIS for monitoring BAI changes during progression so as to study whether BAI can be used as an indicator for progression.

Semi-automatic BAI methods require human input in the spine anatomical landmarks identification. For the best classifier BAItp method, manual procedure is to contour related transverse process features for thoracic and lumbar regions. Our research team has recently reported automatic segmentation of these bony features in standing AP posture through deep learning approaches (Banerjee et al. 2022). The overall architecture of the deep learning network is shown in **Figure 5.1**.

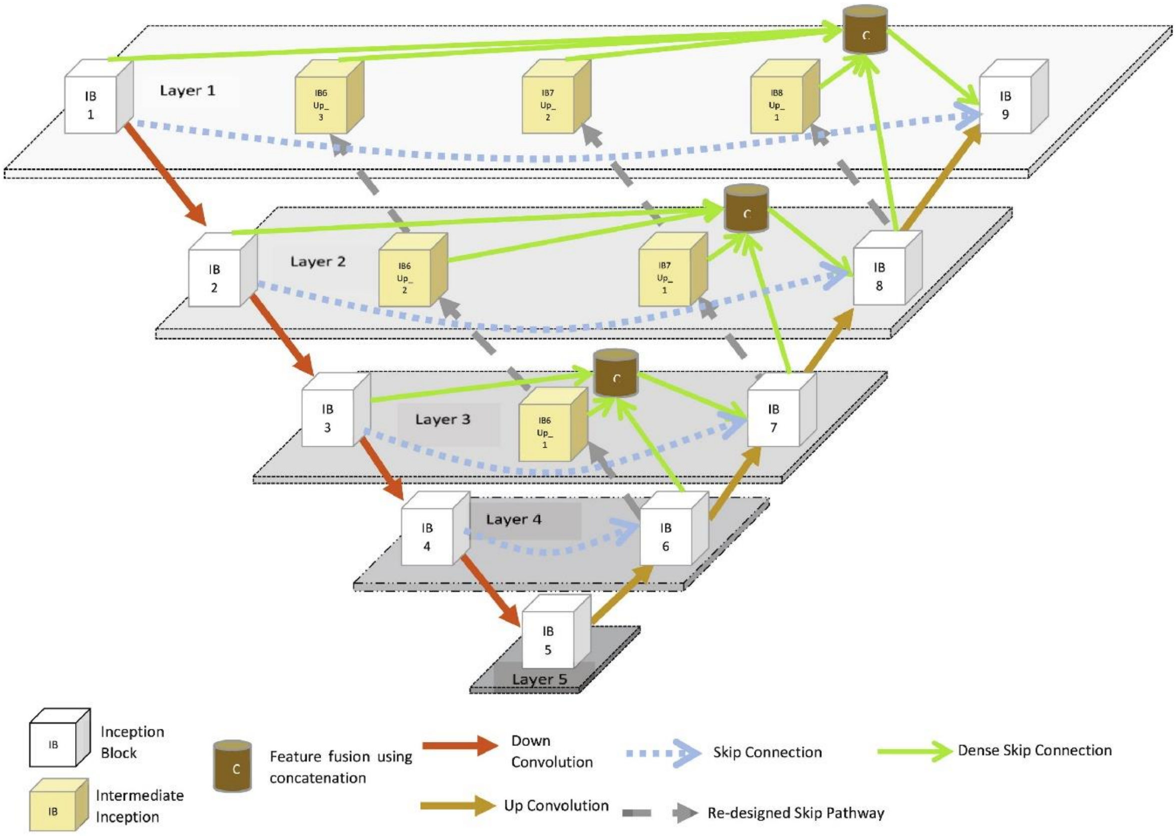

Figure 5.1 Overall architecture of proposed SIU-Net. (Image Courtesy: Banerjee et al. 2022, Fig.3)

This ‘SIU-Net’ model employs the basic U-Net structure as the base framework and contains the improvised Inception blocks, the re-designed Dense-skip connection feature fusion using concatenation and the Down-sample path, and the Up-sample path. This model demonstrated promising segmentation results for transverse process related features in both thoracic region with dice coefficient of 0.85 (thoracic transverse process pairs, **Figure 5.2**); and lumbar region with dice coefficient of 0.90 (lumbar lumps, **Figure 5.3**) against other deep learning approaches. Truth mask (TM) represents the manual annotation of the respective features.

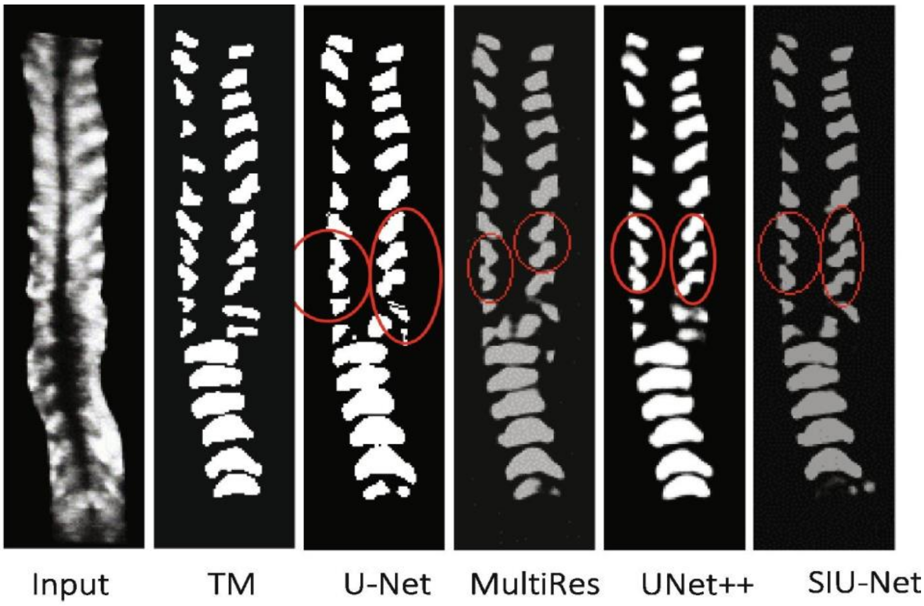

Figure 5.2 Visualization of the segmentation outcomes of proposed SIU-Net and other deep learning approaches in thoracic region. (Image Courtesy: Banerjee et al. 2022, Fig.8a)

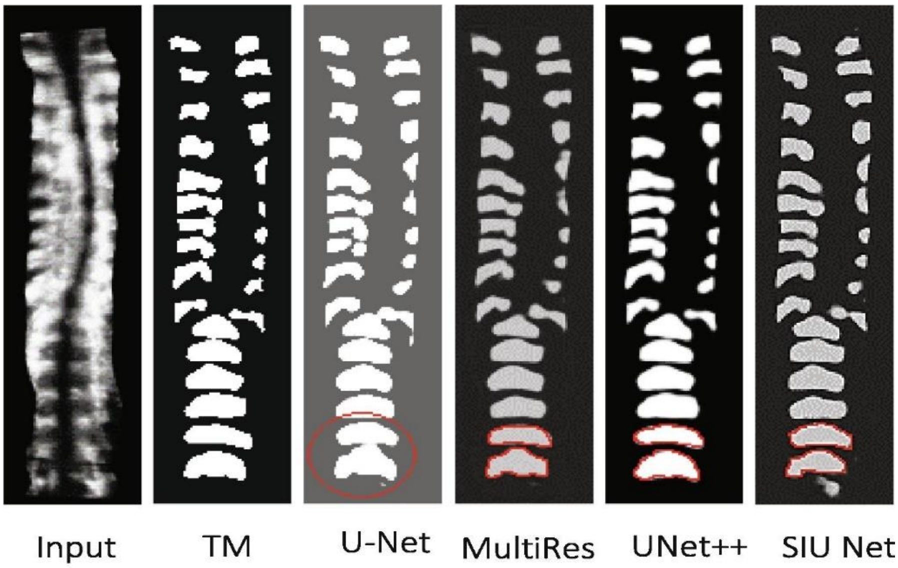

Figure 5.3 Visualization of the segmentation outcomes of proposed SIU-Net and other deep learning approaches in lumbar region. (Image Courtesy: Banerjee et al. 2022, Fig.9a)

The deep learning approaches for segmentation of ultrasound landmarks for lateral bending posture are yet to be delivered and validated. With the future validation of the bone features segmentation and classification method in lateral bending posture, the automatic generation of BAI could be investigated for the subsequent performance with respect to the current semi-automatic methods.

AIS curve progression is another important aspect of future direction of using BAI. Previous studies had been conducted to investigate either the natural course or strategies from the mild AIS stage. The risk of progression can be up to 22% for scoliosis patients overall, and skyrockets to 68% once the Cobb angle passing 20° (Bettany-Saltikov et al. 2015). Skalli's group expressed interest into exploring the progression risk of mild AIS (Skalli et al. 2017). Drevelle et.al (2010) showed that a combination of several biomechanical parameters: gravity, decreased disc stiffness and anterior spinal growth could induce progress for spines with initial mild curvature. 3D ultrasound imaging could be a powerful tool for monitoring and tracking the mild AIS patients for an extended period time; and explore the relationship between the changes of BAI profiles with the curve progression; and investigate whether BAI could be used as a predictive or prognostic parameter for AIS curve progression.

REFERENCES

Adams MA, Dolan P (2005). Spine biomechanics. Journal of Biomechanics, vol.38(10), Oct 2005, pp.1972-1983.

Altaf F, Gibson A, Dannawi Z, Noordeen H (2013). Adolescent idiopathic scoliosis. *British Medical Journal*, vol.346, May 2013, pp.30-34.

AO Surgery Reference. [Online] Available at: https://www2.aofoundation.org/wps/portal/!ut/p/a0/04_Sj9CPykssy0xPLMnMz0vMAfGjzOKN_A0M3D2DDbz9_UMMDRyDXQ3dw9wMDAx8jfULsh0VAdAsNSU!/?bone=Spine&segment=DeformityScoliosis&soloState=lyteframe&contentUrl=srg/popup/additional_material/55/X190-LenkeClassification.jsp Access on: Jan-01-2020.

Baka N, Leenstra S, van Walsum T (2017). Ultrasound aided vertebral level localization for lumbar surgery. *IEEE Transactions on Medical* Imaging, vol.36(10), pp.2138-2147.

Banerjee S, Lyu J, Huang ZX et al. (2022). Ultrasound spine image segmentation using multi-scale feature fusion skip-inception U-Net (SIU-Net). *Biocybernetics and Biomedical Engineering*, vol.42(1), Jan 2022, pp.341-361.

Beauséjour M, Roy-Beaudry M, Goulet L, Labelle H (2007). Patient Characteristics at the Initial Visit to a Scoliosis Clinic, *Spine*: (12) May 2007, pp 1349-1354 doi: 10.1097/BRS.0b013e318059b5f7

Behensky H, Giesinger K, Ogon M, et al. (2002) Multisurgeon assessment of coronal pattern classification systems for adolescent idiopathic scoliosis: Reliability and error analysis. *Spine*. vol.27, Jan 2002, pp.762–767.

Bekki H, Harimaya K, Matsumoto Y et. al (2018), Which side-bending X-ray position is better to evaluate the preoperative curve flexibility in adolescent idiopathic scoliosis patients, supine or prone? *Asian Spine Journal*, vol.12(4), May 2018, pp.632-638.

Bettany-Saltikov J, Weiss HR, Chockalingam N, Taranu R, Srinivas S, Hogg J, et.al (2015), Surgical versus non-surgical interventions in people with adolescent idiopathic scoliosis, Cochrane Systematic Review, vol.4, Apr 2015, pp.1-29.

Bolling T, Schuck A, Pape H, Rube C, Meyer FM, Martini C, Timmermann B, Asadpour B, Kortmann RD, Beck JD, Langer T, Paulides M, Konemann S, Willich N((2007). Register for the evaluation of side effects after radiation in childhood and adolescence, first results. *Klinische Padiatrie*, vol.219(3), May 2007, pp.139-145.

Brignol A, Gueziri HE, Laporte C (2020). Automatic extraction of vertebral landmarks from ultrasound images: a pilot study. *Computers in Biology and Medicine*, vol.122, May 2020, pp.103838.

Brink RC, Wijdicks SPJ, Tromp IN, Schlosser TPC, Kruyt MC, Beek FJA, Castelein RM (2017), A reliability and validity study for different coronal angles using ultrasound imaging in adolescent idiopathic scoliosis, *Spine*, vol.18(6), Jun 2018, pp.979-985

Buchler P, de Oliveria MW, Studer D, et.al (2014), Axial suspension test to assess pre-operative spinal flexibility in patients with adolescent idiopathic scoliosis, *European Journal of Spine*, vol.23, Oct 2014, pp.2619-2625.

Cardinal L (2016), Diagnostic testing in the context of high-value care: Incorporating prior probability, *J Community Hosp Intern Med Perspect*, vol.6(6), doi: 10.3402/jchimp.v6.33674

Chamberlain CC, Huda W, Hojnowski LS, Perkins A, Scaramuzzino A (2000). Radiation doses to patients undergoing scoliosis radiography. *The British Journal of Radiology*, vol.73, May 2000, pp.847-853

Chen HB, Zheng R, Lou EHM, Le LH (2020). Compact and wireless freehand 3D ultrasound real-time spine imaging system: a pilot study, *Annu Int Conf IEEE Eng Med Biol Soc,*Jul 2020, pp.2105-2108.

Chen W, Le LH, Lou EHM (2012), Ultrasound Imaging of spinal vertebrae to study scoliosis, *Open Journal of Acoustics*, vol.2, Aug 2012, pp.95-103.

Cheung CWJ, Zhou GQ, Law SY, Lai KL, Jiang WW, Zheng YP (2015), Freehand three-dimensional ultrasound system for assessment of scoliosis, *Journal of Orthopaedic Translation*, vol.3, Jun 2015, pp.123-133.

Cheung CWJ, Zhou GQ, Law SY, Mak TM, Lai KL, Zheng YP (2015). Ultrasound volume projection imaging for assessment of scoliosis, *IEEE Transactions on Medical Imaging*, vol.34(8), Aug 2015, pp.1760-1768.

Courvoisier A, Drevelle X, Dubousset J, Skalli W (2013), Transverse plane 3D analysis of mild scoliosis, *European Spine Journal*, vol.22, Jun 2013, pp.2407-2432.

Cummings RJ, Loveless EA, Campbell J, Samelson S, Mazur JM. （1998） Inter-observer reliability and intra-observer reproducibility of the system of King et al. for the classification of adolescent idiopathic scoliosis. *J Bone Joint Surg Am*. Vol.80, Aug 1998, pp.1107–1111.

Danielsson AJ, Nachemson AL (2003). Back pain and function 23 years after fusion for adolescent idiopathic scoliosis: a case-control study – part II. *Spine*, vol.28(18), Sep 2003, pp.E373-E383.

Dawson B, Trapp RG (2004). Basic and Clinical Biostatistics. 4th ed. New York: Lange Medical Books/McGraw-Hill; 2004.

de Araujo AEA, da Silva EB, Mello DB, Cader SA, Salgado ASI, Dantas EHM (2012). The effectiveness of the Pilates method: reducing the degree of non-structural scoliosis, and improving flexibility and pain in female college students. *Journal of Bodywork & Movement Therapies*, vol.16, Apr 2012, pp.191-198.

den Boer WA, Anderson PG, Limbeek J, Kooijman MA (1999) Treatment of idiopathic scoliosis with side-shift therapy: An initial comparison with a brace treatment historical cohort. *European Spine Journal*, vol.8, Oct 1999, pp.406–410.

DeLong ER, Delong DM, Clrke-Pearson DL (1988). Comparing the areas under two or more correlated receiver operating characteristic curves: a nonparametric approach. *Biometrics*, pp.837-845.

Department of Radiology, University of Washington (2019), Scoliosis, [Online] Available at: https://rad.washington.edu/about-us/academic-sections/musculoskeletal-radiology/teaching-materials/online-musculoskeletal-radiology-book/scoliosis/, Access at Dec 16 2019

Do T, Fras C, Burke S, Widmann RF, Rawlins B, Boachie-Adjei O (2001). Clinical value of routine preoperative magnetic resonance imaging in adolescent idiopathic scoliosis. A prospective study of three hundred and twenty-seven patients. *J Bone Joint Surg Am*; 83-A:577-9

Dobosiewicz K, Durmala J, Czernicki K, Jendrzejek H (2002), Pathomechanic basics of conservative treatment of progressive idiopathic scoliosis according to Dobosiewicz method based upon radiologic evaluation. *Studies in Health Technology and Informatics*, vol.91, Jan 2002, pp.336–34

Doody MM, Lonstein JE, Stovall M, Hacker DG, Luckyanov N, Land CE (2000). Breast cancer mortality after diagnostic radiography: findings from the U.S. scoliosis cohort study. *Spine*, vol.25(16), Aug 2000, pp.2052-2063.

Drevelle X, Lafon Y, Ebermeyer E, Courtois I, Dubousset J, Skalli W (2010), Analysis of idiopathic scoliosis progression by using numerical simulation, *Spine*, vol.35(10), May 2010, pp. E407-E412.

Dubousset J, Ilharreborde B, Le Huec J-C (2014). Use of EOS imaging for the assessment of scoliosis deformities: application to postoperative 3D quantitative analysis of the trunk. *European Spine Journal*, vol. 23(S4), Jul 2014, pp.397-405.

Dunn J, Henrikson NB, Morrison CC, Blasi PR, Nguyen M, Lin JS (2018). Screening for adolescent idiopathic scoliosis, evidence report and systematic review for the US preventive services task force. *JAMA*, vol.319(2), Jan 2018, pp. 173-187.

Dyson RL, Pretorius DH, Budorick NE, Johnson DD, Sklansky MS, Cantrell CJ, Lai S, Nelson TR (2000) Three-dimensional ultrasound in the evaluation of fetal anomalies. *Ultrasound in obstetrics & gynecology*, vol.16(4), Feb 2000, pp.321-328

Elsebaie HB, Dannawi Z, Altaf F, Zaidan A, Al Mukhtar M, Shaw MJ, Gibson A, Noordeen H (2016). Clinically orientated classification incorporating shoulder balance for the surgical treatment of adolescent idiopathic scoliosis. *European Spine Journal*, vol.25(2), Feb 2016, pp.430-437.

Etier Jr BE, Orr SP, Antonetti J, Thomas SB, Theiss SM (2016). Factors impacting press ganey patient satisfaction scores in orthopedic surgery spine clinic. *Spine*, vol.16(11), Nov 2016, pp.1285-89.

Fairbank MJ (2004). Historical perspective: William Adams, the forward bending test, and the spine of Gideon Algernon. *Spine*, 29, May 2004, pp.1953-5.

Folsch C, Schlogel S, Lakemeier S, Wolf U, Timmesfeld N, Skwara A (2012). Test-retest reliability of 3D ultrasound measurements of the thoracic spine, *PMR*, vol.4, May 2012, pp.335-341.

Fong DYT, Cheung KMC, Wong YW, Wan YY, Lee CF, Lam TP, Cheng JCY, Ng BKW, Luk KDK (2015). A population-based A population-based cohort study of 394,401 children followed for 10 years exhibits sustained effectiveness of scoliosis screening, *Spine*, vol.15(5), May 2015, pp.825-833.

Garbajal G, Gomez A, Ungi T et.al (2015). Portable optically tracked ultrasound system for scoliosis measurement. *Recent Advances in Computational Methods and Clinical Applications for Spine Imaging*, 2015

Glasier CM, Chadduck WM, Leithiser Jr RE, Williamson SL, Seibert JJ (1990). Screening spinal ultrasound in newborns with neural tube defects. *Journal of Ultrasound in Medicine*, vol.9(6), Jun 1990, pp.339-343.

Goldberg CJ, Moore DP, Fogarty EE, Dowling FE (2008), Scoliosis: a review, *Pediatric Surgery International*, vol.24, Sep 2007, pp.129-144.

Grave KC, Brown T (1976). Skeletal ossification and the adolescent growth spurt, American *Journal of Orthodontics*, vol.69(6), Jun 1976, pp.611-619.

Gstoettner M, Sekyra K, Walochnik N, Winter P, Wachter R, Bach CM (2007). Inter- and intraobserver reliability assessment of the Cobb angle: manual versus digital measurement tools. *European Spine Journa*l, vol. 16, Jun 2007, pp.1587-1592.

Haher TR, Gorup JM, Shin TM, Homel P, Merola AA, Grogan DP, Pugh L, Lowe TG, Murray M (1999). Results of the scoliosis research society instrument for evaluation of surgical outcome in adolescent idiopathic scoliosis: a multicenter study of 244 patients. *Spine*, vol.24(14), Jul 1999, p.1435.

Hanley JA, McNeil BJ (1982). The meaning and use of the area under a receiver operating characteristic (ROC) curve. *Radiology*, vol.143(1), Feb 1982, pp.29-36.

He C, To MKT, Cheung JPY, Cheung KMC, Chan CK, Jiang WW, Zhou GQ, Lai KKL, Zheng YP, Wong MS (2017), An effective assessment method of spinal flexibility to predict the initial in-orthosis correction on the patients with adolescent idiopathic scoliosis (AIS), *PLOS ONE*, vol.12(12), Dec 2017

Heary RF, Kumar S, Bono CM (2008). Bracing for scoliosis. Neurosurgery, vol. 63 (S.3), Sep 2008, pp.A125-A130.

Hefti F (2013). Pathogenesis and biomechanics of adolescent idiopathic scoliosis (AIS). *Journal of Children's Orthopaedics*, vol.7(1), Apr 2013, pp.17-24.

Herzenberg JE, Waanders NA, Closkey RF, Schultz AB, Hensinger RN (1990). Cobb angle versus spinous process angle in adolescent idiopathic scoliosis. The relationship of the anterior and posterior deformities. *S*pine, vol.15(9), Mar 1990, pp.874-9.

Himmetoglu S, Guven MF, Bilsel N, Dincer Y (2015). DNA damage in children with scoliosis following X-ray exposure. *Minerva Pediatrica*, vol.67, Oct 2015, pp.1-2.

Hoffman DA, Lonstein JE, Morin MM, Visscher W, Harris III BSH, Boice Jr JD (1989). Breast cancer in women with scoliosis exposed to multiple diagnostic X rays. *Journal of the National Cancer Institute*, vol. 81(17), Sep 1989, pp.1307-1312.

Huang QH, Zeng ZZ, Li XL (2018). 2.5-D extended field-of-view ultrasound. *IEEE Trans Med Imaging,* vol.37(4), Apr 2018, pp.851-859.

Huang QH, Deng QF, Li L et al. (2019). Scoliotic imaging with a novel double-sweep 2.5-dimensional extended field-of-view ultrasound. *IEEE Transactions on ultrasonics, ferroelectrics, and frequency control*, vol.66(8), Aug 2019, pp.1304-1315.

Huang ZX, Wang LW, Leung FHF, Banerjee S, Yang D, Lee TTY, Lyu J, Ling SH, Zheng YP (2020). Bone feature segmentation in ultrasound spine image with robustness to speckle and regular occlusion noise, *2020 IEEE Intl Conf on SMC*, Oct 2020.

Hui SC, Pialasse JP, Wong JY, Lam TP, Ng BK, Cheng JC, Chu WC (2016). Radiation dose of digital radiography (DR) versus micro-dose x-ray (EOS) on patients with adolescent idiopathic scoliosis: 2016 SOSORT- IRSSD "John Sevastic Award" Winner in Imaging Research. *Scoliosis Spinal Disord* Vol.11(46), Dec 2016. doi: 10.1186/s13013-016-0106-7.

Jada A, Mackel CE, Hwang SW, Samdani AF, Stephen JH, Bennett JT, Baaj AA (2017). Evaluation and management of adolescent idiopathic scoliosis: a review, *Neurosurg Focus*, vol.43(4), Oct 2017, E2.

Jalalian A, Tay FEH and Liu G (2017). Mining motion data of scoliotic spine in the coronal plane to predict the spine in lateral bending positions. *Transactions on Machine Learning and Data Mining*, vol.10(1), Mar 2017, pp.25-39.

Jiang WW, Zhou GQ, Lai KL, Zheng YP (2016), Quantitative evaluation of spinal coronal curvature for scoliosis using a fast 3-D ultrasound projection imaging method, *IFMBE Proceedings*, vol.56, May 2016, pp. 313-317.

Jiang WW, Cheng CLK, Cheung JPY, Samartzis D, Lai KKL, T MKT, Zheng YP (2018). Patterns of coronal curve change in forward bending posture: a 3D ultrasound study of adolescent idiopathic scoliosis patients. *European Spine Journal*. Vol.27 (9), May 2018, pp.2139-2147.

Jiang WW, Zhou GQ, Lai KL, Hu SY, Gao QY, Wang XY, Zheng YP (2019), A fast 3-D ultrasound projection imaging method for scoliosis assessment, *Mathematical Biosciences and Engineering*, vol.16(3), May 2019, pp. 1067-1081.

Johnson DD, Pretorius DH, Riccabona M, Budorick NE, Nelson TR (1997). Three-dimensional ultrasound of the fetal spine, *Obstetrics & Gynecology*, vol.89(3), Mar 1997, pp.434-438.

Julien C, Carl-Eric A, Archana S, Hubert L, Stefan P (2010). Correlation between immediate in-brace correction and biomechanical effectiveness of brace treatment in adolescent idiopathic scoliosis. *Spine*, vol.35(18), Aug 2010, pp.1706-1713.

Karimi MT, Rabczuk T, Kavyani M et.al (2019), Evaluation of the efficacy of part-time versus full-time brace wear in subjects with adolescent idiopathic scoliosis (AIS): a review of literature. *Current Orthopaedic Practice*, vol.30(1), Feb 2019, pp.61-68.

Khodaei M, Zheng R, Lou EHM et.al (2018). Intra-and inter-rater reliability of spinal flexibility measurements using ultrasound (US) images for non-surgical candidates with adolescent idiopathic scoliosis: a pilot study, *European Spine Journal*, 27:2156-2164.

King HA, Moe JH, Bradford DS, Winter RB (1983). The selection of fusion levels in thoracic idiopathic scoliosis. *J Bone Joint Surg Am*. Vol.65, 1983, pp.1302–1313.

Knott P, Mardjetko S, Nance, D, Dunn M (2005), Electromagnetic topographical technique of curve evaluation for adolescent idiopathic scoliosis, *Spine*, vol.31(24), Nov 2005, pp.E911-E915.

Konieczny MR, Senyurt H and Krauspe R (2013), Epidemiology of adolescent idiopathic scoliosis, J Child Orthop, vol.7, May 2013, pp.3-9.

Korbel K, Kozinoga M, Stolinski L, Kotwicki T (2014), Scoliosis Research Society (SRS) criteria and Society of Scoliosis Orthopaedic and Rehabilitation Treatment (SOSRT) 2008 guidelines in non-operative treatment of idiopathic scoliosis, *Polish Orthopedics and Traumatology*, vol.79, May 2014, pp.118-122.

Koumbourlis AC (2006). Scoliosis and the respiratory system. *Paediatric Respiratory Reviews*, vol.7(2), Jun 2006, pp.152-160.

Kuru T, Yeldan I, Dereli EE, Ozdincler AR, Dikici F, Colak I (2015), The efficacy of three-dimensional Schroth exercise in adolescent idiopathic scoliosis: a randomized controlled clinical trial, *Clinical Rehabilitation*, vol.30(2), Mar 2015, pp.181-190.

Lam TP, Wong YS, Yip BHK, Ng BKW, Hung ALH, Chu WCW, Zheng YP, Lai KKL, Lee W, Qiu Y, Cheng JCY (2019). Using ultrasound for screening scoliosis to reduce unnecessary X-ray exposure: a prospective diagnostic accuracy study on 442 schoolchildren from a scoliosis screening program, 2019 IMAST, Apr 2019.

Lau K, Carter J, Kapoor S, Nagashima K, Carter J (2013), *The Complete Scoliosis Surgery Handbook for Patients: An In-Depth and Unbiased Look Into What to Expect Before and During Scoliosis Surgery* (2013 edition), U.S, Health In Your Hands, p.89.

Lebel V et.al (2016) Physiotherapy scoliosis-specific exercises: a comprehensive review of seven major schools, *Scoliosis Spinal Disorder*, vol.11(20), Aug 2016, pp.1186-1194.

Lee TTY, Jiang WW, Cheng CLK, Lai KKL, To MKT, Castelein RM, Cheung JPY, Zheng YP (2019), A novel method to measure sagittal curvature in spinal deformities: the reliability and feasibility of 3D ultrasound imaging, *Ultrasound in medicine & biology*, vol.45(10), Dec 2019, pp.2725-2735.

Lee TTY, Lai KKL, Cheung JCY, Castelein RM, Lam TP, Zheng YP (2020). 3D Ultrasound imaging provides reliable angle measurement with accuracy comparable to X-ray on patients with adolescent idiopathic scoliosis. *15th International Society on Scoliosis Orthopaedic Rehabilitation and Treatment Meeting (SOSORT)*, Jun 2020.

Lee TTY, Lai KKL, Cheng JCY, Castelein RM, Lam TP, Zheng YP (2021). 3D ultrasound imaging provides reliable angle measurement with validity comparable to X-ray in patients with adolescent idiopathic scoliosis, *Journal of Orthopaedic Translation*, vol.29, Jul 2021, pp.51-59.

Lenke LG, Betz RR, Harms J, Bridwell KH, Clements DH, Lowe TG, Blanke K (2001). Adolescent idiopathic scoliosis: a new classification to determine extent of spinal arthrodesis. *The Journal of Bone & Joint Surgery*, vol.83(8), Aug 2001, pp.1169-1181.

Lenke LG, Betz RR, Haher TR, Lapp MA, Merola AA, Harms J, Shufflebarger HL (2001). Multisurgeon assessment of surgical decision-making in adolescent idiopathic scoliosis: curve classification, operative approach, and fusion levels. *Spine*, vol.26(21), Nov 2001, pp.2347-2353.

Lenke LG, Edwards, CC II, Bridwell KH (2003). The Lenke classification of adolescent idiopathic scoliosis: how it organizes curve patterns as a template to perform selective fusions of the spine. *Spine*, vol.28(20S), Oct 2003, pp. S199-S207.

Levy AR, Goldberg MS, Mayo NE, Hanley JA, Poitras B (1996). Reducing the lifetime risk of cancer from spinal radiographs among people with adolescent idiopathic scoliosis. *Spine*, vol.21(13), Jul 1996, pp.1540-1547.

Lin H, Sucato D (2004). Identification of Lenke spine deformity classification by simplified 3D spine model. *26th Annual Int Conf. IEEE in Medicine and Biology So*. vol.5, Sep 2004., pp.3144-3146.

Liu YZ, Pan AX, Hai Y, Li WJ, Yin L, Guo RJ (2019). Asymmetric biomechanical characteristics of the paravertebral muscle in adolescent idiopathic scoliosis, *Clinical Biomechanics*, vol.65, May 2019, pp.81-86.

Lonstein JE, Carlson JM. The prediction of curve progression in untreated idiopathic scoliosis during growth (1984). *J Bone Joint Surg Am*, 66 Aug 1984, pp.1061-71.

Loughenbury PR, Murphy E, Dunsmuir R, Gummerson NW, Rowbotham E, Khan AL (2016). Estimated x-ray exposure and additional cancer risk during surgical treatment of scoliosis in the growing spine. *NASS 31st Annual Meeting Proceedings*, S251-S337.

Louis R (2012). Surgery of the Spine: Surgical Anatomy and Operative Approaches. Reprinted (1983) Springer New York: Science & Business Media; 2012.

Lowe LH, Johanek AJ, Moore CW (2007) Sonography of the neonatal spine: part 1, normal anatomy, imaging pitfalls, and variations that may simulate disorders. *Am J Roentgenol*, vol.188(3), Mar 2007, pp.733-738.

Lowe T, Berven S, Shwab FJ, Bridwell KH (2006). The SRS classification for adult spinal deformity: building on the King/Moe and Lenke classification systems. *Spine*, vol.31(19), Sep 2006, pp.S119-S125.

Majdouline Y, Aubin C-E, Robitaille M, Sarwark JF, Labelle H (2007). Scoliosis correction objectives in adolescent idiopathic scoliosis. *Journal of Pediatric Orthopaedics*, vol.27(7), Oct 2007, pp.775-781.

Matusik E, Durmala J, Olszanecka-Glinianowicz M, Chudek J, Matusik P (2020). Association between Bone Turnover Markers, Leptin, and Nutritional Status in Girls with Adolescent Idiopathic Scoliosis (AIS). *Nutrients*; 12(9), Jun 2020,pp.2657. https://doi.org/10.3390/nu12092657

Millner PA, Dickson RA (1996). Idiopathic scoliosis: biomechanics and biology. *European Spine Journal*, vol.5(6), Dec 1996, pp.362-373.

Mirtz TA, Thompson MA, Greene L, Wyatt LA, Akagi CG (2005). Adolescent idiopathic scoliosis screening for school, community, and clinical health promotion practice utilizing the PRECEDE-PROCEED model, *Chiropractic & Osteopathy*, vol.13, Nov 2005, article number: 25 (2005).

Mohanty SP, Pai Kanhangad M, Gullia A (2020). Curve severity and apical vertebral rotation and their association with curve flexibility in adolescent idiopathic scoliosis, *Musculoskeletal Surgery*, Apr 2020, https://doi.org/10.1007/s12306-020-00660-0.

Morrissy RT, Goldsmith GS, Hall EC, Kehl D, Cowie GH (1990). Measurement of the Cobb angle on radiographs of patients who have scoliosis. Evaluation of intrinsic error. *The Journal of Bone & Joint Surgery,* vol.72, Jul 1990, pp.320-327.

Negrini S, Antonini G, Carabalona R, Minozzi S (2003). Physical exercises as a treatment for adolescent idiopathic scoliosis. A systematic review. *Journal of Pediatric Rehabilitation*, vol.6(3), Sep 2003, pp.227-235.

Negrini S, Negrini A, Romano M, Verzini N, Parzini S (2006) A controlled prospective study on the efficacy of SEAS.02 exercises in preparation to bracing for idiopathic scoliosis. *Studies in Health Technology and Informatics,* vol.123, Jan 2005, pp.519–522.

Negrini A, Negrini MG, Donzelli S, Romano M, Zaina F, Negrini S (2015) Scoliosis-Specific exercises can reduce the progression of severe curves in adult idiopathic scoliosis: a long-term cohort study*. Scoliosis* 10, Jul 2015, 20. https://doi.org/10.1186/s13013-015-0044-9

Nguyen DV, Vo QN, Le LH, Lou EHM (2015). Validation of 3D surface reconstruction of vertebrae and spinal column using 3D ultrasound: a pilot study. *Medical Engineering & Physics*, vol. 37(2), Feb 2015, pp.239-244.

Ovadia D, Bar-On E, Fragniere B, Rigo M, Dickman D, Leitner J, Wientroub S, Dubousset J (2006), Radiation-free quantitative assessment of scoliosis: a multi-center prospective study, *European Spine Journal*, vol.16(1), pp.97-105.

Ovadia D (2013). Classification of adolescent idiopathic scoliosis (AIS). *Journal of Children's Orthopaedics*, vol.7(1), Feb 2013, pp.25-28.

Pasha S, Capraro A, Cahill PJ, Dormans JP, Flynn JM (2016). Bi-planar spinal stereoradiography of adolescent idiopathic scoliosis: considerations in 3D alignment and functional balance, *European Spine Journal*, vol.25(10), Oct 2016, pp.3234-3241.

Pasha S (2019). 3D deformation patterns of S shaped elastic rods as a pathogenesis model for spinal deformity in adolescent idiopathic scoliosis. *Scientific reports*, vol.9, Nov 2019:16485.

Phan P, Mezghano N, Wai EK, de Guise J (2013). Artificial neural networks assessing adolescent idiopathic scoliosis: comparison with Lenke classification, *Spine*, vol. 13(11), Nov 2013, pp.1527-1533.

Pil-Neo H (2016), Psychological and physical effects of Schroth and Pilates exercise on female high school students with idiopathic scoliosis. *Journal of Korean Physical Therapy*, vol.28(6), Dec 2016, pp.364-368.

Pooh RK, Pooh KH (2005) Fetal vertebral structure detected by three-dimensional ultrasound, *The Ultrasound Review of Obsterics and Gynecology*, vol.5(1), Dec 2005, pp.29-33.

Ramirez N, Johnston CE, Browne RH (1997). The prevalence of back pain in children who have idiopathic scoliosis. J Bone Joint Surg Am1997;79:364-8

Richard BS, Bernstein RM, D'Amato CR, Thompson GH (2005). Standardization of criteria for adolescent idiopathic scoliosis brace studies: SRS committee on bracing and nonoperative management. *Spine*, vol.30(18), Sep 2005, pp.2068-2075.

Romano M, Negrini A, Parzini S, Tavernaro M, Zaina F, Donzelli Sm Negrini S (2015). SEAS (Scientific Exercises Approach to Scoliosis): a modern and effective evidence based approach to physiotherapic specific scoliosis exercises. Scoliosis, vol.10, Feb 2015. Article number: 3 (2015).

Rose PS, Lenke LG (2007). Classification of operative adolescent idiopathic scoliosis: treatment guidelines, *Orthopedic Clinics of North America*, vol.38(4), Oct 2007, pp.521-529.

Sekiya T, Aota Y, Yamada K, Kaneko K, Ide M, Saito T (2018). Evaluation of functional and structural leg length discrepancy in patients with adolescent idiopathic scoliosis using the EOS imaging system: a prospective comparative study, *Scoliosis and Spinal Disorders*, vol.13(7), Apr 2018, pp.10-15.

Seo JH, Hong SG (2014). The pilates effects about scoliosis. *Journal of the Korean Society of Radiology*, vol.8(7), Dec 2014, pp.397-400.

Shea QTK, Yip PYM, Zheng YP (2015). Development of flexible 2D ultrasound arrays for scoliosis assessment. *IFMBE Proceedings*, Dec 2015, pp.256-258.

Simony A, Hansen EJ, Christensen SB, Carreon LY, Andersen MO (2016). Incidence of cancer in adolescent idiopathic scoliosis patients treated 25 years previously. *Eur Spine J*, vol. 25, Sep 2016, pp.3366–3370 https://doi.org/10.1007/s00586-016-4747-2

Skalli W, Vergari C, Ebermeyer E, Courtois I, et al (2017), Early detection of progressive adolescent idiopathic scoliosis, a severity index, *Spine*, vol.42(11), Jun 2017, pp.823-830.

Solomon E, Shortland AP, Meyer AK, Lucas JD (2016). The development and validation of a 3D ultrasound system for monitoring curve progression of patients with scoliosis, *Spine*, vol.16(4), Apr 2016, pp. S51-52.

The EOS Imaging System Official Website. Available at: https://www.eos-imaging.com/, Access on 24 Dec 2019.

Torres MFL, DiPietro MA (2014). Spine ultrasound imaging in the newborn, Seminars in Ultrasound, CT and MRI, vol.35(6), Dec 2014, pp.652-661.

Ungi T, King F, Kempston M (2014), Spinal curvature measurement by tracked ultrasound snapshots, *Ultrasound Medical Biology*, vol.40, pp.447-454.

US Preventive Services Task Force (2018). Screening for adolescent idiopathic scoliosis US Preventive Services Task Force Recommendation Statement. *JAMA*, vol.319(2), Jan 2018, pp.165-172

Vergari C, Skalli W, Abelin-Genevois K et.al (2021). Effect of curve location on the severity index for adolescent idiopathic scoliosis: a longitudinal cohort study, *European Radiology*, Apr 2021, https://doi.org/10.1007/s00330-021-07944-4.

Vo QN, Le LH, Lou EHM (2019). A semi-automatic 3D ultrasound reconstruction method to assess the true severity of adolescent idiopathic scoliosis, *Medical & Biological Engineering & Computing* 2019, 57:2115-2128.

Vrtovec T, Pernus F, Likar B et.al (2009), A review of methods for quantitative evaluation of spinal curvature, *European Spine Journal*, vol.18(5), Feb 2009, pp.593-607.

Wang Q, Li M, Lou EHM, Wong MS (2015), Reliability and validity study of clinical ultrasound imaging on lateral curvature of adolescent idiopathic scoliosis, *Plos One*, Published: August 12, 2015, https://doi.org/10.1371/journal.pone.0135264

Wang Q, Li M, Lou EHM, Chu WCW, Lam TP, Cheng JCY, Wong MS (2016), Validity study of vertebral rotation measurement using 3D ultrasound in adolescent idiopathic scoliosis*, Ultrasound in Medicine and Biology*, 42(7): 1473-1481.

Wang S, Qiu Y, Zhu Z, Ma Z, Xia C, Zhu F (2007). Histomorphological study of the spinal growth plates from the convex side and the concave side in adolescent idiopathic scoliosis. *Journal of Orthopaedic Surgery and Research*; 2:19

Weinstein SL, Dolan LA, Cheng CY, Danielsson A, Morcuende JA (2008). Adolescent idiopathic scoliosis. *The Lancet*, vol.371(9623), May 2008, pp.1527-1537.

Weiss HR, Goodall D (2008). The treatment of adolescent idiopathic scoliosis (AIS) according to present evidence. A systematic review, *European Journal of Physical and Rehabilitation Medicine*, vol.44(2), Jun 2008, pp.177-193.

Wong HK, Hui JHP, Rajan U, Chia HP (2005). Idiopathic scoliosis in Singapore schoolchildren: a prevalence study 15 years into the screening program, *Spine,* vol.30(10), May 2005, pp.1188-1196.

Wong YS, Lai KKL, Zheng YP, Wong LLN, Ng BKW, Hung ALH, Yip BHK, Chu WCW, Ng AWH, Qiu Y, Cheng JCY, Lam TP (2019). Is radiation-free ultrasound accurate for quantitative assessment of spinal deformity in idiopathic scoliosis(IS): a detailed analysis with EOS radiography on 952 patients, *Ultrasound in Med. & Biol.,* vol.45(11), Oct 2019, pp.2866-2877.

Wren TAL, Ponrartana S, Poorghasamians E et.al (2017). Biomechanical modeling of spine flexibility and its relationship to spinal range of motion and idiopathic scoliosis. *Spine Deformity*, 5, Jan 2017, pp.225-230.

Ylikoski M (2005). Growth and progression of adolescent idiopathic scoliosis in girls, *Journal of Pediatric Orthopaedics B,* vol.14(5), Sep 2005, pp.320-324.

Young M, Hill DL, Zheng R, Lou EHM (2015), Reliability and accuracy of ultrasound measurements with and without the aid of previous radiographs in adolescent idiopathic scoliosis (AIS), *European Spine Journal*, vol.24, Mar 2015, pp.1427-1433.

Zapata KA, Sucato DJ, Jo CH (2019). Physical therapy scoliosis-specific exercises may reduce curve progression in mild adolescent idiopathic scoliosis curves. *Journal of Pediatric Physical Therapy*, vol.31(3), Jul 2019, pp.280-285.

Zheng R, Hill D, Lou EHM et.al (2018). Assessment of curve progression on children with idiopathic scoliosis using ultrasound imaging method. *European Spine Journal* 2018, 27: 2114-2119.

Zheng YP, CW Cheung. A three-dimensional (3D) ultrasound imaging system for assessing scoliosis. Patent issued: US 8,900,146 B2; China 201080040696.0; Japan 5849048. Pending in Canada, Australia, and EU. Filled in Jul 2009.

Zheng YP, Lee TTY, Lai KKL, Yip BHK, Zhou GQ, Jiang WW, et.al (2016). A reliability and validity study for Scolioscan: a radiation-free scoliosis assessment system using 3D ultrasound imaging, *Scoliosis and Spinal Disorders*, vol.11(1), Sep 2016, pp.1.

Zhou GQ, Jiang WW, Lai KL, Zheng YP (2017), Automatic measurement of spine curvature on 3-D ultrasound volume projection image with phase features, *IEEE Transactions on Medical Imaging*, vol.36(6), Jun 2017, pp.1250-1262.

Zhou GQ, Li DS, Zhou P, Jiang WW, Zheng YP (2020). Automating Spine Curvature Measurement in Volumetric Ultrasound via Adaptive Phase Features. Ultrasound in Medicine and Biology, vol.46(3), Oct 2020, pp.828-841.

Zhou XH, Obuchowski NA, McClish DK (2011). Statistical methods in diagnostic medicine. Wiley-Blackwell.